THE UNIVERSITY OF OKLAHOMA

GRADUATE COLLEGE

VISCOELASTIC BEHAVIOR OF SIMPLE HYDROCARBONS AT HIGH PRESSURE

A DISSERTATION

SUBMITTED TO THE GRADUATE FACULTY

in partial fulfillment of the requirements for the

degree of

DOCTOR OF PHILOSOPHY

BY

ROBERT GOTTFRIED REIN, JR.

Norman, Oklahoma

1967

VISCOELASTIC BEHAVIOR OF SIMPLE HYDROCARBONS

AT HIGH PRESSURE

APPROVED BY

C. M. Sliepcevich

Stanley E. Babb Jr.

Raymond B. Daniels

Gerald Thomas

DISSERTATION COMMITTEE

ACKNOWLEDGMENT

I wish to express my gratitude to the members of my doctoral committee for the inspiration, guidance and support they have provided. In particular I am grateful to Professor C. M. Sliepcevich who initiated the research program and whose influence assured its continuance; to Professor S. E. Babb, Jr. for the use of his high pressure equipment, his assistance during the experimental phase of the work and for his constructive criticisms; to Professor G. Tuma for the guidance and insight he provided in matters concerning electronics; and to Professor R. D. Daniels for his counsel throughout my graduate work.

In addition I wish to thank Mr. Gene Scott, who was instrumental in constructing much of Professor Babb's equipment, for making the rotating crystal holder and the crystal holder used in the high pressure cell. Mr. Scott's assistance during the experimental phase of the work is also appreciated. The assistance of Professor W. J. Ewbank who supplied the National Bureau of Standards liquids and calibration data for the National Bureau of Standards liquids is also appreciated.

I am indebted to Autoclave Engineers, Inc. and to the National Science Foundation for financial support.

Finally I wish to express my deep gratitude to my parents whose sacrifice made a college education much easier.

ABSTRACT

The possible viscoelastic behavior of simple hydrocarbons at high pressure was investigated. The viscosity-measuring technique consisted of a torsionally oscillating quartz rod. When the oscillating rod is immersed in a liquid, measurements of the resonant frequency and the resistance of the rod at resonance can be used to calculate the viscous and elastic behavior of the liquid. This viscometer reproduced, within experimental accuracy, Newtonian (non-viscoelastic) viscosity versus pressure data obtained by other investigators using different viscosity measuring techniques.

When using the torsionally oscillating rod as a high pressure viscometer, the effect of pressure on the resonant frequency of the rod must be considered. This pressure effect on the resonant frequency was measured for 20-kc and 60-kc crystals at pressures up to 8×10^3 atmospheres. The change in resonant frequency with pressure was found to vary inversely with the crystal length according to:

$$\frac{f_o(P) - f_o}{f_o} = -2.601 \times 10^{-5} + 1.689 \times 10^{-4} P + 1.216 \times 10^{-5} P^2.$$

P is the pressure in kiloatmospheres and f_o is the resonant frequency in cycles per second.

Of the liquids investigated, propane, n-pentane, i-pentane, n-octane, methylcyclohexane and toluene, only toluene exhibited viscoelastic behavior. By using a simple Maxwell model for a viscoelastic fluid and a frequency variable which reduced frequency measurements at various pressures to a series of frequencies at atmospheric pressure, it was deduced that toluene has a shear relaxation time between 7.5×10^{-9} and 2.4×10^{-8} sec.

TABLE OF CONTENTS

LIST OF TABLES

LIST OF ILLUSTRATIONS

VISCOELASTIC BEHAVIOR OF SIMPLE HYDROCARBONS AT HIGH PRESSURE

CHAPTER I

INTRODUCTION

Often when a shear stress is applied to a liquid it flows and when the stress is removed the liquid ceases to flow. If one considers a small element of such a liquid, it does not revert to its original position when the stress is removed. Work done on the liquid cannot be recovered.

On the other hand if a shear stress--such that the response remains in the elastic region--is applied to a solid and then removed, the small element will revert to its original position. The work done in deforming the solid may be recovered.

In between these different types of behavior is a class of substances which exhibit viscoelasticity. They are liquids in the sense that any applied stress causes some irrecoverable flow. They also behave like solids in that some recoil or strain recovery occurs upon release of the stress. Many polymers, polymer solutions and slurries behave viscoelastically.

In this chapter, a brief mathematical description will be given for each of three types of material behavior under the influence of shear stress. (1) Viscous behavior, (2) Elastic behavior and (3) Viscoelastic behavior. The mathematical descriptions of behavior under stress are followed by a review of pertinent investigations of viscoelastic behavior and a summary of related high pressure phenomena and experimental techniques.

Viscous Behavior

Consider the motion of a simple liquid, such as water, under the influence of an applied shear stress. It is common to consider the motion of the liquid contained between two parallel plates separated by a distance y. The upper plate is held stationary and the lower plate moved in the x direction. The plates are assumed to have infinite length in the z and x directions. After steady state laminar flow has developed it is found that a shear stress τ_{yx} must be applied to maintain motion. The situation is illustrated in Figure 1, where u(y) is the displacement in the x direction. The shear stress is

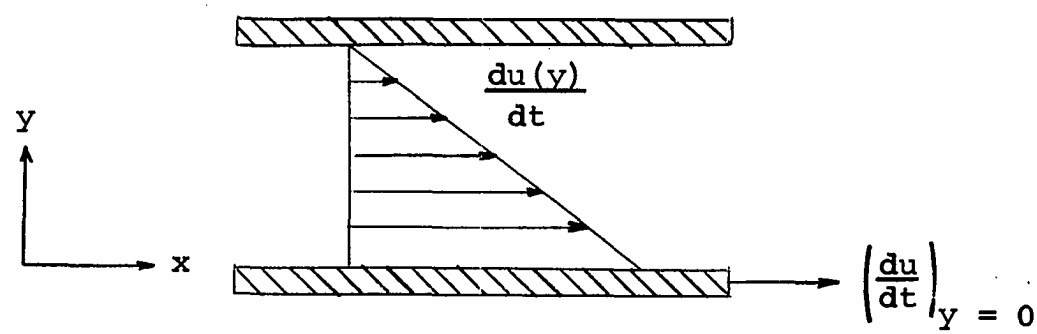

Figure 1. Velocity profile for steady state, laminar flow in a Newtonian liquid.

found to be related to u(y) by Newton's law of viscosity.

$$\tau_{yx} = -\eta \frac{d}{dy} \frac{du(y)}{dt} = \eta\dot{\gamma} \qquad (1)$$

η is the coefficient of viscosity and $\dot{\gamma}$ is the rate of shear. Similarly, if the fluid were in a dashpot (Figure 2), the applied stress is represented by Equation (1). The dashpot is a mechanical analogue of a Newtonian liquid. The electrical analogue is a resistor.

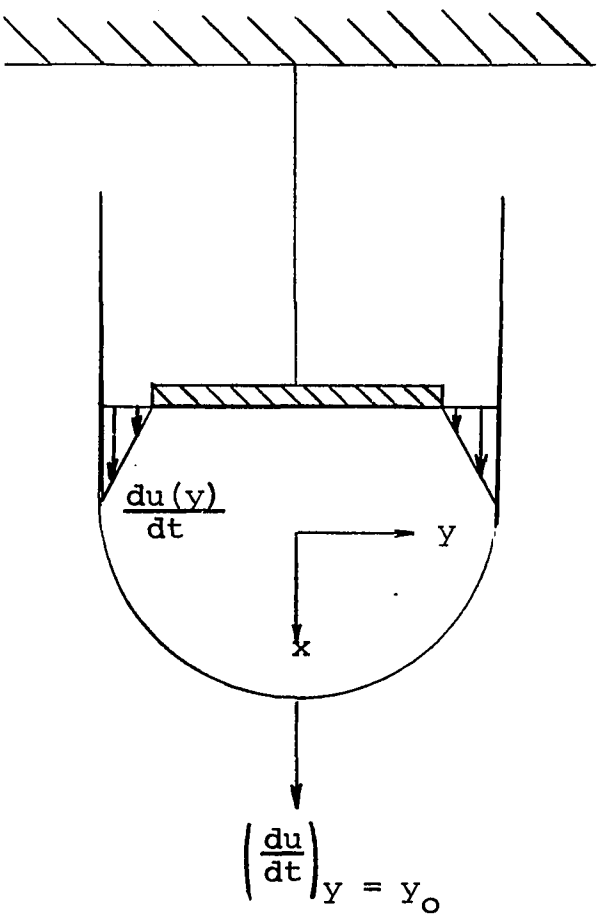

Figure 2. Velocity profiles for steady state, laminar flow in a dashpot filled with a Newtonian liquid.

Elastic Behavior

Now consider the motion of an elastic solid. The shear stress is found to be independent of the rate of x motion: it depends only on the amount of motion. The situation is illustrated in Figure 3. The shear stress is related to the x displacement by Hooke's Law with a shear

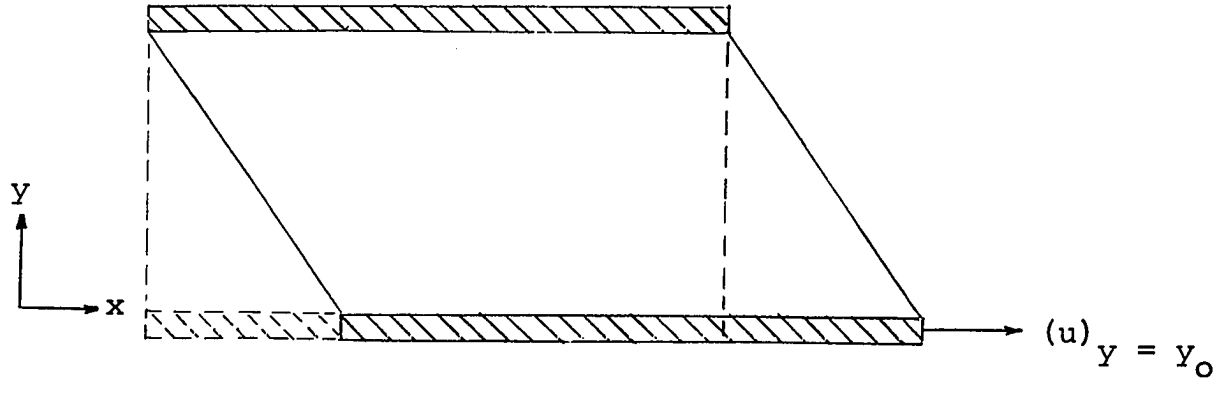

Figure 3. Shear strain in a solid with modulus G. Dashed lines indicate the original position of the solid.

modulus G

$$\tau_{yx} = -G \frac{du}{dy} = -G\gamma . \qquad (2)$$

If τ_{yx} is removed, the solid will recover to its original state. This property of elasticity is analogous to the behavior of a spring, and indeed a spring is the mechanical analogue of a Hookean solid. A capacitor is the electrical analogue.

Viscoelastic Behavior

If a spring and dashpot were connected in series, as per Figure 4, the total extension of the combination would be

the sum of the elongation of the spring and the dashpot.

$$\gamma_s + \gamma_d = \frac{\tau_{yx}}{G} + \frac{\tau_{yx}dt}{\eta} = D \qquad (3)$$

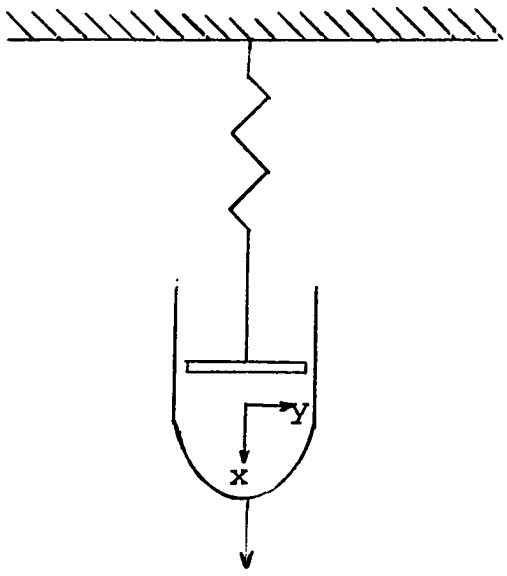

Figure 4. Series combination of spring and dashpot.

Differentiation of Equation 3 with respect to time, t, and setting $\lambda = \eta/G$, gives the operator equation

$$\eta \frac{dD}{dt} = (\lambda \frac{d}{dt} + 1)\ \tau_{yx} \qquad (3a)$$

This equation expresses the deformation of the combination in terms of the applied stress. λ is the relaxation time of the system, the time required for the stress caused by a sudden extension to relax to 1/e of its initial value when the extension is stopped. The first term on the right represents the elastic contribution, and the second term represents the viscous contribution to the stress. By analogy Equation (3a)

expresses the deformation of a Maxwellian viscoelastic fluid, one that expresses both the fluidity of a Newtonian liquid and the elasticity of a Hookean solid. Its applicability is restricted to materials which can be represented by a single viscosity and shear modulus. Polymers and polymer solutions which have a distribution of chain lengths and configurations cannot be expected to obey Equation (3a) in any but a quantitative manner.

In more general terms, Equation (3a)is

$$2\eta\ \dot{\gamma}_{jk} = (\lambda\ \frac{d}{dt} + 1)\ \tau_{jk} \qquad (4)$$

where

$$\dot{\gamma}_{jk} = \frac{1}{2}\left(\frac{\partial v_k}{\partial x_j} + \frac{\partial v_j}{\partial x_k}\right) \quad : \quad j \neq k$$

$v_k = (dx_k)/dt$ is the velocity in the k direction, and v_j is the velocity in the j direction.

If small amplitude oscillatory measurements, with period ω, are made one may assume steady state behavior of τ_{jk} : $\tau_{jk} = (\tau_{jk})_o e^{i\omega t}$. Defining η_o as a viscosity measured at low ω, Equation (4) then becomes

$$\eta_o\ \dot{\gamma}_{jk} = (i\omega\lambda + 1)\ \tau_{jk} \qquad (4a)$$

Defining a complex viscosity η^* to represent this situation gives:

$$\eta^* = \frac{\tau_{jk}}{\dot{\gamma}_{jk}} = \eta_1 - i\eta_2 = \eta_o(i\omega\lambda + 1)^{-1} \qquad (5)$$

Equating the real and imaginary terms of Equation (5) gives

$$\frac{\eta_1}{\eta_o} = \frac{1}{1 + \lambda^2 \omega^2} \tag{6}$$

and

$$\frac{\eta_2}{\eta_o} = \frac{\lambda \omega}{1 + \lambda^2 \omega^2} \tag{7}$$

where η_1 represents the viscous term in η^* and η_2 represents the effect of elasticity, by analogy with Equation (3a). The behavior of η_1/η_2 and η_2/η_o for a given substance can be represented graphically as shown in Figure 5.

Consider the predicted behavior of η_1, the real part of η^*, as a function of $\omega = 2\pi f$ (Equation (6)). At a very low frequency, $\lambda\omega << 1$, $\eta_1 = \eta_o$. The material exhibits a Newtonian viscosity. The viscosity is also independent of frequency as long as ω is very small. Non-Newtonian effects are observed as ω increases ($\lambda\omega \rightarrow 1$). As predicted by Equation (6), η_1 becomes less than η_o and becomes frequency dependent. By definition a Newtonian viscosity is independent of frequency. Therefore, the frequency dependence of η_1 as predicted by Equation (6) and illustrated in Figure 5 suggests non-Newtonian behavior. All Newtonian materials will exhibit viscoelasticity if a high enough frequency is used in the viscosity measuring process. In Figure 6 the qualitative viscosity dependence on frequency (shear rate) is illustrated for several types of liquids.

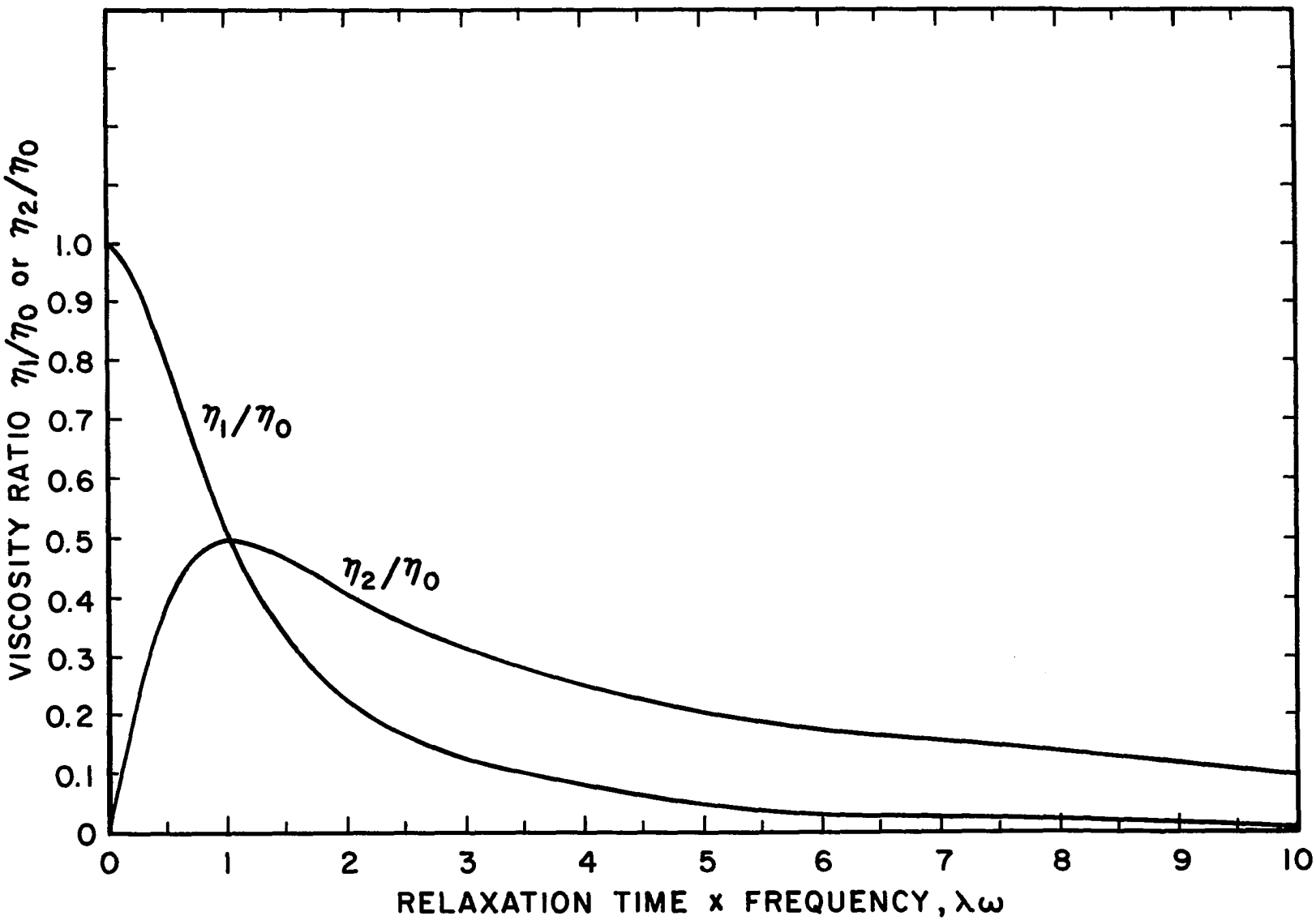

Figure 5. Changes in the Real and Imaginary Parts of the Complex Viscosity, η^*, with the Product of Frequency and Relaxation Time.

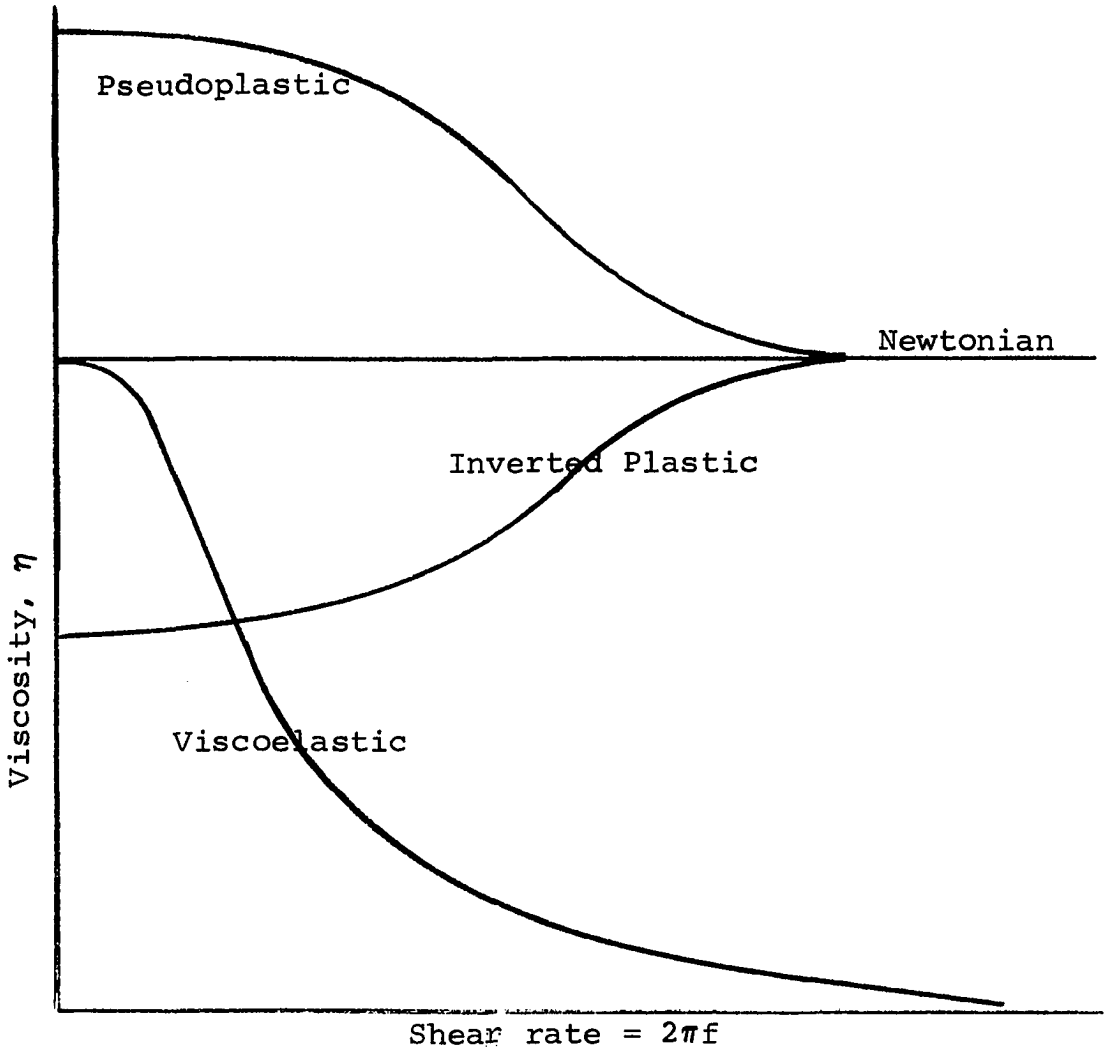

Figure 6. Qualitative Viscosity Dependence on Frequency for Some Common Types of Liquids.

Likewise a Newtonian material exhibits no elasticity. Consider the predicted behavior of η_2 (Equation 7) which represents the elastic contributions of a viscoelastic material. As long as ω is very small $\eta_2 \approx 0$. However, the predicted value of η_2 increases as ω increases as again shown in Figure 5. η_2 reaches a maximum at the relaxation frequency

$\omega = 1/\lambda$. The existence of η_2 further suggests non-Newtonian behavior because Newtonian liquids exhibit no elasticity, $\eta_2 = 0$.

The frequency dependence of η_1 and the existence of η_2 as predicted by Equations (6) and (7) both suggest non-Newtonian behavior and are not observed at low frequencies. However, as ω increases, the frequency dependence of η_1 and the existence of η_2 become apparent, and non-Newtonian behavior results.

As mentioned, this analysis is valid only for a substance which can be represented by a single zero shear rate viscosity and a single relaxation time. A generalized Maxwell model, which is a parallel combination of N springs and N dashpots connected in series and may be more representative of the behavior of polymers is represented by

$$\dot{\gamma}_{jk} \sum_{n=1}^{N} \eta_o(n) = \sum_{n=1}^{N} \lambda_n \frac{d}{dt} (\tau_{jk(n)}) + \sum_{n=1}^{N} \tau_{jk(n)} \qquad (4b)$$

Now a series of relaxation times and a series of zero shear rate viscosities must be considered.

Equations such as Equation (4b) and other more general linear and non-linear equations may help predict the behavior of polymers; but they are overly complicated for substances with relatively simple structures, such as short chain paraffins and simple ring compounds. The development of the two parameter Maxwell model represented by Equation (4a) or Figure 5 should be adequate to describe the behavior of simple compounds.

If Equation (3) instead of Equation (3a) had been used as the basis of the development one would have been led to consider a complex shear modulus

$$G^* = i\omega\eta^* = G_1 + iG_2 \tag{8}$$

instead of a complex viscosity.

$$G_1 = \frac{\eta_o\lambda}{1+\omega^2\lambda^2} \tag{9}$$

and

$$G_2 = \frac{\eta_o\omega^2\lambda}{1+\omega^2\lambda^2}. \tag{10}$$

Occasionally viscoelasticity data are interpreted in terms of G^* instead of η^*.

Pertinent Investigations on Viscoelastic Behavior

Barlow and Lamb (3) investigated the viscoelastic behavior of three different lubricating oils. Spectra of relaxation frequencies were observed because different oils had different compositions and because the oils were mixtures. From analysis of the frequency dependence of $G_1 = i\omega\eta_2$ and the variation in composition of these oils the authors concluded that "the principal contributions of the hydrocarbon types to the relaxation spectrum are, in ascending order of

frequency: tri-aromatics, di-aromatics, mono-aromatics, and saturates." Di-aromatic hydrocarbons were found to have a relaxation frequency of roughly 10^8 cps. (cycles per second); mono-aromatics roughly from 10^9-10^{10} cps.; and saturated hydrocarbons above 10^{11} cps.

Rouse and Sittel (22) investigated viscoelastic behavior of polystyrene solutions in toluene as a function of frequency, polystyrene concentration and polymer molecular weight. The frequency range investigated was 200 cps. to 60 kc. (kilocycles). All data for η_1 as a function of frequency, $\eta_1(f)$, approach the viscosity of toluene at the highest frequency. Therefore, it is apparent that toluene does not possess a relaxation frequency below 60 kc. at 30°C. and atmospheric pressure. If toluene did possess a relaxation frequency near or below 60 kc., η_1 would be less than measured at low shear rates, as quantitatively indicated in Figures 5. η_1 for the solution would then be less than η_1 for toluene. However the data of Rouse and Sittel do not indicate this decrease of η_1, thereby indicating that toluene's shear relaxation frequency must be above 60 kc. in accordance with Barlow's and Lamb's findings.

Harrison, Lamb and Matheson (14) also investigated viscoelastic properties of solutions of polystyrene in toluene. In their experiments, the combined use of temperature as a variable and reduced frequencies extended the range of effective frequencies considerably. Agreement of $\eta_1/\eta_o(f)$ and

$G_1(f)$ with predicted behavior was good for solutions of polystyrene fractions with molecular weights up to 2.39×10^5 gm./mol. For heavier fractions η_1/η_o (f) is below the predicted curve at low frequencies, but it agrees at higher frequencies. $G_1(f)$ is always below the predicted curve for the heavier fractions. Although the authors suggest that this anomalous behavior is caused by temporary association of molecules, the behavior may well be explained if toluene has a shear relaxation time of approximately 10^{-6}-10^{-7} sec., which would correspond to a relaxation frequency of 10^6-10^7 cps. Indeed the authors' data give evidence that toluene does have a relaxation time of 10^{-6}-10^{-7} sec.

A graph of η_1/η_o versus reduced frequency for a 1.53×10^5 gm./mol. fraction has not reached its asymptotic minimum at 1 megacycle, which was the highest frequency measured. At 1 megacycle $\eta_1/\eta_0 \approx 0.4$. $\eta_o = 1.46$ centipoises, (cp), for this solution, therefore $\eta_1 \approx 0.584$ cp. at 1 megacycle. At $30^oC.$, the temperature to which all frequency measurements were reduced, η_o toluene = 0.526 cp. Apparently, the only contribution affecting $\eta_1(f)$ is caused by the polymer relaxation times; for if the frequency were near the frequency associated with a relaxation time for toluene, it would be expected that η_1 would be less than η_o for toluene, as Figure 5 again demonstrates.

However, the magnitude of η_1 associated with the polymer might be large enough to obscure changes in $\eta_1(f)$ associated with toluene. In this case, experimental $\eta_1/\eta_o(f)$

and G_1 (f) curves would be expected to obey the theoretical curves which were based on relaxation of only the polymer. If the polymer relaxation frequencies could be shifted to lower frequencies, a relaxation frequency of toluene might then be observed.

Shifting the relaxation frequencies of the polymer to lower frequencies may be accomplished by using a higher molecular weight fraction of the polymer. Then the polymer relaxation processes may not overshadow a relaxation frequency of toluene. Indeed a relaxation frequency is revealed when solutions of higher molecular weight fractions of polymer are investigated. η_1/η_o versus reduced frequency for a 3.64×10^5 gm./mol. fraction has almost approached its axymtotic minimum at 1 megacycle. At this frequency, $\eta_1/\eta_o \approx 0.25$. $\eta_o = 1.49$ cp. Therefore $\eta_1 \approx 0.372$ cp. A viscosity of 0.372 cp. is even less than the viscosity of the solvent toluene, indicating that reduced frequency is approaching a value corresponding to the relaxation frequency of toluene. Because not only the polymer but also toluene is exhibiting some shear relaxation at 1 megacycle, it may be expected that solutions of 3.64×10^5 gm./mol. and higher molecular weight polystyrene fractions in toluene will not agree with curves of η_1/η_o (f) and G_1 (f) based on relaxation of only the polystyrene.

Therefore, from this data it can be concluded that toluene has a shear relaxation time of about 10^{-6}-10^{-7} sec. and that the relaxation effect of toluene in lower molecular

weight fractions is overshadowed by the magnitude of η_1 for the polymer. The deviation of experimental data from predicted curves for higher molecular weight polymer fractions might be explained by the shear relaxation of toluene.

Spriggs and Bird (25) analyzed data for 5% polyisobutylene in Decalin taken by DeWitt et al. (10) in terms of a generalized, non-linear viscoelastic model. The experimental curve of η_1/η_o versus frequency agreed well with that predicted by the model. The agreement of η_2/η_o with the predicted curve is not as good. Because the highest frequency used was about 400 cps., and because Decalin probably will not have a relaxation frequency below 10^8 cps., no relaxation effects attributable to Decalin were observed.

Reiner (21) believes to have found a viscoelastic effect in toluene. The essential parts of the apparatus are shown schematically in Figure 7. When the rotor was rotated at velocities $60 \leq \Omega \leq 260$ rad./sec. an axial force was required to maintain the original separation of the rotor and stator. Reiner postulates that this force is to balance a cross stress, which is related to a cross viscosity by

$$\tau_{zz} = \tau_{rr} - \tau_{\theta\theta} = \eta_c \dot{\gamma}^2 \qquad (11)$$

Equation (11) involves a non-linear relation between stress and shear rate, which Reiner represents by

$$\tau_{ij} = -p\delta_{ij} + \frac{r\Omega}{d} \begin{Vmatrix} 0 & 0 & 0 \\ 0 & \frac{\eta_c r\Omega}{d} & \eta \\ 0 & \eta & \frac{\eta_c r\Omega}{d} \end{Vmatrix} \qquad (12)$$

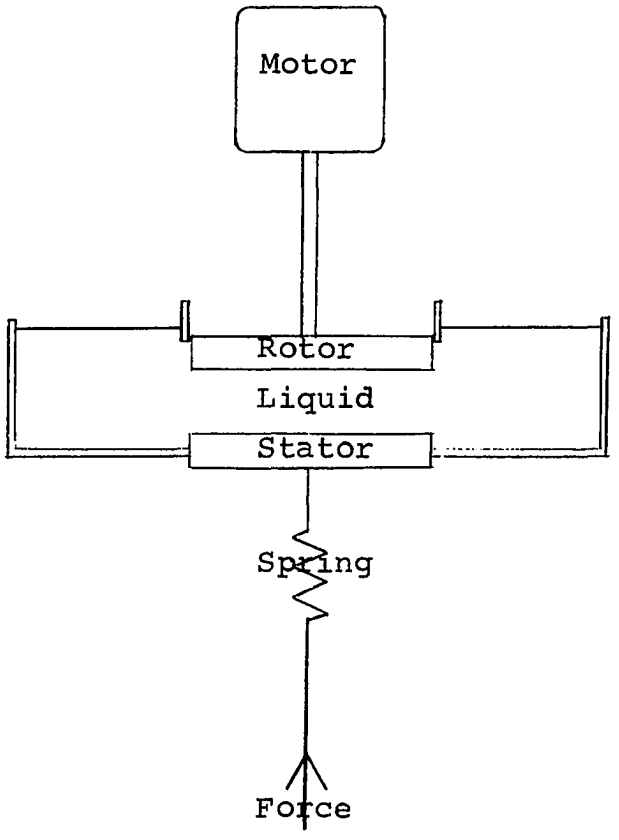

Figure 7. Schematic diagram of the apparatus Reiner used to investigate viscoelastic effects in toluene.

where d is the separation between the rotor and stator. Reiner found $\eta_c = -2 \times 10^{-7}$ sec. poise; a Maxwellian relaxation time of $2\text{-}3 \times 10^{-5}$ sec.; and calculated a shear modulus $G = 2 \times 10^2$ dyne/cm.^{2}. Although a non-linear relation between stress and

shear rate is required to interpret the results, Reiner claims that this experiment gives evidence of viscoelasticity in toluene.

High Pressure Viscosity Measuring Techniques

The most common viscometers used for high pressure viscosity measurements on liquids are those in which the time of fall for a weight is related to viscosity. These viscometers are known as falling weight and rolling ball viscometers. However, these viscometers do not lend themselves to investigations of viscoelastic phenomena because the range of available shear rates is much too low. Consider Bridgman's (4) falling weight viscometer for example. The time required for the weight to fall usually was 5-10 seconds; the distance of fall was 3 cm.; and the distance from the weight to the cylinder wall was about 0.05 cm. Therefore, a rough estimate of the shear rate existing during his experiments can be obtained.

$$\dot{\gamma} = \frac{\Delta}{\Delta y}\frac{\Delta \ell}{\Delta t} = \frac{3 \text{ cm.}}{5\text{-}10 \text{ sec.}} / .05 \text{ cm.} = 6\text{-}12 \text{ sec.}^{-1}$$

Using a Maxwellian relaxation time $\lambda = \eta/G$, a 100-fold increase in relaxation time may be expected at pressures of approximately 10 kiloatmospheres (katm.) if any increase in G is neglected. A 100-fold increase in relaxation time is expected because viscosities often increase 100 fold in the pressure range, atmospheric to 10 katm. Therefore, using the data of Barlow and Lamb as a guide, relaxation times on

the order of 10^{-7} to 10^{-8} sec. might be expected for monoaromatic hydrocarbons at 10 katm. Clearly, the condition $\lambda\dot{\gamma} \rightarrow 1$ cannot be obtained with the falling weight viscometer, even at high pressure, so it is not suited to investigations of viscoelastic phenomena in simple hydrocarbons. Instead data from this type of instrument give the low shear rate viscosity $\eta_o(P)$ which appears in the Maxwell theory of a viscoelastic substance, which indeed is the data for which the instrument was designed.

The torsionally oscillating crystal viscometer introduced by Mason (16), modified and further explained by Rouse et al. (23), and used by Philippoff (20), Rouse and Sittel (22) and Harrison et al. (14) is particularly adaptable to investigating viscoelastic phenomena at high pressure although its use is limited to substances with low conductivity. The crystals commonly used have resonant frequencies from 20 kc. to 100 kc., which are equivalent to shear rates of 1.25×10^5 to 6.25×10^5 sec.$^{-1}$.

The simplicity of the viscometer is beneficial for high pressure work.

A quartz rod oriented as shown in Figure 8 has been shown to oscillate in a torsional mode (11). Although there is coupling to a lengthwise mode, the lengthwise mode of oscillation is neglible if the length to diameter ratio of the crystal is at least 10/1 (17). The frequency of torsional oscillation for such a rod is

$$f = \frac{1}{2\ell}\sqrt{\frac{c_{66}}{\rho_c}} \qquad (13)$$

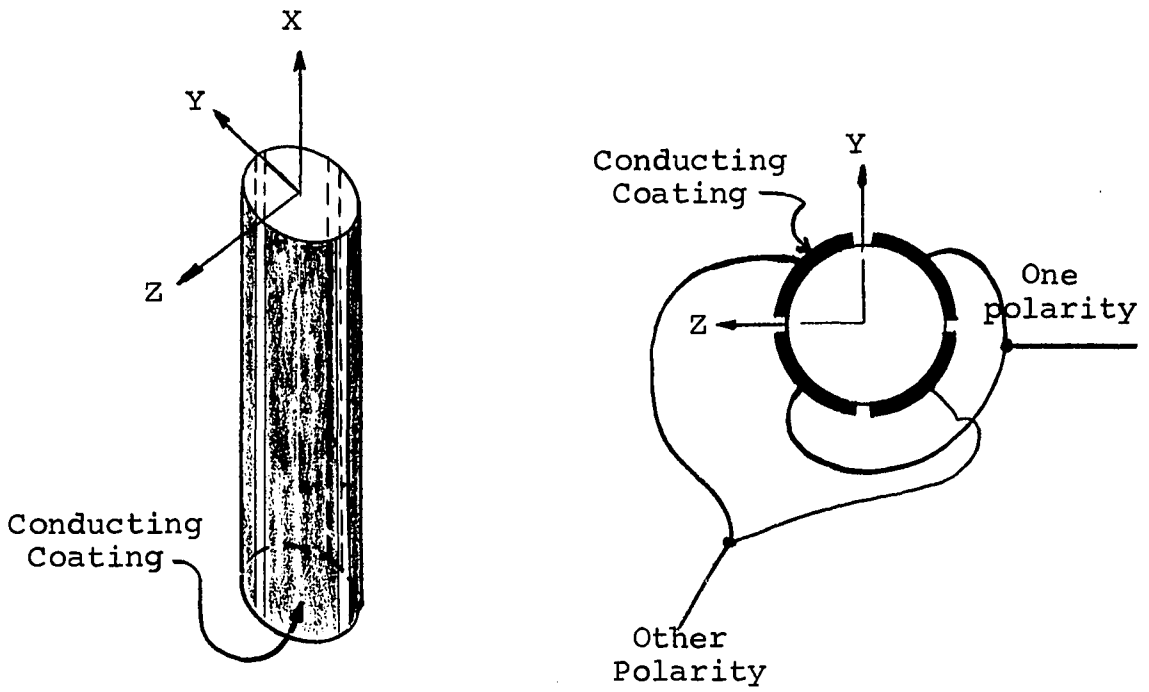

Figure 8. Orientation of quartz rod necessary to get torsional oscillation (X, Y, and Z are quartz crystallographic directions).

where ℓ is the length of the rod, ρ_c is its density, and c_{66} is the elastic shear modulus for displacement in the Y direction with respect to X. $c_{66} = 40.5 \times 10^{10}$ dyne/cm.^{2} for quartz (18).

Consider the motion in a liquid of viscosity η and density ρ caused by such a torsionally oscillating rod. The motion is everywhere tangent to the surface of the rod and shears the liquid adjacent to the surface with respect to the liquid removed from the surface. This shearing motion sets

up a transverse wave which propagates radially from the crystal surface. Using the cylindrical coordinates r,θ and z and assuming that v_θ, the tangential velocity, is independent of θ, the displacement in the tangential direction; Newton's law of viscosity is:

$$\tau_{r\theta} = -\eta \frac{dv_\theta}{dr} \qquad (1a)$$

Assuming no liquid motion in the z direction, the equation of motion in the liquid is

$$\rho \frac{\partial v_\theta}{\partial t} = -\frac{1}{r} \frac{\partial}{\partial r} \left(r\tau_{r\theta} \right) = \frac{\eta}{r} \frac{\partial}{\partial r} \left(r \frac{\partial v_\theta}{\partial r} \right) . \qquad (14)$$

The equation of motion is applicable for $a \leq r \leq \infty$ where a is the radius of the quartz crystal. Assuming that the motion of the liquid will be periodic in time gives $v_\theta(r,t) = v_\theta(r)e^{i\omega t}$, and Equation (14) becomes

$$\frac{d^2v_\theta}{dr^2} + \frac{1}{r}\frac{dv_\theta}{dr} - \frac{i\omega\rho}{\eta} v_\theta = 0 = r^2 \frac{d^2v_\theta}{dr^2} + r\frac{dv_\theta}{dr} - r^2q^2v_\theta \qquad (14a)$$

where $q^2 = i\omega\rho/\eta$. The boundary conditions applicable to Equation (14a) are $v_\theta(a,t) = v_o e^{i\omega t}$, and $v_\theta(\infty,t)$ must remain finite. $\omega = 2\pi f$ is equivalent to the shear rate $\dot{\gamma}$. Equation (14a) is a modified Bessel's equation of zero order. A solution to Equation (14a), subject to the boundary conditions, is

$$v_\theta(r,t) = [v_o e^{i\omega t} K_o(qr)]/K_o(qa). \tag{14b}$$

Using the approximation $K_o(x) \sim \frac{\pi e^{-x}}{2x}$ applicable for large values of x, an approximate solution to Equation (14a) is

$$v_\theta(r,t) = v_o e^{i\omega t} e^{-q(r-a)} \tag{14c}$$

A mechanical impedance, analogous to an electrical impedance is defined by

$$Z_M = R_M + iX_M = \tau_{r\theta}/v_\theta \tag{15}$$

where the subscript M denotes a mechanical impedance, resistance or reactance. Using the relation between $\tau_{r\theta}$ and v_θ given by Equation (1a), obtaining dv_θ/dr from Equation (14c) and substituting for $\tau_{r\theta}$ and v_θ into Equation (15) gives

$$Z_M = i\omega\rho\eta \tag{16}$$

where η possess a real and imaginary part. Recalling the definition of a complex viscosity in relation to a Maxwell viscoelastic liquid, Equation (5), Equation (16) gives

$$\eta^* = \eta_1 - i\eta_2 = (Z_M)^2/i\omega\rho \tag{17}$$

Equating the real and imaginary parts of Equation (17) and using the definition of Z_M gives

$$\eta_1 = (2X_M R_M)/\omega \rho \qquad (18)$$

and

$$\eta_2 = (R_M^2 - X_M^2)/\omega \rho. \qquad (19)$$

Mason (16) showed that R_M and X_M could be related to the resonant frequency of the crystal and its resistance at resonance by

$$R_M = (R_E - R_{Eo})/ K_r \qquad (20)$$

and

$$X_M = (f_o - f)/ K_f. \qquad (21)$$

K_r and K_f are crystal constants. R_E is the electrical resistance of the crystal at resonance in a liquid, and R_{Eo} is the electrical resistance of the crystal at resonance in air. Likewise, f is the resonant frequency of the crystal in a liquid, and f_o is the resonant frequency of the crystal in air. R_E and f of an oscillating crystal can be measured with an impedance bridge and an electronic frequency counter.

An oscillating crystal can be represented by a series RLC combination in parallel with a capacitor C_o (see Figure 9a).

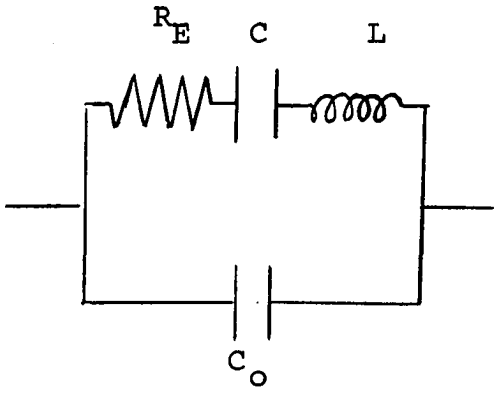

Figure 9a. Electrical representation of an oscillating crystal.

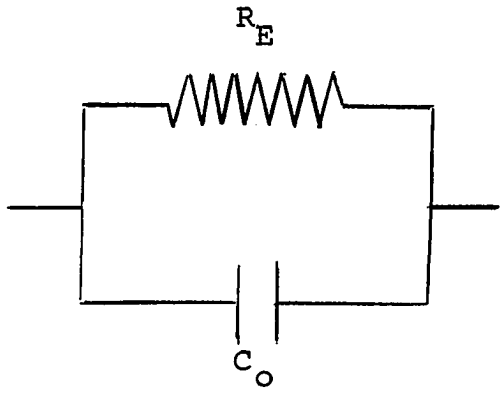

Figure 9b. Electrical representation of an oscillating crystal at resonance.

The combination RLC represents the frequency dependence of the crystal. The static capacitance of the crystal, capacitance between leads from the crystal to the impedance bridge and capacitance across the divisions between electrodes on the crystal are all combined in the term C_o.

At resonance the reactances X_L and X_C cancel, and the current through the crystal is a maximum. Thus, the resonant frequency can be determined by measuring the crystal conductance, with an impedance bridge, as a function of frequency. The frequency at which the conductance is maximum is the resonant frequency. At resonance, the crystal can be represented as in Figure 9b, where the reactances X_L and X_C are cancelled. Thus the resistance of the crystal at resonance, R_E, will be the minimum resistance, which corresponds to the

maximum conductance, measured by an impedance bridge which measures parallel R and C combinations. At resonance the resistance of this parallel combination (Figure 9b) is equal to the resistance R_E of the crystal.

K_f and K_r, which are needed to relate R_E to R_M and f to X_M by Equations (18) and (19), can be readily obtained from calibration measurements with Newtonian liquids of known η and ρ. For Newtonian liquids $\eta_2 = 0$ and $R_M = X_M$. Then, combination of Equations (18) and (20) gives

$$R_E = R_{Eo} + K_r \sqrt{\omega \rho \eta / 2} \tag{22}$$

Similarly, combination of Equations (19) and (21) gives

$$f = f_o - K_f \sqrt{\omega \rho \eta / 2} \tag{23}$$

Thus, a graph of R_E versus $\sqrt{\omega \rho \eta / 2}$ will give a straight line with intercept R_{Eo} and slope K_r. Likewise, a graph of f versus $\sqrt{\omega \rho \eta / 2}$ will give a straight line with intercept f_o and slope K_f. Having obtained the constants, Equations (18) and (20) may be used to calculate η_1 for liquids of unknown viscosity. Likewise, Equations (19) and (21) may be used to calculate η_2 after obtaining the appropriate constants.

K_f and K_r are theoretically related to physical and electrical properties of the crystal by

$$K_f = \frac{1}{\pi \rho_c} \left[\frac{1}{r} + \frac{1}{\ell}\right] \tag{24}$$

and

$$K_r = 4\pi L_c K_f, \tag{25}$$

where:

ρ_c = density of crystal

r = radius of crystal

ℓ = length of crystal

L_c = inductance of crystal

as given by Appeldoorn et al. (1).

High Pressure Phenomena

Bridgman (4) (5) investigated the viscosities of many pure liquids as a function of pressure by measuring the time required for a weight to fall through the liquid while under pressure. Because the shear rate was very low in his experiments, Bridgman's measurements give η_o as a function of pressure.

Figure 10 shows the viscosity dependence on pressure for the liquids he investigated. Curve A, with log η always concave towards the pressure axis is common. However, the behavior shown by curve B, in which log η versus pressure becomes convex to the pressure axis at high pressure may be the general case. In the later investigation (5) which

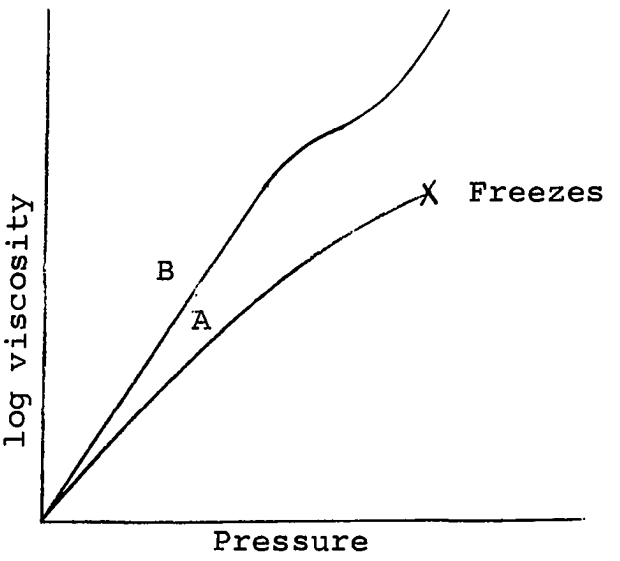

Figure 10. Typical changes of viscosity with pressure.

measured viscosities at pressures to about 29 katm. all fluids that did not freeze exhibited the reverse curvature.

For most of the simple compounds investigated the viscosity increased about 100 fold as pressure was increased from atmospheric to 10 katm. In the pressure range atmospheric to 29 katm. the viscosity of simple compounds increased 400 to 700 fold. For instance, the viscosity of iso-pentane at 29 katm. is 493 times its viscosity at atmospheric pressure of 0.198 cp. at 30°C. Thus, using a Maxwellian relaxation time, $\lambda = \eta/G$ for iso-pentane, increases in relaxation time of the order of 490 fold above atmospheric relaxation times may be expected at 29 katm. if changes in the shear modulus with pressure are neglected.

Babb and Scott (2) have measured the viscosity of several simple hydrocarbons to pressures of about 8-10 katm., using a rolling ball viscometer. The viscosity versus pressure curves are all of the type represented by curve A in Figure 8.

Philippoff (20) and Appeldoorn et al (1) investigated viscoelastic effects in hydrocarbons and polymer blends up to 15,000 psi. They found that the hydrocarbons exhibited no viscoelasticity in this pressure range. The effect of pressure on the polymer blends (9.5% polyalkylmethacrylate in a 33 cp. paraffinic base oil) was to increase both η_1 and η_2. The ratio η_2/η_1 decreased with increasing pressure, indicating a relative decrease in elastic effects as pressure increased. The decrease in η_2/η_1 with pressure is unexpected and is not observed in pure polymers, concentrated polymer solutions, or polymer solutions in very low viscosity solvents. As would be expected, both η_1 and η_2 decreased with increasing frequency (See Figure 5 for $\omega\lambda > 1$). Unexpectedly, η_1 does not appear to approach the solvent viscosity at high frequencies.

Michels and Perez (19) report that increasing pressure changes the resonant frequency of AT and BT cut quartz crystals.* For the AT cut crystal, with a resonant frequency of 942 kc. at atmospheric pressure, the change in frequency with pressure is approximately $\frac{1}{f}\left[\frac{\Delta f}{\Delta P}\right] = 8.03 \times 10^{-6}$ cm.^{2}/kg. For the BT cut

---

*The geometrical configuration resulting from cutting crystals in various manners are designated by convention as AT-, BT-, etc. cuts. (Consult Ref. 17)

crystal, f_o = 6040 kc., $\frac{1}{f}\left[\frac{\Delta f}{\Delta P}\right] = -2.03 \times 10^{-6}$ cm.^{2}/kg. Measurements were taken at pressures up to 0.97 katm.

Philippoff (20) reported no noticeable change in resonant frequency of a torsionally oscillating quartz rod for pressures up to 15,000 psi.

Philippoff (20) also shows that the viscosity of dilute polymer solutions may be represented in terms of reduced temperature, pressure and frequency variables. The effect of increasing temperature is the same as decreasing pressure or frequency; or vice versa. Increasing temperature, decreasing pressure and decreasing frequency all decrease the reduced frequency. Use of a reduced frequency allows correlations of measurements at one frequency and various temperatures and pressures to cover effectively a range of frequencies reduced to a reference temperature and pressure. The reduced variables are:

$$f_r = (f_{meas.})(a_{TP})$$

$$a_{TP} = \left[\frac{T_o\rho_o}{T\rho_{TP}}\right]\left[\frac{\eta_T}{\eta_o}\right]\left[\frac{\eta_P}{\eta_o}\right] \qquad (26)$$

$$\eta_{1r} = \eta_1 \left(\frac{\eta_o}{\eta_T}\right)_P \left(\frac{\eta_o}{\eta_P}\right)_T$$

$$\eta_{2r} = \eta_2 \frac{T_o\rho_o}{T\rho}$$

The subscripts T and P refer to the absolute temperature and pressure of the measurements. The subscript o refers to the conditions at the reference temperature and pressure. η_T and

η_p are low shear rate viscosities. Philippoff observed that $(\eta_{solution})/(\eta_{solvent}) = \eta_{rel.}$ is independent of pressure. Therefore, the effect of pressure on the solution viscosity could be replaced by the pressure effect on the solvent viscosity.

CHAPTER II

EXPERIMENTAL EQUIPMENT AND PROCEDURE

The most critical aspects of the experimental work were the preparation and mounting of the crystals and the design of the electronic measuring system. The high pressure system used in these studies had previously been developed by Professor S. E. Babb.

Preparation of Quartz Crystals

Quartz rods, with their axes parallel to the X crystal direction were purchased from P. R. Hoffman Company. The Y crystal axis was also indicated on the crystals. The crystal dimensions and approximate fundamental frequencies were:

0.375 ± 0.001 inch diameter x 1.300 ± 0.001 inch long - 60 kc.

0.375 ± 0.001 inch diameter x 3.875 ± 0.001 inch long - 20 kc.

While it is suggested that a length/diameter ratio of 10/1 is desirable to eliminate longitudinal motion of the crystal (17), Appeldoorn et al. (1) mention that high viscosities can be measured more accurately with the 60-kc crystal, and no adverse effects caused by longitudinal loading are encountered if the above dimensions are used.

The final preparations of these crystals for use as viscometers followed the suggestions of Greenidge (12). They are as follows:

(1) Final dimensions were obtained by grinding with #600 abrasive. This work was performed by P. R. Hoffman Company.

(2) Orientation of the Z crystal axis was checked by examination between crossed polarized lens as suggested by Cady (9).

(3) The crystals were etched 12-15 minutes in agitated 48% hydroflouric acid, rinsed in distilled water and dried. This step removed any loose quartz dust that might have been left from the machining operations and provided a uniform surface. Etching has been found to improve the efficiency and stability of crystals greatly.

(4) The crystals were cleaned for about 1 hour in boiling aqua regia, rinsed with distilled water and dried in air. This process removed any foreign particles, grease or fingerprints from the surfaces.

(5) A narrow ring of silver paint (a suspension of metallic silver with a borosilicate filler in xylene solvent) was applied midway between the ends of the crystal, where the crystal would be held by the mounting. This ring of paint put a thicker coating on the crystal than was obtained by the subsequent evaporation process and thus protected the evaporated coating from harmful scratches in this vulnerable area.

(6) A conductive silver film was evaporated onto the cylindrical surface of the crystal. For this operation the crystal was mounted in a motor-driven, rotating, vice-like device shown in Figure 11. It was then placed in a vacuum evaporation unit and the evaporation was carried out. The

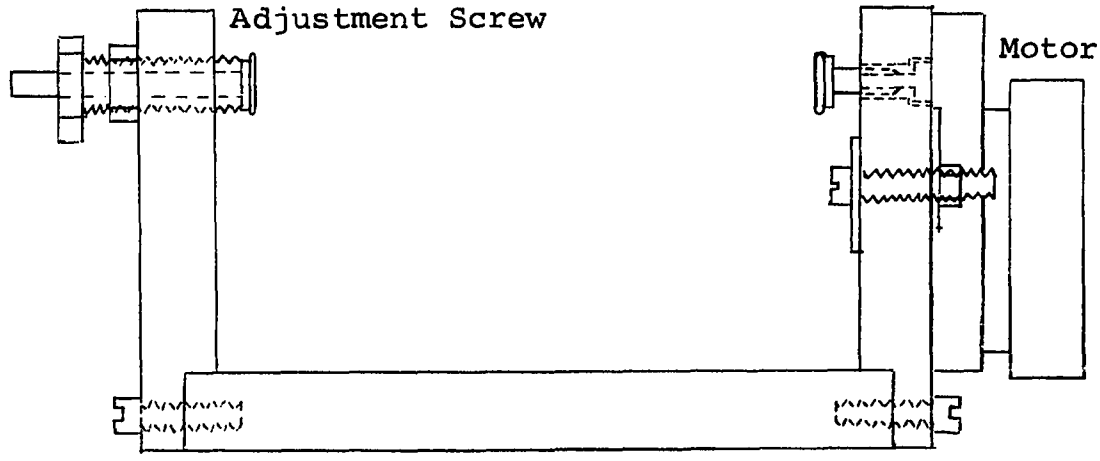

Figure 11. Motor driven crystal holder for silver evaporation.

motor rotated the crystal at ½ RPM.

(7) Finally the silver film was divided to obtain four separated electrodes, oriented as shown in Figure 8. Division of the silver film was accomplished by scraping the film off of the crystal with a piece of abrasive material. Although this scraping did mar the crystal surface, the damage was very slight and did not affect the performance of the crystal. Electrical isolation of the electrodes was tested with an ohmmeter. The resistance between electrodes was at least 100 megohms.

Electronic Equipment and the Impedance Bridge

Figure 12 indicates the electrical components used to determine the resonant frequency and resistance. The oscillator was a Hewlett-Packard Model #200CD with a frequency range of 5 cps. to 600 kc. The frequency counter was a Hewlett-Packard Model #521G which could be used up to 1.2 Mc. The counter was precise to ± 1 cps. in the range used.

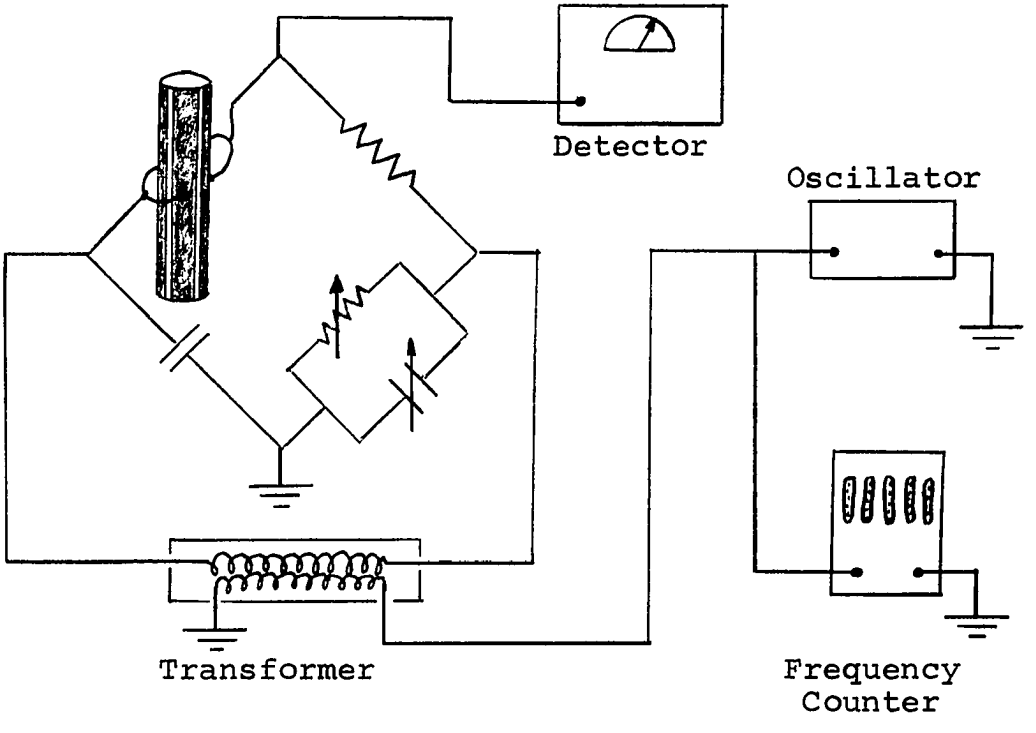

Figure 12. Electrical components used in determining the resonant frequency and resistance.

Philippoff (20) and Appeldoorn et al. (1) used a Wien type bridge to determine the electrical properties of the crystal, which are then related to the complex viscosity η^* by Equations (16) and (17). Barlow and Lamb (3) used a Wayne-Kerr Type B601 bridge. Other commercially available bridges

either do not cover the desired frequency range or do not give sufficient accuracy to allow their use in this type of determination. Therefore, an impedance bridge was constructed from available components. Both a Wien and a Schering circuit were constructed; the Schering circuit was selected after experimentation because greater accuracy was obtainable with it. The bridge circuit, with electric shielding and important residual capacitances, is shown in Figure 13. R and C represent the unknown resistance and capacitance.

It will be noted that in the Schering circuit of Figure 13 the combination RC is in series whereas in Figure 9b the combination $R_E C_o$ is in parallel. To convert from the measurements obtained from the series combination to the desired values representing the physical situation in the viscometer, wherein the combination is parallel, the following equations apply:

$$R_E = \frac{R^2 + (1/\omega C)^2}{R} = \frac{1}{G_E} \tag{27}$$

also

$$C_o = \omega^{-1} \left(\frac{\frac{1}{\omega C}}{R^2 + (\frac{1}{\omega C})^2} \right) \tag{28}$$

where R and C are measured by the impedance bridge.

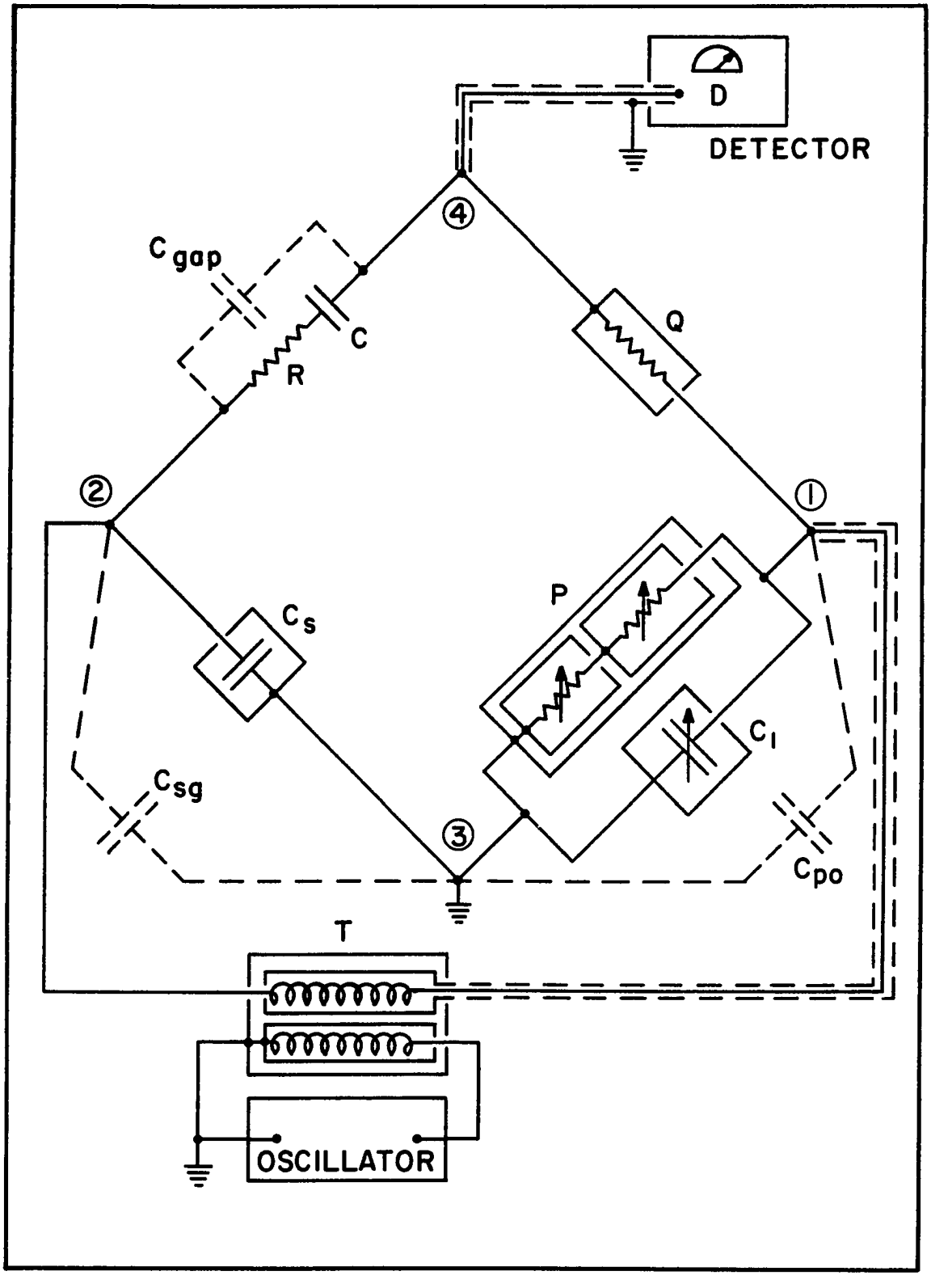

Figure 13. Details of the Impedance Bridge

The balance equations give R and C in terms of the other circuit elements.

$$R = (C_1/C_s)\ Q$$
$$C = (P/Q)\ C_s \qquad (29)$$

Notice that if C_1 and P are chosen as the adjustable circuit elements, as they were, the R and C balances are independent of each other. The balance equations (29) are modified by the presence of the circuit residuals: C_{po}, C_{sg} and C_{gap} shown in Figure 11. The circuit elements are arranged so that the effects of C_{po} and C_{sg} are easily accounted for. C_{po}, the capacitance of point 1 to ground is effectively in parallel with the variable capacitor C_1. Thus the effective value of C_1 for measurements is $C_{1eff} = C_1 + C_{po}$. Similarly, C_{sg}, which includes the inter-shield capacitances of the transformer, shunts C_S and $C_{Seff} = C_S + C_{sg}$. C_{gap} accounts for the capacitance between the leads from the crystal to the impedance bridge and the capacitance caused by connecting these leads to the crystal and to the bridge. As mentioned in the Introduction, the effect of C_{gap} is included in C_o, which is a quantity being measured by the impedance bridge, and thus it does not introduce error into the balance equations when measurements are being made on the crystal.

The values of C_{po} and C_{sg} are obtained by using a resistor and capacitor with known values in the RC arm of the bridge

and balancing the bridge. If the known values of R and C are chosen so that R/X is small, the effect of C_{gap} is negligible. Upon rearrangement, and with C_{leff} replacing C_l and C_{Seff} replacing C_S, the balance equations become:

$$C_{po} = R(C_S + C_{sg})/Q - C_l$$

$$C_{sg} = (Q/P)C - C_S \qquad (29a)$$

The values of C_{po} and C_{sg} thus may be obtained from Equations (29a) if R and C are known. After C_{po} and C_{sg} have been determined, Equations (29) may be used to calculate unknown values of R and C; by replacing C_l with C_{leff} and replacing C_S with C_{Seff}.

The effect of shielding is to make indeterminate capacitances from the circuit elements to ground constant. The circuit elements were shielded as suggested by Hague (13) and (15). The connections to the shields are such that in most cases the current through the residual capacitance to ground actually flows to a grounded part of the circuit, thereby leading to the least possible inaccuracy in measurement. The circuit elements were kept as far apart as possible to minimize coupling between elements.

Table 1 gives details about the circuit elements.

TABLE 1

DESCRIPTION OF CIRCUIT ELEMENTS OF

THE IMPEDANCE BRIDGE

Element	Description
P*	Series combination of (a) 1Ω to 11.11 kΩ precision resistor in 1Ω steps, and (b)* 1kΩ to 1.1 megΩ ± 1% in 10 kΩ steps where Ω is in ohms, kΩ is kilo ohms and megΩ is megohms
Q**	10kΩ to 1.1megΩ ± 1% in 10kΩ steps
C_S**	0μμf to 1100 μμf ± 1% in 100 μμf steps
C_1	General Radio precision variable air capacitor; 50 μμf to 4100 μμf continuous
D***	General Radio 1232-A Tuned Amplifier and Null Detector. Maximum sensitivity of 2 μV/full scale at 20 kc and 6 μV/full scale at 60 kc
T	General Radio 578-C Shielded Transformer, for use in the range 2 kc to 500 kc

Notes *Resistor in part (b) of this combination rarely used.

**This element used only as a range switch.

***It was possible to use a filter in the 20 kc range but not in the 60 kc range with this detector.

In order to determine the accuracy of the measurements obtained from the impedance bridge of Figure 13, several resistors and capacitors, whose resistances and capacitances were determined by a precision circuit, were installed in the arm ② - ④ of Figure 13. The readings of P and C_1 (Figure 13) were converted to R and C by Equations (29), and these values were then

compared with those previously obtained. It was found that the discrepancies between the two sets of readings correlated best with the ratio R/X_C, the resistance divided by the reactance of the capacitor. These errors are reported as percentages in Table 2.

TABLE 2

AVERAGE ERROR IN ELECTRICAL RESISTANCE MEASUREMENTS

20 kc		60 kc	
R/X_C	Average Error	R/X_C	Average Error
125	+1.8%	8.5	+2.7%
39.8	-1.3%	6.2	+2.8%
19.6	-2.1%	0.40	-3.5%
6.00	-3.6%	0.10	-20.6%*
0.013	-4.6%		

*Obtained after high pressure measurements were completed.

Experimental Procedure

After the crystals had been prepared as previously described, the following steps were taken with each crystal to obtain the data necessary for viscosity calculations.

(1) The crystal was mounted in a crystal holder and the holder screwed onto the snout of a closure for the high pressure cell, as shown in Figure 14. An O-ring was used to keep the crystal securely mounted. Rough calibration curves

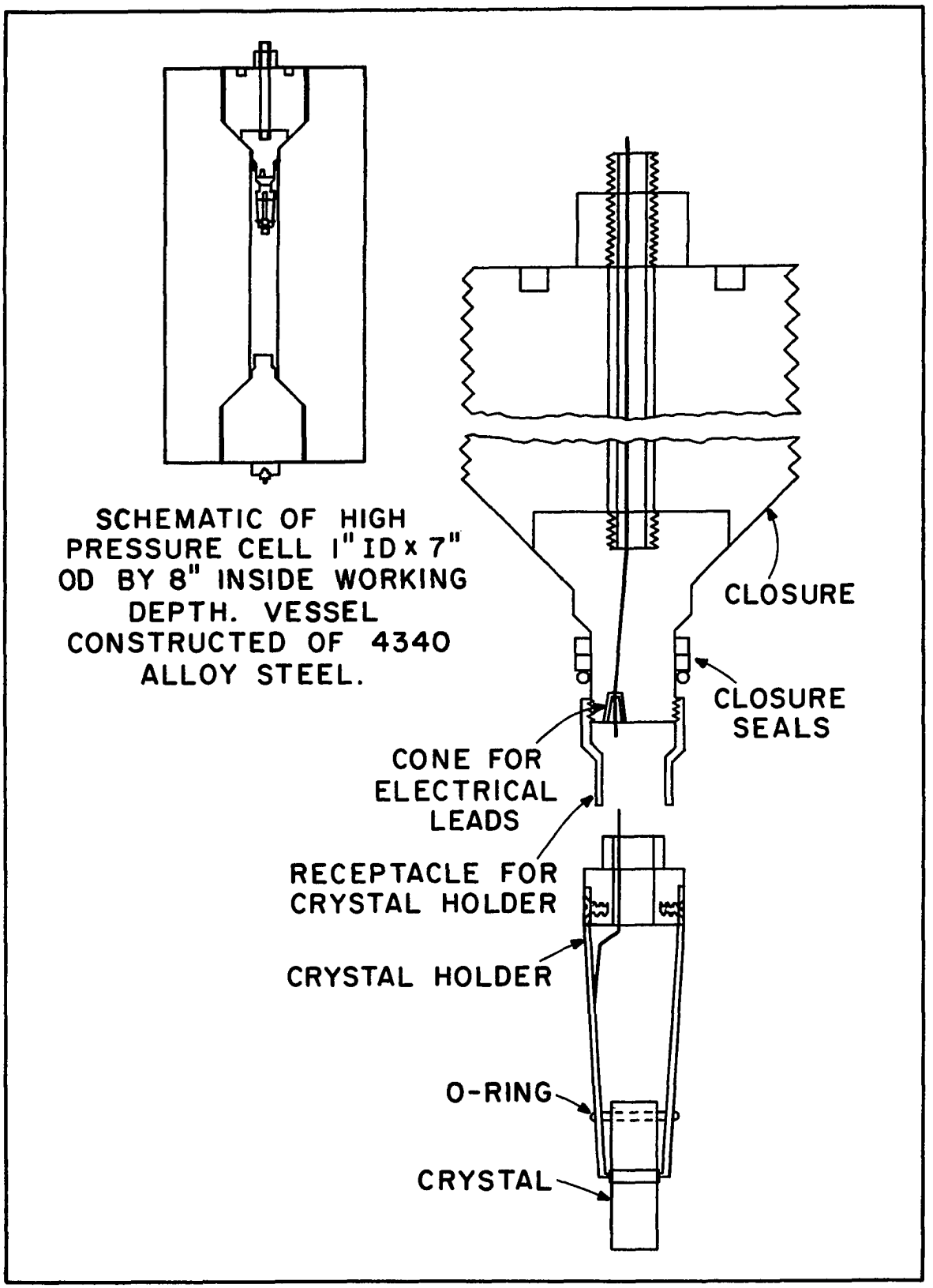

Figure 14. Cross Section of the High Pressure Closure and Crystal Holder.

of R_E versus $\sqrt{\omega \rho \eta/2}$ and f versus $\sqrt{\omega \rho \eta/2}$ were obtained from several liquids with known ρ and η.

All determinations of resonant frequency were made by using the impedance bridge to measure R and C as functions of frequency. R_E as a function of frequency was then calculated by using Equation (20). The frequency at which R_E was a minimum was taken as the resonant frequency. As indicated by Equation (27) the minimum R_E is equivalent to the maximum conductance, G_E. The resistance used for the calibration curve, R_E versus $\sqrt{\rho \omega \eta/2}$ was R_E at the resonant frequency.

The crystal was adjusted in the mounting until R_E versus $\sqrt{\rho \omega \eta/2}$ and f versus $\sqrt{\rho \omega \eta/2}$ were linear, and until R_{Eo} was a minimum. When these calibration curves were linear, it was assumed that coupling of the torsional mode to other modes of oscillation was negligible. This assumption is reasonable because Equations (22) and (23) which resulted from considering only torsional motion predicts this linear dependence. Other modes of oscillation will result in R_E versus $\sqrt{\rho \omega \eta/2}$ or f versus $\sqrt{\rho \omega \eta/2}$ being non-linear.

The crystal was adjusted in its mounting to obtain a minimum R_{Eo} in order to obtain the highest possible Q for the mounted crystal. The crystal can be treated as a series RLC circuit, for which $Q = X/R_E$ at resonance. Q is indicative of the sharpness of the $R_E(f)$ curve, and X is the reactance of either L or C. In a given fluid, air for instance, adjusting the crystal in its mounting for a minimum R_{Eo} is equivalent to adjusting for a maximum Q and maximum conductance at resonance.

A mounted crystal with a high Q is desirable because Q decreases considerably as $\rho\eta$ increases, thereby decreasing the sharpness of the $R_E(f)$ curve and increasing the uncertainty in obtaining the minimum of the $R_E(f)$ curve, which occurs at the resonant frequency.

(2) After rough calibration indicated linearity of the calibration curves and the minimum R_{Eo}, the crystal was soldered in the mounting with an Indium alloy solder. The solder joints insured good electrical contact between the mounting arms and the crystal at high pressures. A final calibration in fluids of known ρ and η was then performed.

(3) The crystal was inserted in the high pressure cell and the resonant frequency and resistance in air again checked. If the resonant frequency and resistance measured in air in the cell did not agree with the values obtained in step 2, the crystal was removed from the cell and the calibration procedure repeated. After R_{Eo} and f_o values were obtained in the cell which agreed with those obtained from out of cell measurements, the liquid whose viscosity was to be investigated was introduced into the cell from the liquid reservoir. A flow diagram of the high pressure apparatus is given in Figure 15.

Preliminary pressurization of the cell was obtained after isolating the air pump and the hand pump designated "high pressure" in Figure 15 from the rest of the system. Sufficient liquid could be pumped into the cell with the hand pump designated "low pressure" to bring the pressure in the cell to about 1 katm. After the necessary measurements of frequency (f)

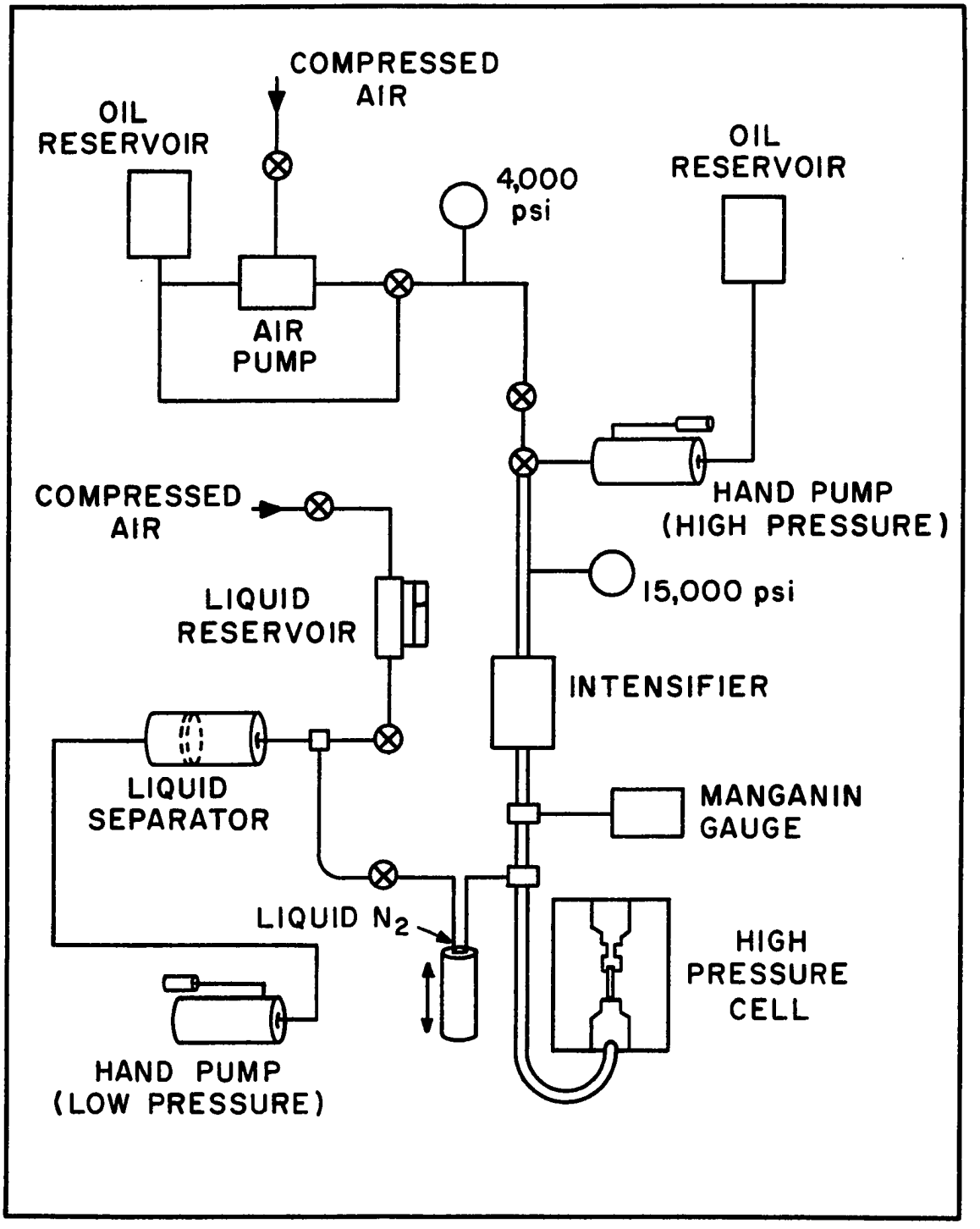

Figure 15. High Pressure Flow Diagram

and resistance (R_E) were obtained in the pressure range, atmospheric to about 1 katm., the low pressure end of the flow diagram was isolated by closing the frozen valve.* Further pressure in the cell was obtained by driving the intensifier piston down with either the air pump or the "high pressure" hand pump. Pressure in the cell could then be lessened by allowing the pressure in the cell to drive the intensifier piston back up. Thus pressure in the cell was increased or decreased by either driving the intensifier piston down with the air pump or hand pump, or by driving it up with the pressure of the liquid in the cell.

Measurements were made to determine the resonant frequency and resistance of the crystal immersed in the fluid as a function of pressure. Measurements were taken both as pressure was being increased and decreased. When measurements taken at a given pressure, obtained by increasing the pressure, did not agree with measurements taken at the same pressure, but obtained by decreasing pressure, or vice versa, the pressure was cycled to determine if a hysteresis effect existed. If a hysteresis effect existed, it was usually an indication of a bad electrical connection to the crystal or a short of the electrical leads. If hysteresis was observed, the crystal was removed from the cell, the electrical malfunction corrected and the procedure started over.

---

*Babb, S. E. Simple High Pressure Valves, The Review of Scientific Instruments, 35, 917 (1964).

(4) After the necessary data were obtained with one liquid, that liquid was removed from the cell, and the cell was cleaned with petroleum ether. After the solvent was removed from the cell, the cell was put under a vacuum for several hours. Cleaning the cell was accomplished without removing the crystal from the cell, which eliminated the need for replacing the seals and recalibrating the crystal. The cell was then filled with the next liquid to be investigated and the high pressure measurements were repeated. A data run was terminated after all the desired liquids had been investigated and the crystal removed from the cell.

In order to differentiate data obtained during different runs the following notation is used. First the approximate resonant frequency in air of the crystal used as the viscometer is given. The approximate resonant frequency is followed by a Roman numeral indicating the order of the run. Thus 20kc-I designates the first data run with the 20-kc crystal, and 60kc-II indicates the second data run with the 60-kc crystal. Data runs 20kc-I and 60kc-I were preliminary runs in which equipment malfunctions were soon discovered. Therefore, no data for 20kc-I or 60kc-I are presented. The designation 60kc-IIa does not refer to a separate data run but rather refers to a crystal calibration obtained in the high pressure cell at the conclusion of data run 60kc-II.

(5) With data run 20kc-II, after the final liquid had been investigated at high pressure, the crystal was removed from the cell, and its calibration was checked for

deviation from the original calibration. No deviations were observed. This calibration check could not be repeated after data run 20kc-III because when it was removed from the cell a loose electrical connection to the crystal was discovered.

With the exception of the 60kc-IIa calibration, all calibrations were obtained by inverting the crystal and holder in a glass vessel which was successively filled with each calibration fluid. 60kc-IIa calibration curves were obtained by calibration in the high pressure cell instead of in the glass vessel. Calibration in the high pressure cell was done to determine the effect of the different electrical environment of the steel cell on the calibration curves.

CHAPTER III

RESULTS AND DISCUSSION OF RESULTS

The calibrations, viscosity data, analysis of errors and the viscoelastic effects are discussed in turn in this chapter.

Viscometer Calibration

As previously mentioned, the crystal viscometer is calibrated by obtaining the linear relations R_E versus $\sqrt{\rho\eta\omega/2}$ and f versus $\sqrt{\rho\eta\omega/2}$ for Newtonian liquids with known η and ρ. The following non-conducting calibration liquids were used for which data for ρ as a function of temperature $\rho(T)$ as well as η as a function of temperature $\eta(T)$ were obtained from the International Critical Tables: n-pentane, n-octane, n-decane, toluene and carbon tetrachloride. The following calibration liquids were hydrocarbon oil samples obtained from the National Bureau of Standards who supplied $\eta(T)$ and $\rho(T)$ data: Oil I, Lot #12; Oil L, Lot #27; Oil N, Lot #16. In addition hydrocarbon oils designated as Sample #1 and Sample #2 were obtained. $\eta(T)$ and $\rho(T)$ data for Samples #1 and #2 were measured by the author. $\eta(T)$ and $\rho(T)$ data for the National Bureau of Standards liquids, Sample #1 and Sample #2 are summarized in Appendix B. All of these liquids were assumed to be non-viscoelastic at

atmospheric pressure and below 10^8 cps. in accordance with the conclusion of Barlow and Lamb (3) on hydrocarbons. Note, however, that at higher frequencies these liquids can become viscoelastic, Figure 5.

The results of calibrations preceding each data run are summarized in Table 3. For each of the calibrations the measured R_E and f data were fitted by a least squares straight line in accordance with Equations (22) and (23). The resulting slopes and intercepts, which are K_r, K_f, R_{Eo} and f_o, as explained in Chapter 2, together with the standard errors, s, and correlation coefficients, r, for each calibration are summarized in Table 4. In Tables 3 and 4 data for the calibration preceding data run 60kc-II were obtained in the glass calibration vessel, and data for calibration 60kc-IIa were obtained in the high pressure cell. In these tables the subscripts r and f refer to resistance and frequency respectively.

Calibration data for air, toluene, n-octane, n-decane and carbon tetrachloride were not included in any of the calculations of f_o and K_f for the 60-kc crystal. These data were omitted because they give a much higher K_f than the remaining data, which agreed with theoretical predictions. This behavior, a high K_f value at low $\sqrt{\rho\eta\omega/2}$ with a much lower K_f value at higher $\sqrt{\rho\eta\omega/2}$, was also observed by Harrison et al. (14) who attributed the discontinuous f versus $\sqrt{\rho\eta\omega/2}$ curve to surface roughness of the crystal.

When the data on the 60-kc crystal mentioned above are omitted from calculations the calibration data are correlated

TABLE 3

SUMMARY OF CALIBRATION DATA

Calibration for Data Run	Calibrating Fluid	$\sqrt{\rho\eta\omega/2}$	R_E (kΩ)	f (cps)	Temperature (°C.)
20kc-II	Air	0.0	22	19,905	26
	n-pentane*	9.23	79	19,900	26
	toluene*	17.1	135	19,897	26
	Oil I-12	71.5	530	19,879	26
	Oil L-27**	222	1590	19,844	22.5
	Sample #1**	327	2215	19,824	22.5
	Sample # 2	410	3100	19,797	25
20kc-III	Air	0.0	44	19,901	22.5
	n-pentane	9.6	83	19,896	
	toluene	17.7	138	19,890	
	Oil I-12	81.5	564	19,872	
	Oil L-27	222	1425	19,840	
	Sample #1	327	1908	19,813	
	Sample #2	455	2650	19,780	
60kc-II	Air	0.0	135	59,470	25
	toluene	30	180	59,424	
	n-decane	35	205	59,420	
	CCl_4	52	265	59,390	
	Oil I-12	127	488	59,413	
	Oil L-27	353	950	59,340	
	Sample #1	520	1191	59,300	
	Sample #2	718	1588	59,240	
60kc-IIa**	Air	0.0	75	59,430	26
	n-octane	29	158	59,410	26
	CCl_4	51.3	234	59,382	26
	Oil L-27	354	1102	59,335	25
	Sample #1	556	1430	59,279	23.2
	Sample #2	739	1870	59,212	24.2
	Oil N-2	1364		59,040	23.4

*Calibration data obtained both before and after high pressure measurements.

**Calibration data obtained after high pressure measurements.

TABLE 4

RESULTS OF LEAST SQUARES FIT

OF CALIBRATION DATA

Quantity	Calibration for Data Run			
	20kc-II	20kc-III	60kc-II	60kc-IIa
R_{Eo} (kΩ)	4.2	14.4	160.6	111.0
f_o (cps)	19,902	19,897	59,447	59,437
K_f (cps/gm/cm-sec)	-0.262	-0.262	-0.289	-0.293
K_{ftheo} (cps/gm/cm-sec)	-0.264	-0.264	-0.289	-0.289
% deviation of K_f from K_{ftheo}.	0.8	0.8	0.0	1.4
s_f (cps)	4.47	4.26	4.24	9.57
r_f	0.995	0.979	0.998	0.999
K_r (kΩ/gm/cm-sec)	7.231	5.787	2.026	2.431
s_r (kΩ)	91	37	52	65
r_r	0.998	1.000	0.996	0.996

very well by a straight line, as evidenced by the fact that all correlation coefficients are very nearly one.

Also, when the frequency data on the 60-kc crystal mentioned above are omitted, values of K_f obtained by calibration agree very well with the K_f values predicted by Equation (24),

as shown in Table 4. As expected, K_f has the same value regardless of whether the calibration is made inside the high pressure cell or in the glass container, as evidenced by the 60-kc calibration data in Table 4. K_f is not expected to vary with changing electrical surroundings because as Equation (24) indicates, it is independent of electrical quantities.

However, from the calibration data for the 60-kc crystal it appears that K_r depends on whether the data are taken in the cell or in the glass container. This dependency is expected because, as Equation (25) indicates K_r depends on the inductance of the crystal. The inductance of the crystal might be different when in the environment of a glass container from when in the steel high pressure cell.

In addition, another method of calibration was used which, in effect, resulted in calibrating the crystal while the actual high pressure viscosity data were being obtained.

In Figures (16-18) the resonance frequency versus resistance for each liquid investigated is plotted as a function of pressure for each crystal.

If the liquids considered are Newtonian, $R_M = X_M$, and equating Equations (20) and (21) predicts that f versus $R_E - R_{Eo}$, for a series of liquids at a given pressure, will be a straight line with slope $-(K_f/K_r)$:

$$f = f_o - (K_f/K_r)(R_E - R_{Eo}) \qquad (30)$$

The intercept of $f(R_E)$ with $R_E = R_{Eo}$, at a given pressure,

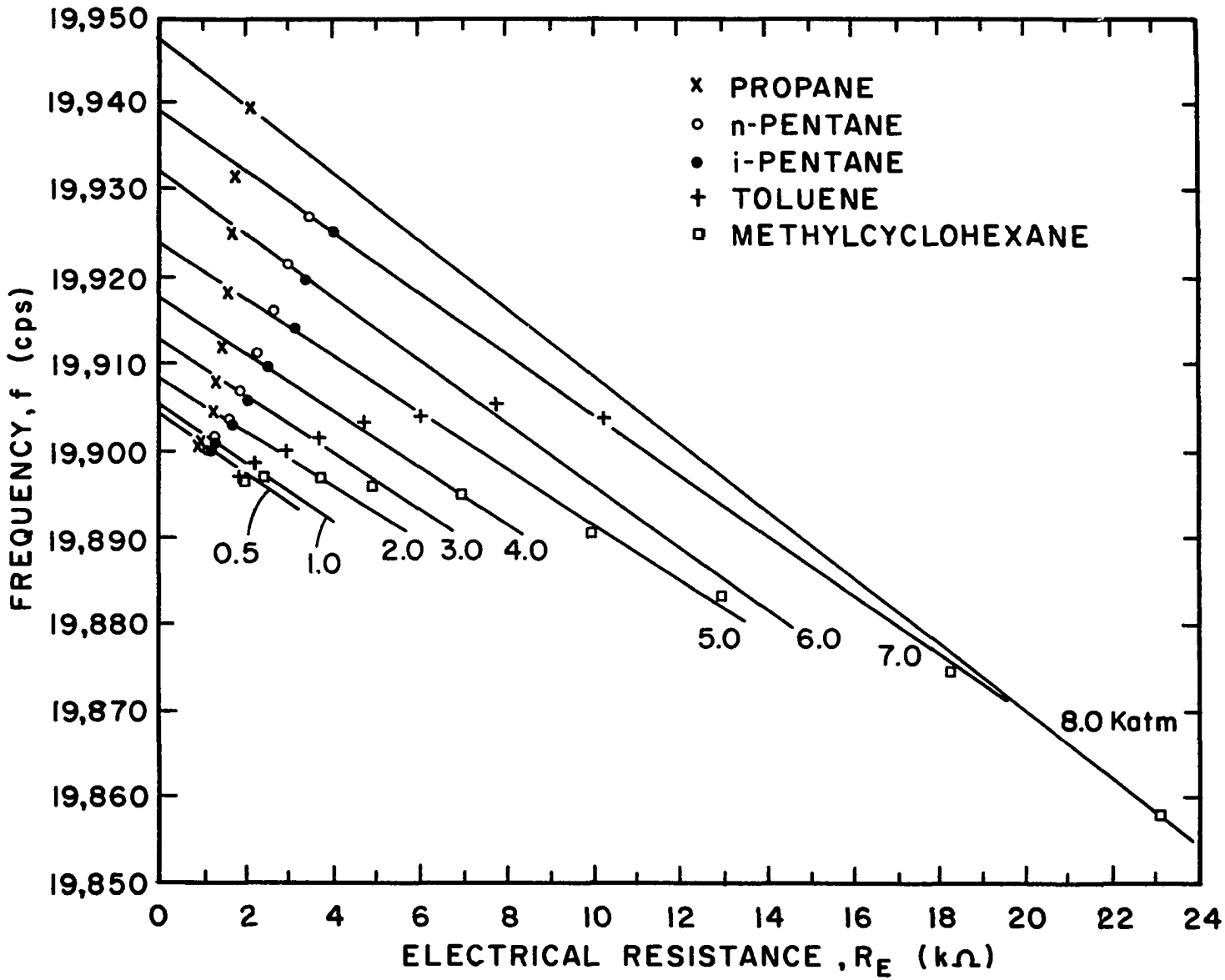

Figure 16. The Change in Resonant Frequency with Resistance at Various Pressures for Run 20kc-II.

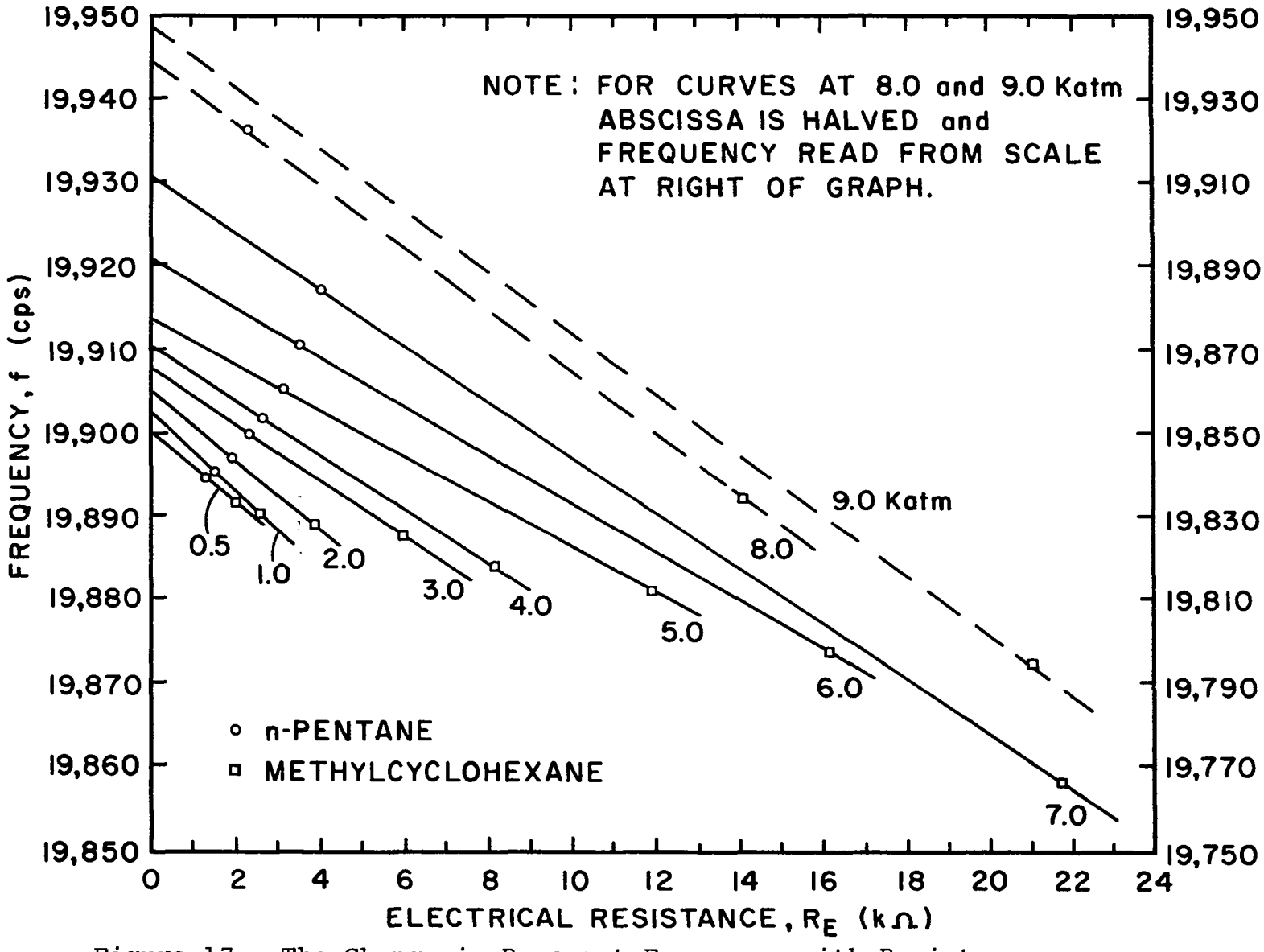

Figure 17. The Change in Resonant Frequency with Resistance at Various Pressures for Run 20kc-III.

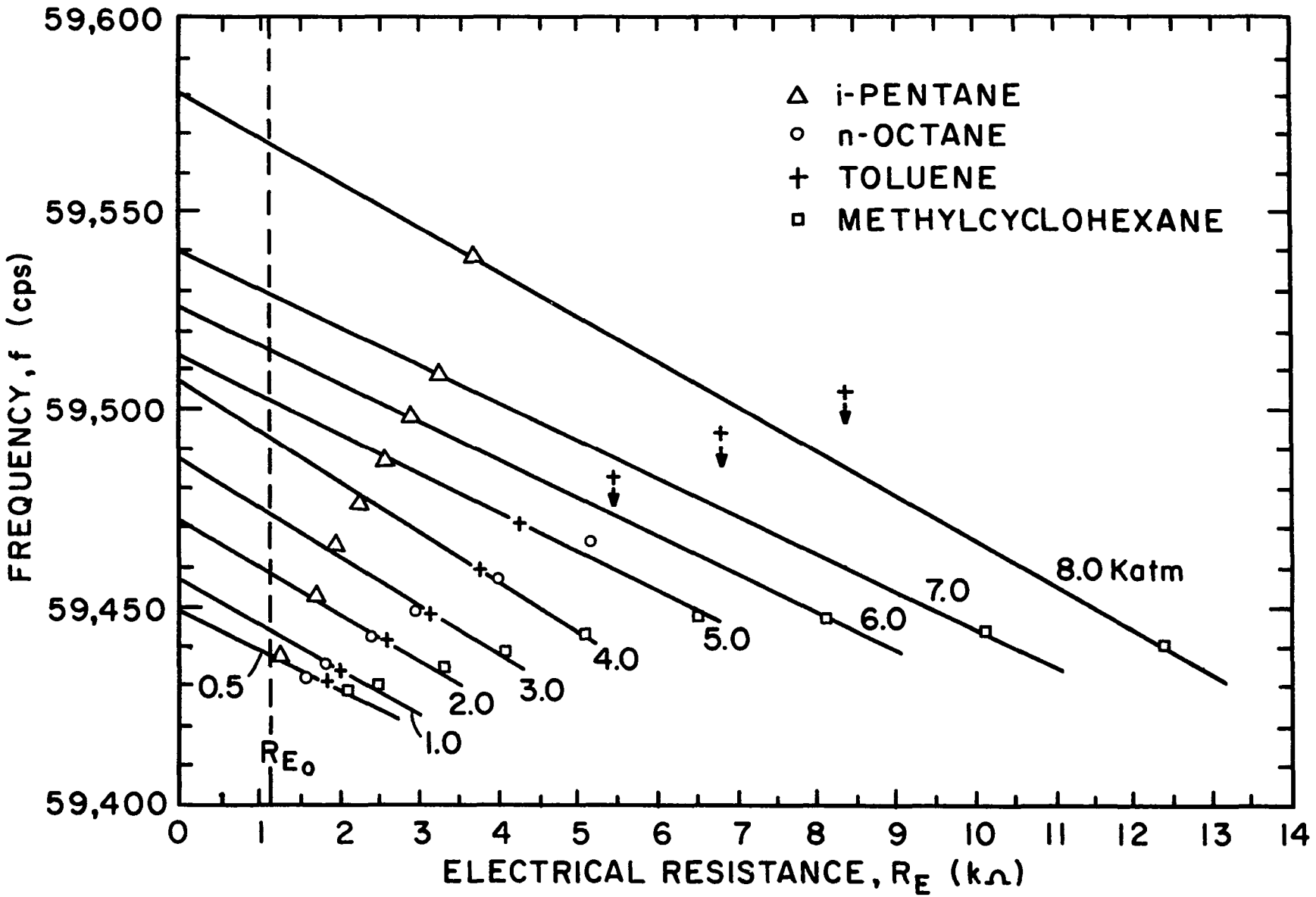

Figure 18. The Change in Resonant Frequency with Resistance at Various Pressures for Run 60kc-II.

gives the resonant frequency of the crystal, which is equivalent to the resonant frequency in air at that pressure. The slopes and intercepts as a function of pressure are summarized in Table 5. These slopes and intercepts result from least squares fit of the data. The data for all fluids investigated fall on a straight line at a given pressure, as predicted, with the exception of the toluene data obtained at high pressures with the 60-kc crystal. The slight variation of slopes between different pressures is caused by uncertainties in measurement of R_E and f.

Because Equation (24) predicts that K_f is independent of electrical surroundings and the calibration data summarized in Table 4 support this prediction, it is assumed that the K_f values given in Table 4 are effective during the high pressure data runs. Equation (25) also predicts that K_r is dependent on electrical surroundings and the 60-kc calibration data support this conclusion. Therefore, it is desirable to know the K_r value for each crystal which is effective in the high pressure cell during the actual data runs. This K_r value may be obtained from the data of Tables 4 and 5.

If it is assumed that K_f is constant and accurate, rearrangement of Equation (30) gives

$$K_r = -(\Delta R_E/\Delta f)K_f. \qquad (30a)$$

The random variation of $\Delta f/\Delta R_E$ with pressure for the runs (See Table 5) indicates that $\Delta f/\Delta R_E$ is probably independent of pressure. Since it is assumed that $\Delta f/\Delta R_E$ is independent

TABLE 5

SUMMARY OF THE RESONANT FREQUENCY IN AIR, f_o,

AND THE CHANGE IN FREQUENCY

AS FUNCTIONS OF PRESSURE

Data Run	Pressure (KAtm.)	$f_o(P)$ (cps)	$\Delta f/\Delta R_E$ (cps/kΩ)	$f_o(P)_{corr}$ (cps)	Δf_o (cps)
20kc-II	0.5	19,904.00	.0365	19,903.50	1.50
	1.0	19,905.00	.0318	19,905.25	3.25
	2.0	19,908.25	.0302	19,909.00	7.00
	3.0	19,912.50	.0314	19,913.25	11.25
	4.0	19,917.50	.0317	19,918.50	16.50
	5.0	19,924.00	.0322	19,924.50	22.50
	6.0	19,932.25	.0368	19,930.50	28.50
	7.0	19,939.00	.0352	19,938.00	36.00
	8.0	19,947.75	.0390	19,941.50	39.50
Average			.0340		
20kc-III	0.5	19,900.25	.0421	19,899.00	2.00
	1.0	19,902.50	.0467	19,900.00	3.00
	2.0	19,905.25	.0419	19,903.50	6.50
	3.0	19,908.00	.0356	19,908.00	11.00
	4.0	19,910.50	.0315	19,913.00	16.00
	5.0	19,914.00	.0277	19,920.00	23.00
	6.0	19,921.00	.0296	19,927.50	30.50
	7.0	19,931.00	.0341	19,933.50	36.50
	8.0	19,939.50	.0367	19,939.00	42.00
	9.0	19,947.50	.0367	19,947.50	50.50
Average			.0363		
60kc-II	0.5	59.437.50	.0960	59,438.00	1.00
	1.0	59,445.00	.1097	59,944.00	7.00
	2.0	59,458.50	.1113	59,457.50	20.50
	3.0	59,473.50	.1213	59,470.00	33.00
	4.0	59,492.00	.1186	59,488.50	51.50
	5.0	59,502.50	.0964	59,506.00	69.00
	6.0	59,518.50	.0953	59,520.00	83.00
	7.0	59,540.00	.0942	59,537.00	100.00
	8.0	59,573.00	.1113	59,563.50	126.50
Average			.1058		

of pressure, an average of $\Delta f/\Delta R_E$ values for all pressures was taken for each run. These average values are also given in Table 5. The average of $\Delta f/\Delta R_E$, for each run, together with the appropriate experimental K_f was used in Equation (30a) to calculate the K_r which was assumed to be effective while data were being obtained. K_r values thus calculated are compared with K_r values obtained from atmospheric calibration in Table 6. In all cases K_r values calculated by

TABLE 6

COMPARISON OF K_r CALCULATED BY EQUATION (30a) AND K_r OBTAINED FROM ATMOSPHERIC CALIBRATION

Data Run	K_r from Equation (30a) (Ω/gm/cm-sec)	K_r from atmospheric calibration (Ω/gm/cm-sec)
20kc-II	7765	7231
20kc-III	7220	5787
60kc-II	2750	2431
60kc-IIa	2750	2026

using Equation (30a) and data obtained during viscosity determinations at high pressure were greater than K_r values obtained at atmospheric pressure. Because the K_r values calculated by Equation (30a) were obtained from data taken during the actual high pressure runs, they were assumed to be more

applicable and reliable than K_r values listed in Table 4. Consequently, K_r values obtained from Equation (30a) were used in Equations (18) and (20) to calculate viscosities.

Figures 16-18 also indicate that the resonant frequency which is equivalent to the resonant frequency in air, f_o, is a function of pressure, $f_o(P)$, and increases with increasing pressure. Table 5 contains a summary of $f_o(P)$.

For each data run at each pressure a straight line with the average slope, K_f/K_r, mentioned above, was made to pass through the average value of the R_E determinations at that pressure. The intercepts of these lines with $R_E = R_{Eo}$ give $f_o(P)_{corr.}$, which are $f_o(P)$ corrected by using the average slope; they are listed in Table 5.

Information about the change in f_o with pressure for each data run is also summarized in Figure 19, where

$$\Delta f_o = f_o(P)_{corr.} - f_o \qquad (31)$$

In Figure 19 least squares parabolas fitting the data for each run are indicated. From Figure 19, $f_o(P)_{corr.}$, which is required to calculate X_M, can be found at any pressure.

Table 7 lists the constants for the least squares parabola, $\Delta f_o = a_o + a_1 P + a_2 P^2$, obtained for each data run and indicates the maximum deviation and the standard error or root-mean-square deviation of the least squares curve from experimental Δf_o values. P has the units of kiloatmospheres (katm) and Δf_o has the units cycles per second (cps).

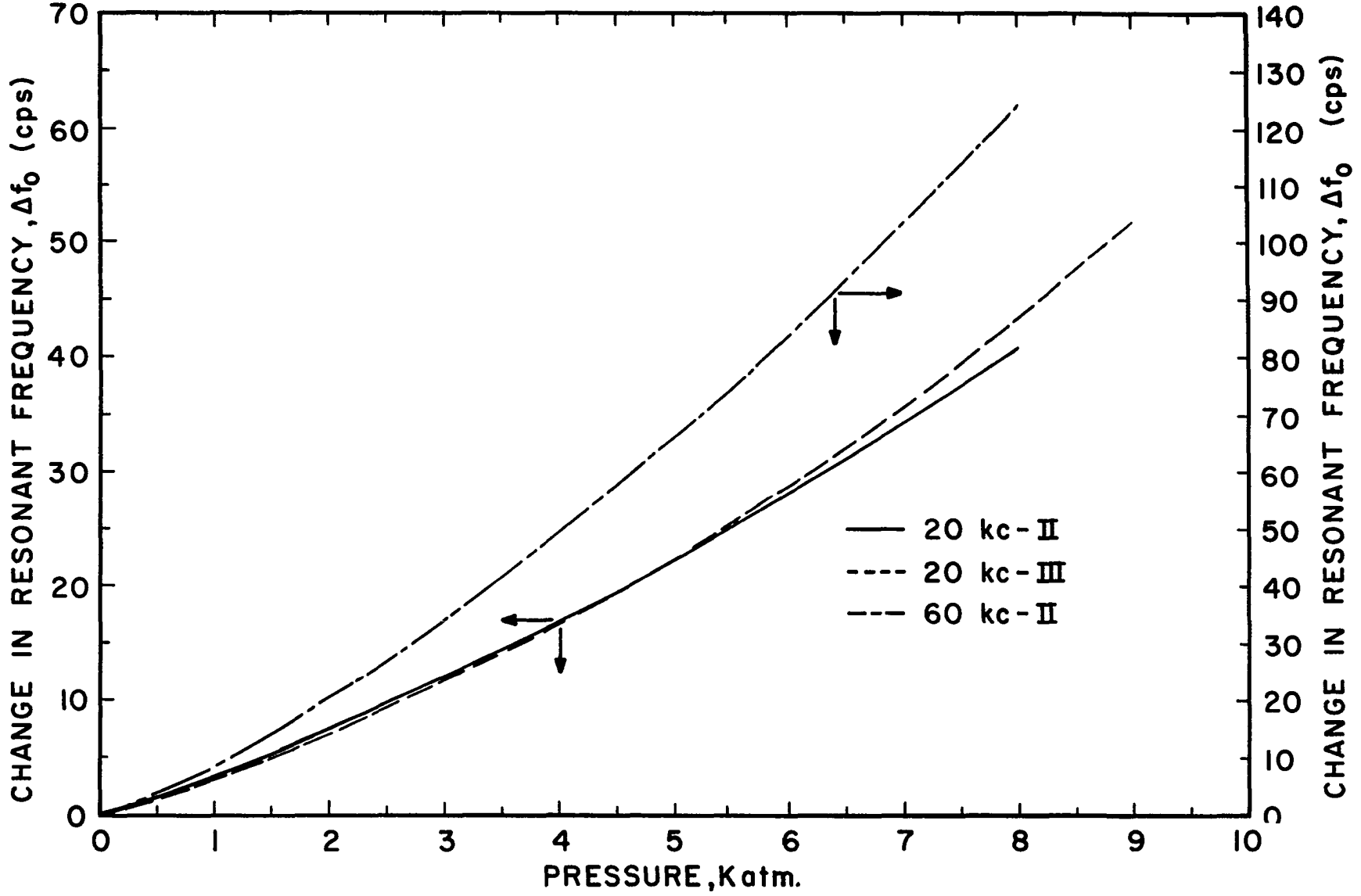

Figure 19. The Effect of Pressure on Crystal Resonant Frequencies in Air.

TABLE 7

CONSTANTS FOR LEAST SQUARES FIT OF Δf_o DATA

Data Run	a_o	a_1	a_2	Maximum Deviation (cps.)	Standard Error (cps.)
20kc-II	-0.413	3.480	0.211	1.5	0.8
20kc-III	-0.336	3.229	0.273	1.0	0.8
60kc-II	-2.400	10.075	0.723	3.0	2.3

The information in Tables 5 and 7 and Figure 18 indicates that $\Delta f_o(P)$ is different for the 60-kc crystal from the 20-kc crystals. This difference in $\Delta f_o(P)$ between 60-kc and 20-kc crystals is to be expected. Equation (13) gives the resonant frequency for a torsionally oscillating crystal:

$$f_o = (1/2\ell)\sqrt{c_{66}/\rho} \qquad (13)$$

For a given material the resonant frequency is uniquely determined by the crystal length.

$$f_o(\ell) = A/\ell \qquad (13a)$$

The effect of pressure on the shear elastic modulus of quartz, c_{66}, and the density, ρ, is assumed to be independent of crystal dimensions. Assuming that the only effect of changing pressure is to alter the crystal length gives

$$\frac{d\, f_o(\ell)}{dP} = -\frac{A}{\ell^2}\frac{d\ell}{dP} = -\frac{A}{\ell^2}\,\ell_o\,(g(P)) \qquad (13b)$$

for the effect of pressure on the resonant frequency. g(P) is obtained from compressibility measurements. If the compressibility is small, a reasonable assumption for quartz, $\ell \approx \ell_o$ and $d f_o/dP$ is proportional to ℓ_o^{-1}. Thus, it is expected that pressure increases cause an increase in resonant frequency of a 60-kc crystal which is three times as great as the increase of a 20-kc crystal. Because Δf_o differs from $f_o(P)$ only by a constant, f_o, the effect of pressure on Δf_o will be the same as the effect on $f_o(P)$. The Δf_o versus pressure curve shown in Figure 19 for the 60-kc data has three times the slope of the 20-kc curves, within experimental precision. Also, differentiation of the least squares curve of $\Delta f_o(P)$ for the 60-kc data gives $(1/3)[d(\Delta f_o)]/dP = 3.358 + 0.482P$. This equation agrees very well with the slope obtained by differentiating both $\Delta f_o(P)$ curves for the 20-kc data and taking the average of the values: $d(\Delta f_o)/dP = 3.354 + 0.484P$. The maximum deviation between $(1/3)[d(\Delta f_o)]/dP$ for the 60-kc data and $d(\Delta f_o)/dP$ for either calculation with the 20-kc data amounts to 4% in the first term and 12% in the second term. Thus it is apparent that the slope of Δf_o versus pressure is inversely related to the crystal length.

The constants for all data runs indicated in Table 7 can be averaged to give a single curve representing $\Delta f_o(P)$ which is independent of the resonant frequency in air at atmospheric pressure, f_o, and which will not deviate from the data for any run by more than 1 cps. This curve is

$\Delta f_o/f_o = -2.601 \times 10^{-5} + 1.689 \times 10^{-4}P + 1.216 \times 10^{-5}P^2$.

This curve is valid between 0.5 katm. and 8.0 katm. pressure and for f_o between 20 kc and 60 kc.

The inductance of the crystal used for each data run can be obtained from Equation (25).

$$L_c = (K_r/K_f)\cdot\frac{1}{4\pi} \qquad (25a)$$

Using K_r as calculated by Equation (30a) and high pressure data (See Table 6) and using K_f obtained from calibration at atmospheric pressure (See Table 4), the L_c applicable for each data run was calculated. These values are given in Table 8.

The quality factor of the crystal, as mounted for each data run, is given by $Q = X/R_E$ where $X = \omega L_c$. A maximum Q for each data run occurred in air, when R_E was the minimum. Likewise, the minimum Q occurred in the most viscous liquid. The maximum and minimum limits of Q are also given in Table 8.

TABLE 8

CRYSTAL INDUCTANCE AND VALUES OF

QUALITY FACTOR APPLICABLE FOR EACH DATA RUN

Data Run	L_c (Henries)	Q_{max}	Q_{min}
20kc-II	2,358	7.02×10^4	131
20kc-III	2,193	1.93×10^4	80
60kc-II	747	1.74×10^4	229

Viscosity Data at High Pressure

As discussed in the Introduction, four constants; K_r, K_f, f_o and R_{Eo} are required in order to calculate η_1 (Equations (18) and (20)) and η_2 (Equations (19) and (21)). For each data run K_f was obtained from calibration at atmospheric pressure, K_r was obtained from high pressure data by using Equation (30a) and $f_o(P)$ was obtained from Figure 19. R_{Eo} was chosen so as to obtain the best fit of $\eta_1(P)$ with accepted low shear rate viscosity data.

As determined from calculations using Equation (28), C_o, the capacitance in parallel with the crystal, was about 15 $\mu\mu$f for the 20-kc crystals and about 10 $\mu\mu$f for the 60-kc crystal. C_o was independent of pressure and independent of the liquid in which the crystal was immersed. These properties indicate that changes in dielectric constant with pressure in a given liquid, and changes in dielectric constant between different liquids, were too small to change the capacitances across the separation of electrodes on the crystal measurably.

If a liquid does not exhibit viscoelasticity $\eta_2 = 0$ and $X_M = R_M$. In this case η_1 may be calculated by

$$\eta_1 = \eta_R = (2R_M^2)/\omega\rho \qquad (18a)$$

Likewise,

$$\eta_1 = \eta_X = (2X_M^2)/\omega\rho \qquad (18b)$$

η_1 was calculated from Equation (18a) for all liquids except toluene at 60 kc, for which Equations (18) and (19) were used at high pressures. Use of Equation (18a) is justified because, as discussed previously, for the series of liquids, with the exception of toluene at 60 kc and high pressure, correlations of R_E versus f at given pressures fell on straight lines with slopes equal to $\Delta f/\Delta R_E$ as was predicted for Newtonian liquids. Furthermore, as will be discussed later, R_M did equal X_M, for all liquids except toluene at 60 kc and high pressure, within the limits of experimental precision. In addition, resistance measurements were much more sensitive to changes in viscosity than were frequency measurements. For example, using Equations (18a) and (20) for data run 20kc-II with a hypothetical liquid of density 0.800 gm/cc, a change in resistance of 1 kΩ, the smallest change that could be measured in this resistance range, from 300 kΩ to 301 kΩ represents a change in viscosity from 0.0252 p. to 0.0254 p. or about 0.8%. A frequency change of 1 cps., the smallest frequency change that could be measured, from 19,920 cps. to 19,921 cps. represents a viscosity change from 0.0236 p. to 0.0291 p. or about 23%. For all of these reasons η_1 was calculated from Equation (18a), except as noted for toluene for which Equation (18) had to be used.

The results, η_R as functions of pressure, with estimated maximum limits of error, are shown in Figures 20-30. The dashed curves on these graphs indicate viscosity versus pressure data obtained by Bridgman (4) with a falling weight, or low shear rate viscometer. Bridgman's data have been corrected from 30°C.

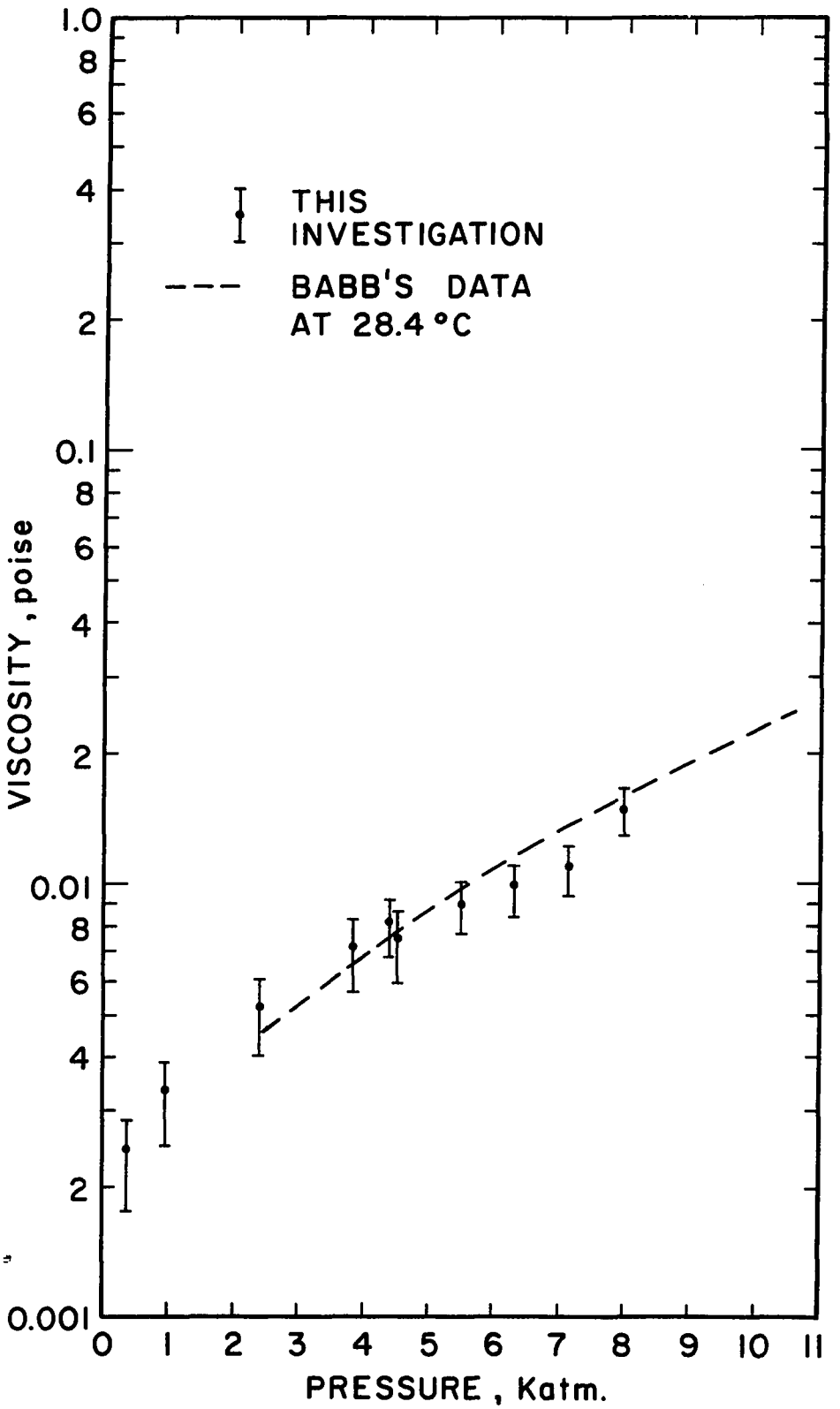

Figure 20. The Effect of Pressure on the Viscosity of Propane at 26°C. (20kc-II).

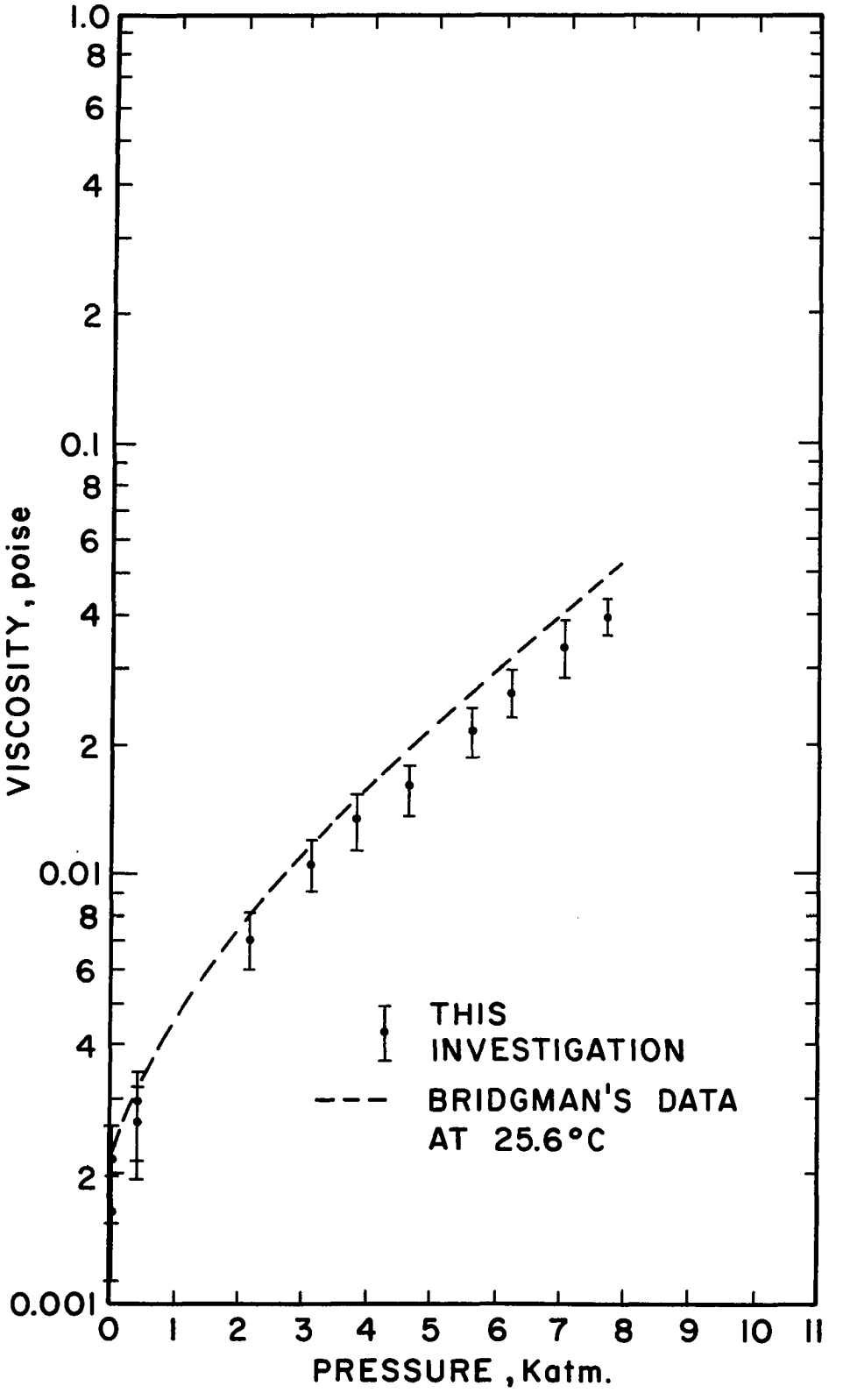

Figure 21. The Effect of Pressure on the Viscosity of n-Pentane at 25.6°C. (20kc-II).

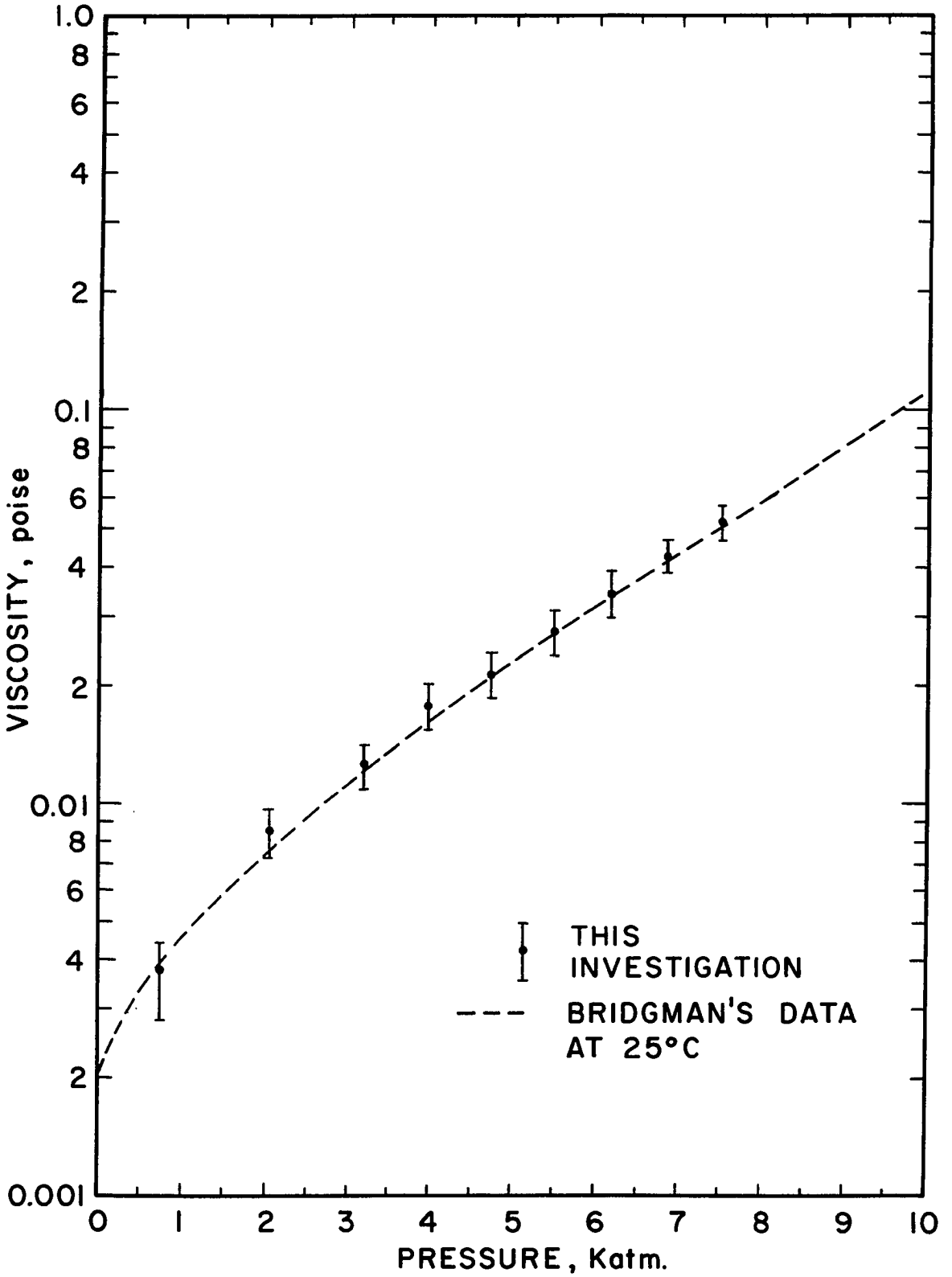

Figure 22. The Effect of Pressure on the Viscosity of i-Pentane at 25°C. (20kc-II).

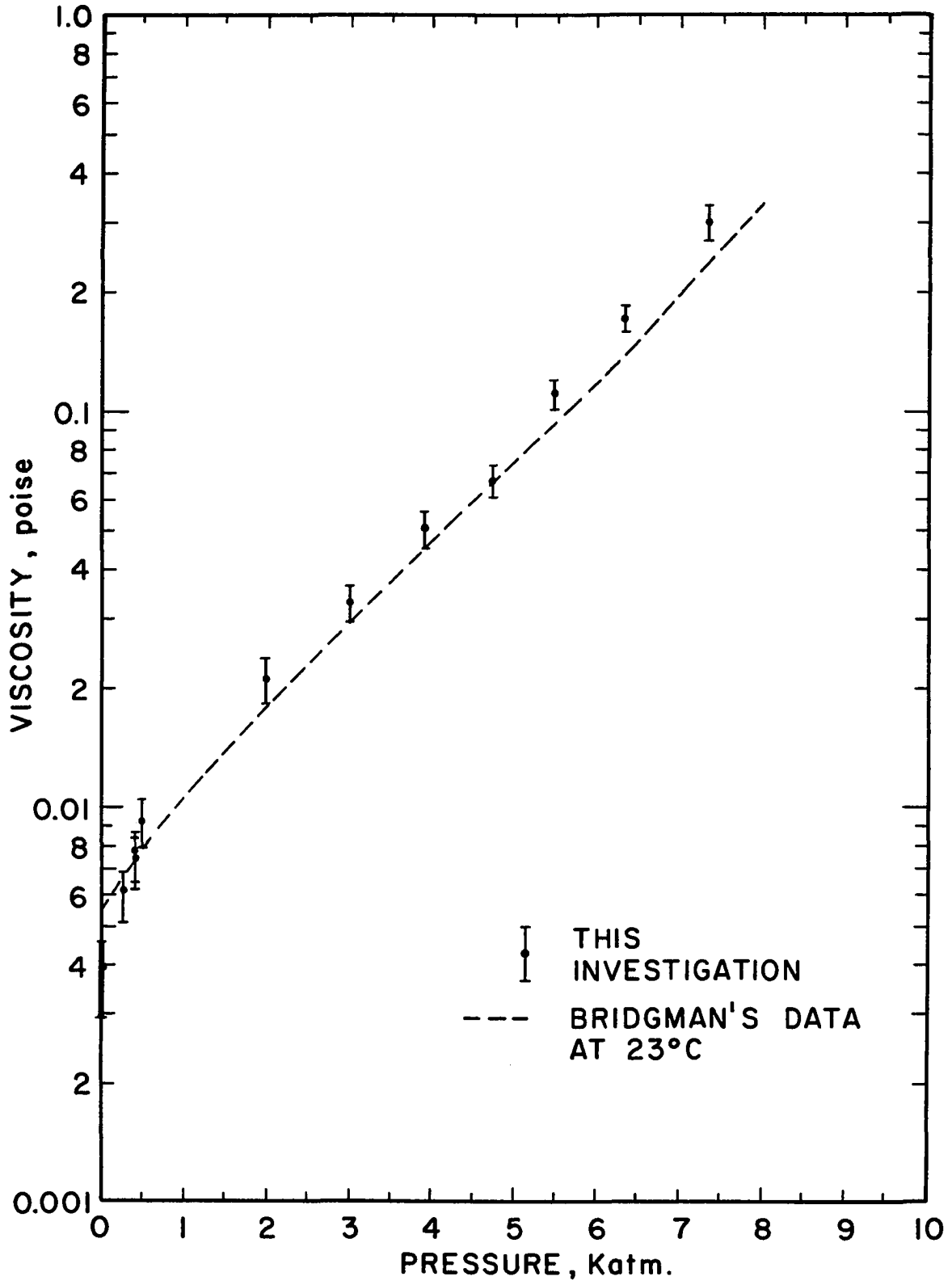

Figure 23. The Effect of Pressure on the Viscosity of Toluene at 23°C. (20kc-II).

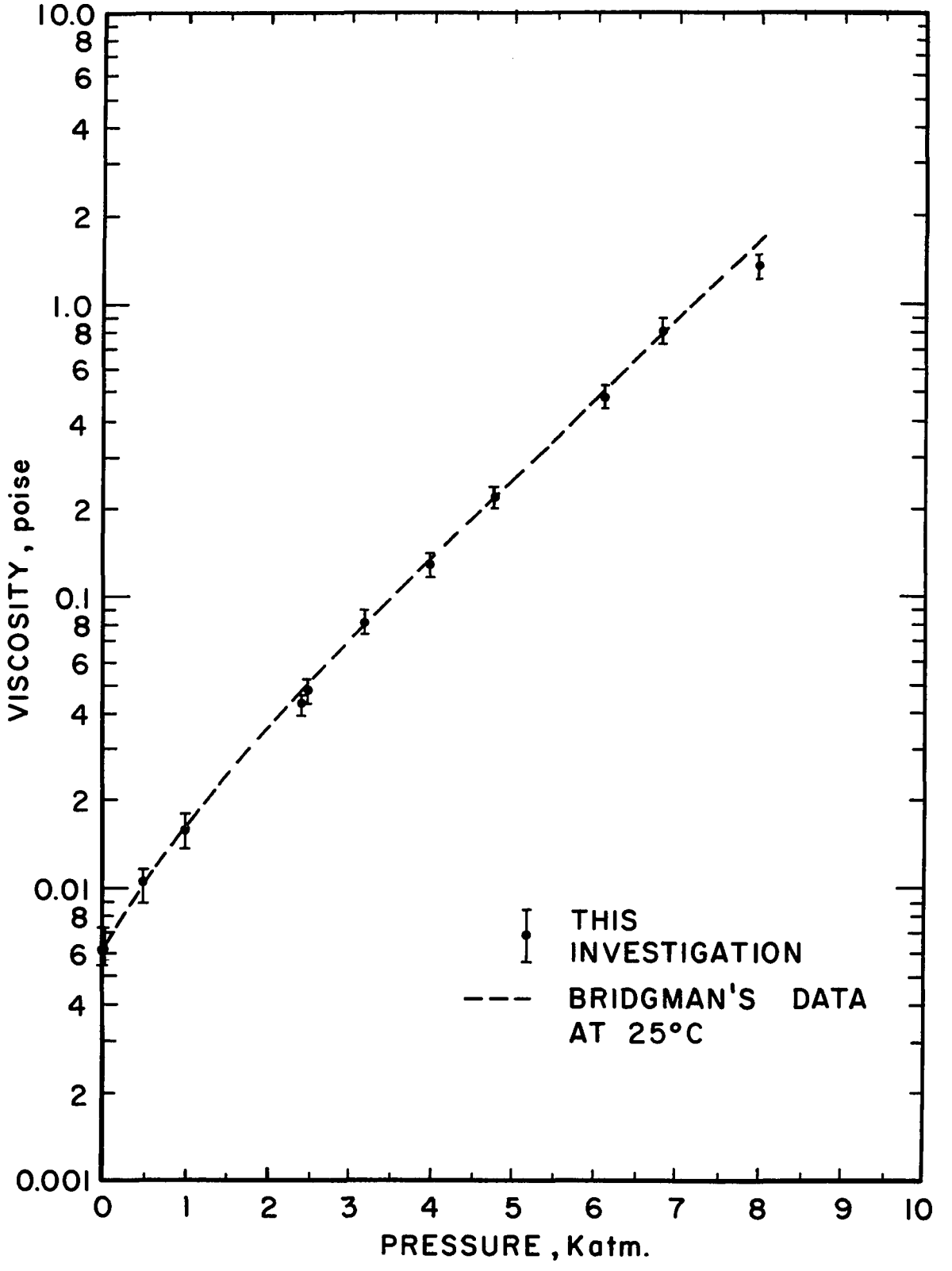

Figure 24. The Effect of Pressure on the Viscosity of Methylcyclohexane at 25°C. (20kc-II).

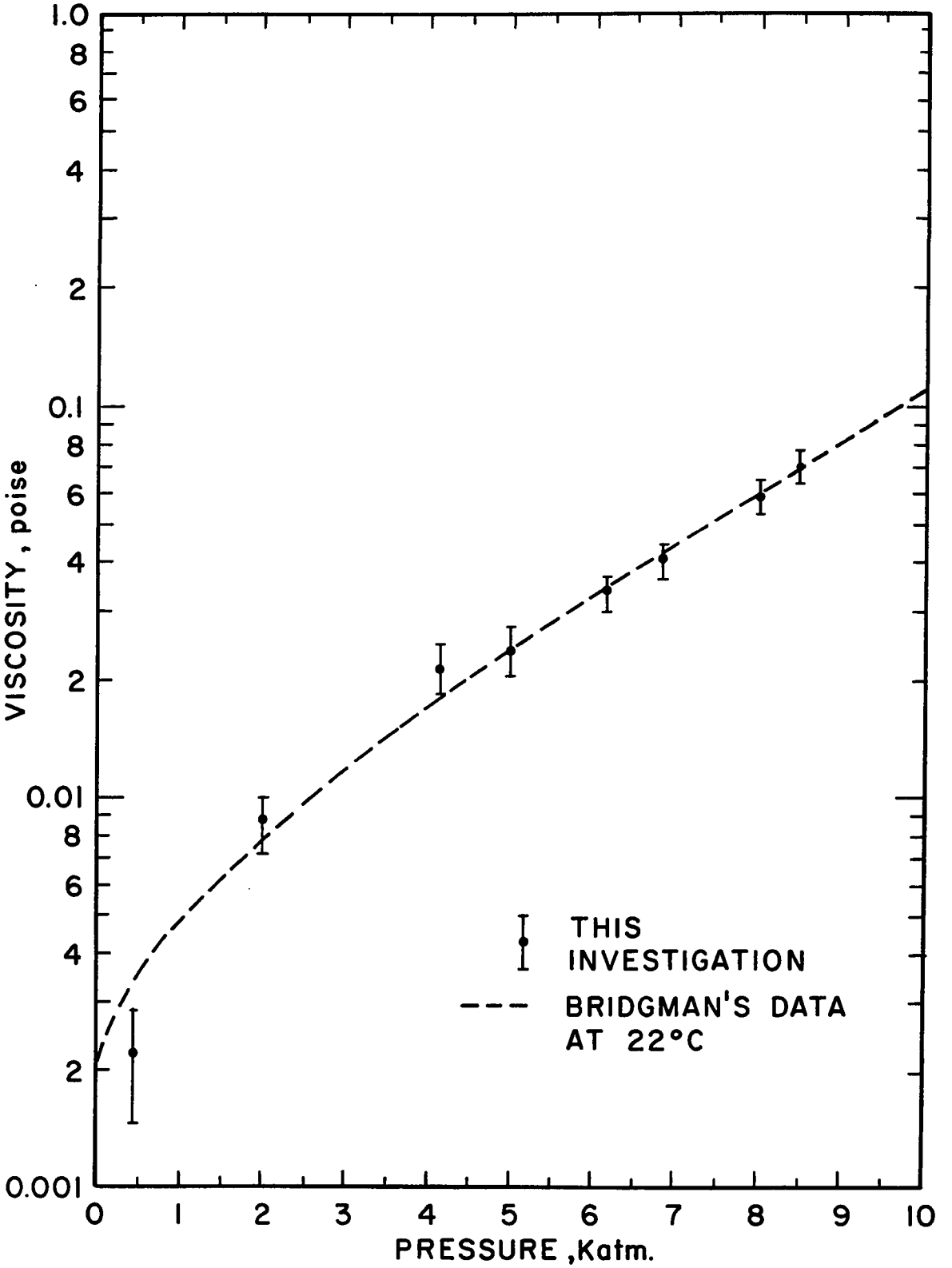

Figure 25. The Effect of Pressure on the Viscosity of n-Pentane at 22°C. (20kc-III).

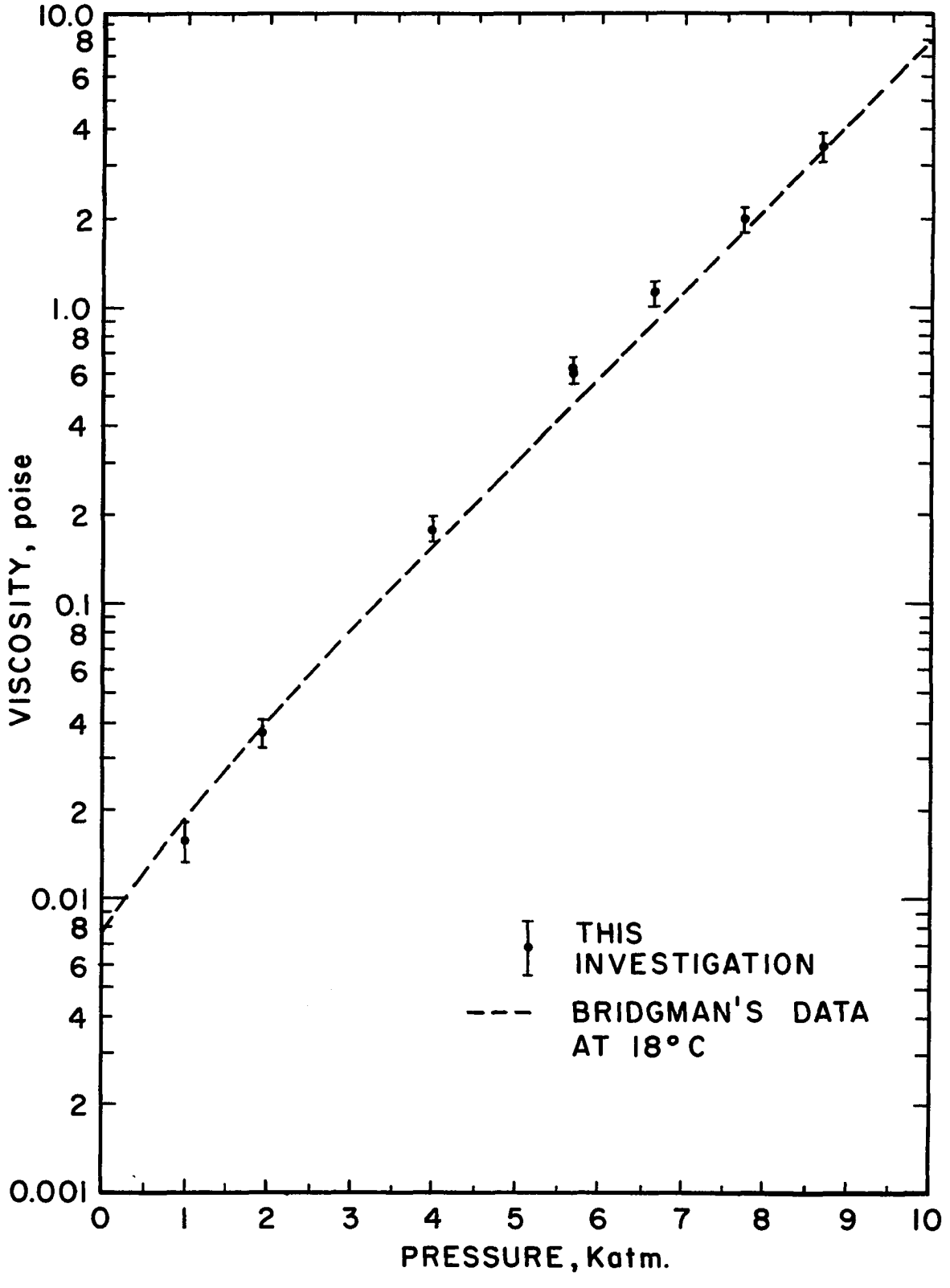

Figure 26. The Effect of Pressure on the Viscosity of Methylcyclohexane at 18°C. (20kc-III).

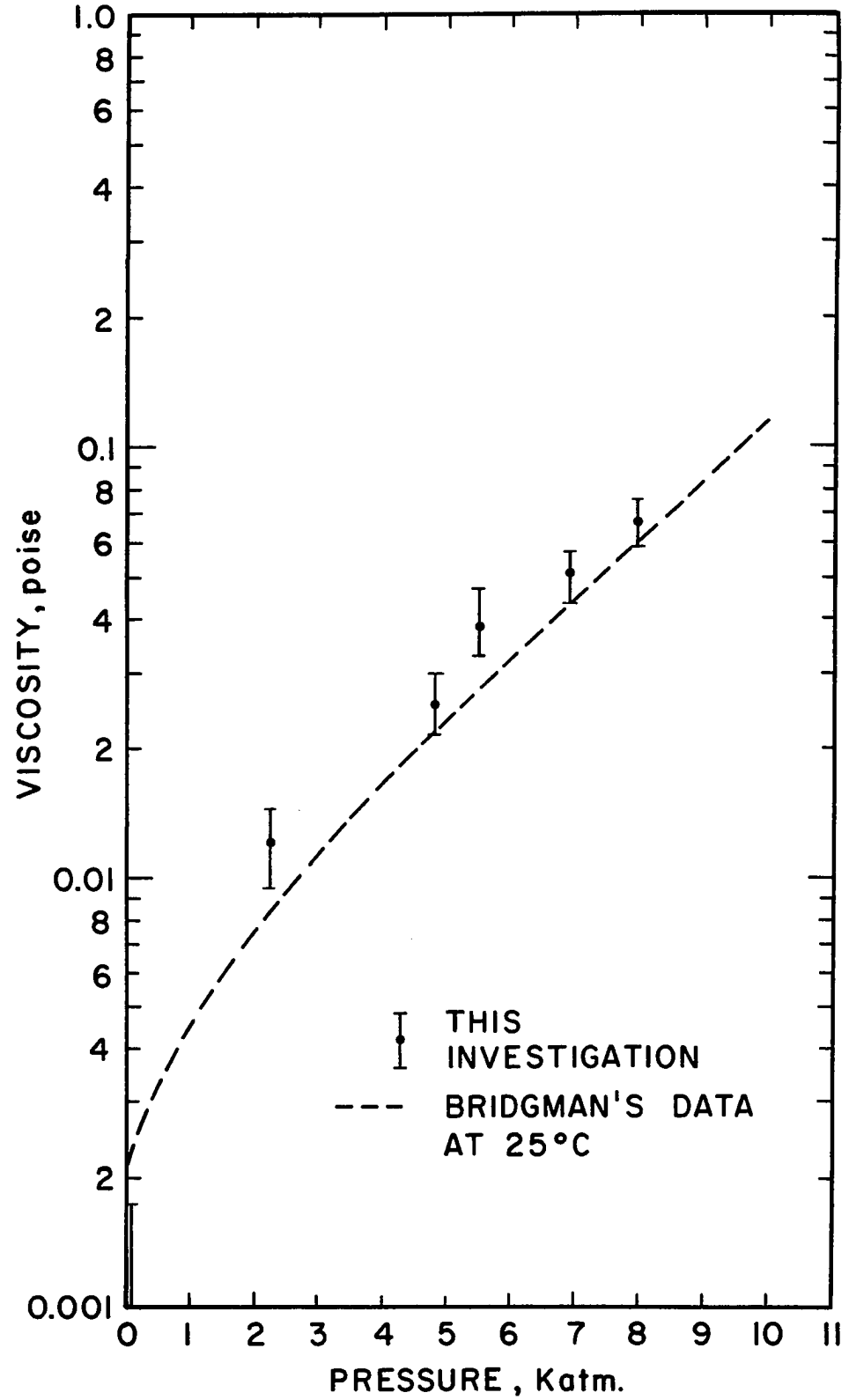

Figure 27. The Effect of Pressure on the Viscosity of i-Pentane at 25°C. (60kc-II).

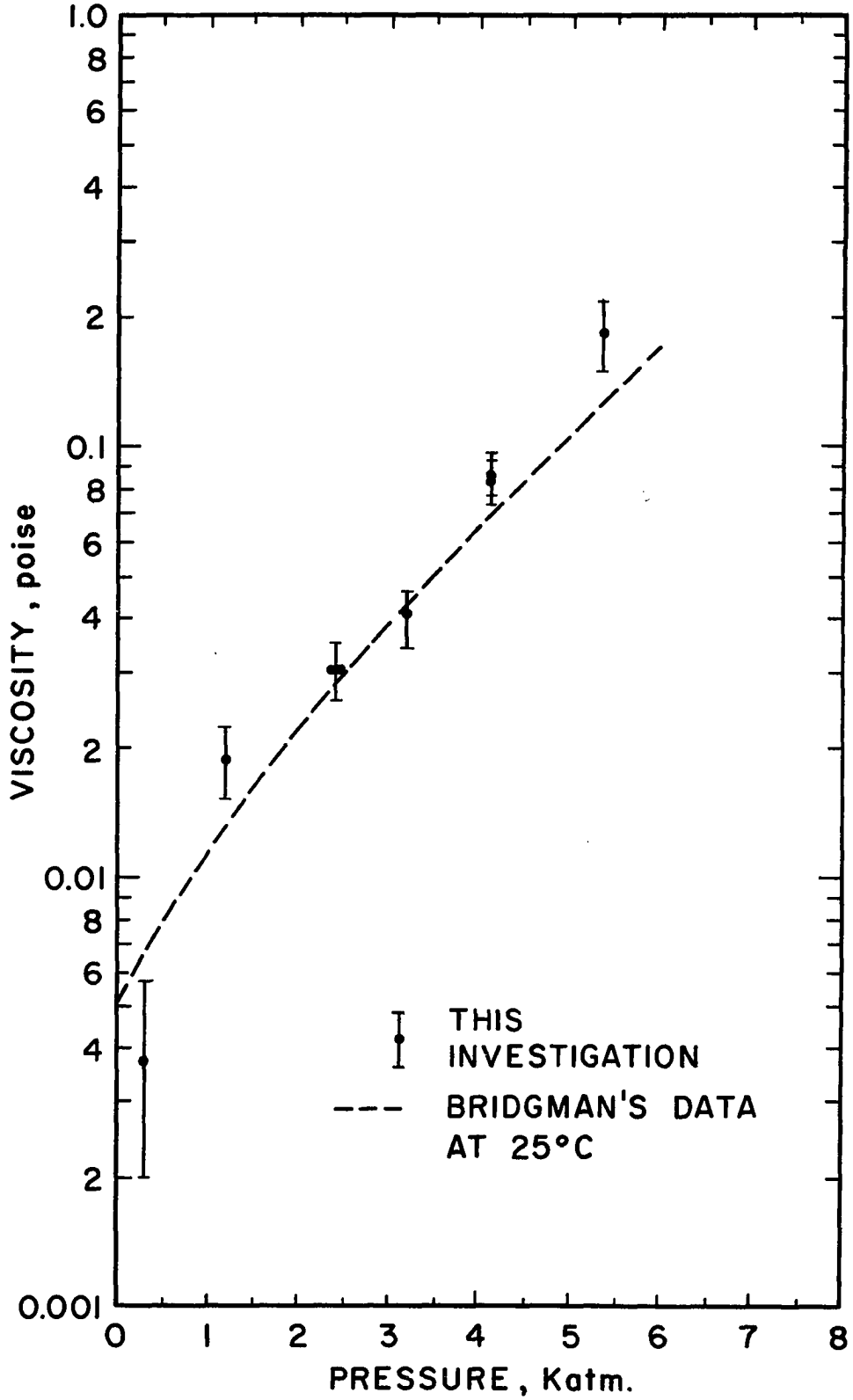

Figure 28. The Effect of Pressure on the Viscosity of n-Octane at 25°C. (60kc-II).

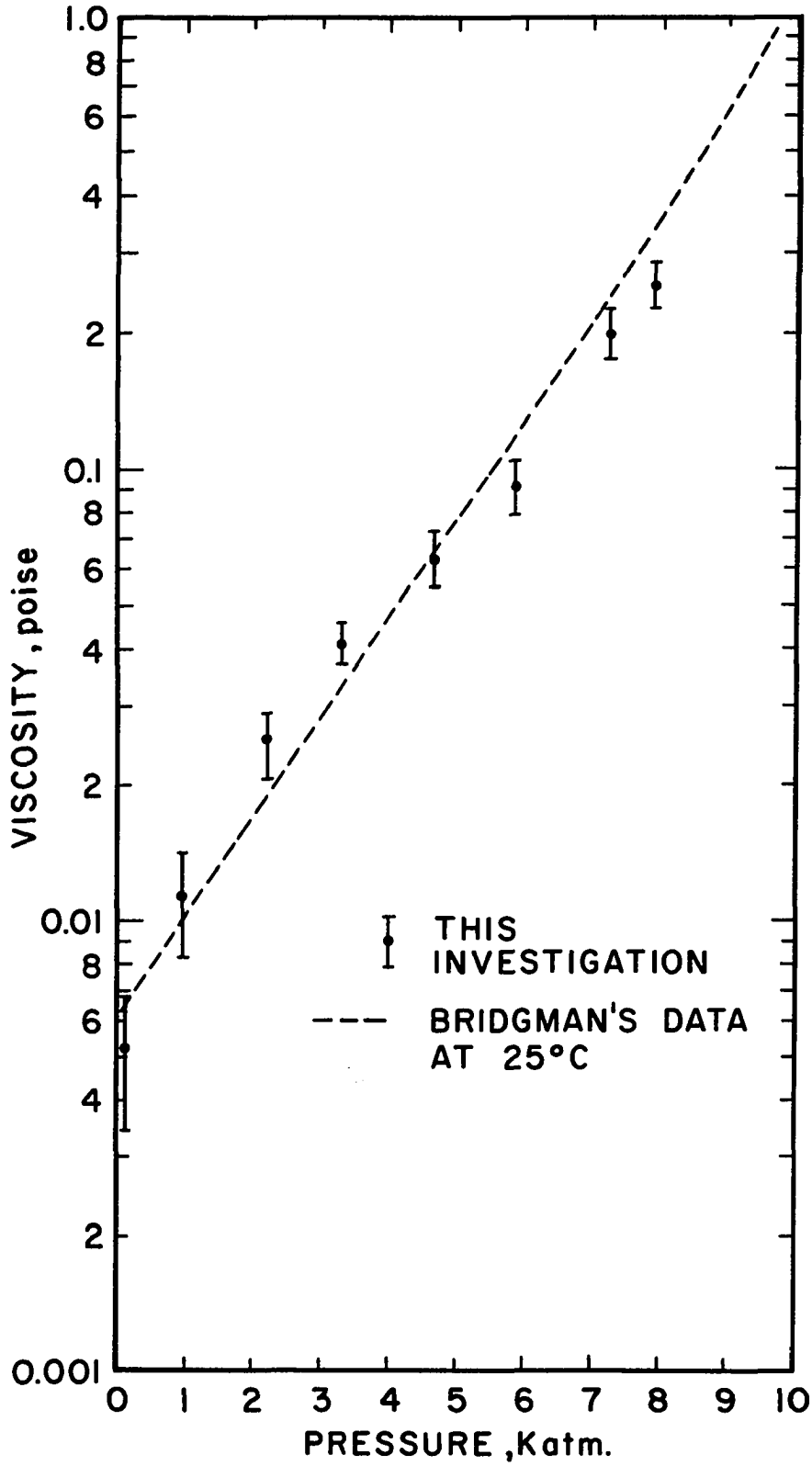

Figure 29. The Effect of Pressure on the Viscosity of Toluene at 25°C. (60kc-II).

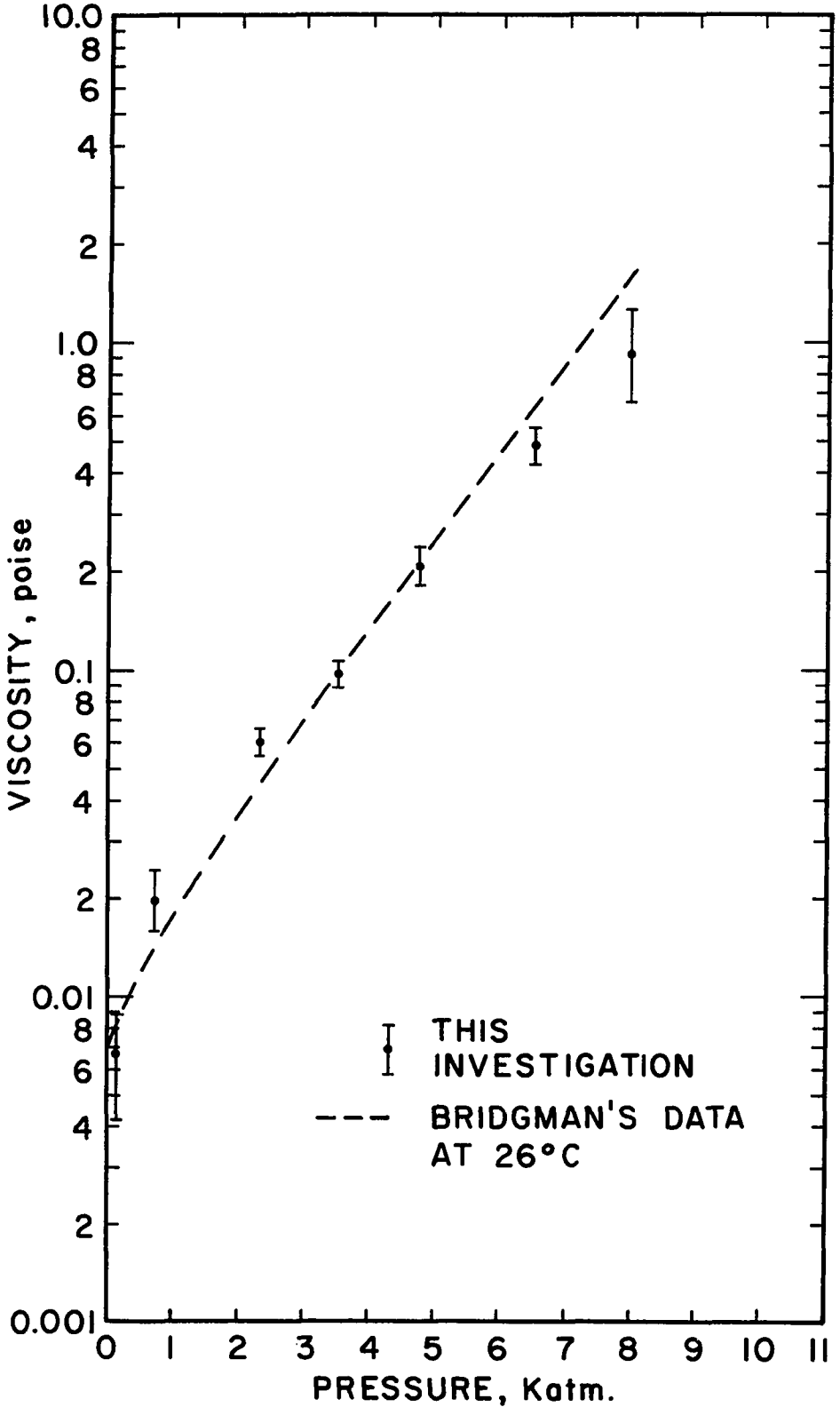

Figure 30. The Effect of Pressure on the Viscosity of Methylcyclohexane at 26°C. (60kc-II).

to the temperature existing during this investigation. The dashed line on the viscosity versus pressure graph for propane, Figure 18, represents the data of Babb (2) and is not corrected for temperature differences.

Temperature corrections to Bridgman's viscosity data were made by assuming viscosity to be related exponentially to temperature, $\eta = \eta_o e^{(B/T)}$, as is observed. Bridgman's viscosity as a function of pressure at 30°C. and 75°C. data were then used to determine B at various pressures. The viscosity data at 30°C. could then be corrected to the temperature of these investigations. Temperature corrections were not made to Babb's data because information was insufficient.

It is necessary to know the density of each liquid as a function of pressure in order to use Equations (18), (18a), or (18b). This information is available from the work of Bridgman (6) for iso-pentane, normal-pentane and normal-octane over the entire pressure range and at 0°C., 50°C., and 95°C. For these liquids $\rho(P)$ at the temperature of the measurements was obtained by approximate interpolation between the curves for $\rho(0^{\circ}C.)$ and $\rho(50^{\circ}C)$. Typically, $\rho(0^{\circ}C.) - \rho(50^{\circ}C.)$ is about 0.10 gm./cc., so the interpolated value is probably not in error by more than 0.01 gm./cc.

The concept of the average fluid (7) was used to extend the range of propane and methyl-cyclohexane compressibility data to 10 katm. and to calculate the compressibility of toluene over the entire pressure range. Bridgman found

that shapes of volume versus pressure curves for eleven liquids above 500 kg./cm.^{2} (1 kg./cm.^{2} = 0.9679 atm.) were very similar and that the change in volume with pressure for any liquid could be represented by an average liquid for which

$$\Delta V/V_{500} = K\left[\alpha\left(\frac{P-500}{1000}\right)^{.8} + \beta\left(\frac{P-500}{1000}\right)^{.6} + \gamma\left(\frac{P-500}{1000}\right)^{.4} + \delta\left(\frac{P-500}{1000}\right)^{.2}\right] \quad (32)$$

where $\alpha = -0.0029$, $\beta = -0.0546$, $\gamma = 0.2969$ and $\delta = 0.1804$. P is the pressure (kg./cm.^{2}) and V_{500} is the volume at 500 kg./cm.^{2} For the liquids Bridgman investigated K varied from 0.8126 to 1.104.

For propane, V_{500} was obtained from Sage and Lacey (24) and is 1.757 cc./gm. at 24°C. Because there was insufficient information to indicate otherwise, K was assumed to be one.

Bridgman (8) gives compressibility data for methyl-cyclohexane at 25°C. up to 5,000 kg./cm.^{2} V_{500} for methyl-cyclohexane was obtained from his data and K = 1.011 determined by making the experimental and calculated values of $\Delta V/V_{500}$ agree at 2,000 kg./cm.^{2} Values of V(P) calculated from Equation (32) agreed with experimental values up to 5,000 kg./cm.^{2} to within 2 parts in 1,100. Equation (32) was used to calculate V(P) up to 10 katm., and this information was used to obtain ρ(P) over the pressure range.

No data on the compressibility of toluene are available. Because the structures of toluene and methyl-cyclohexane are somewhat similar, the density as a function of pressure information obtained by use of Equation (32) for methyl-

cyclohexane was also used for toluene. However, to obtain $\rho(P)$ for toluene, 0.096 gm./cc. was added to all computed $\rho(P)$ values for methyl-cyclohexane to reflect the fact that the density of toluene at 25°C. and one atmosphere is 0.096 gm./cc. greater than the density of methyl-cyclohexane. This procedure may introduce a small error into η_1 and η_2 calculations for toluene, but it is adequate in the absence of detailed volume-pressure data. Calculated $\rho(P)$ information is in Appendix C.

Effects of Errors in Measurement

The errors in measurement consist of resistance and frequency measurements and temperature changes due to compression of the liquid.

Errors in Resistance Measurements

There are three sources of error in R_E calculated from balances of the impedance bridge. These sources are discussed below and are: (A) Inaccuracy of the impedance bridge, (B) Uncertainty in locating the minimum of the R_E versus frequency curve and (C) The effect of oscillator frequency instability on R_E.

Inaccuracy of the impedance bridge. Table 2 gives data which related the error in calculated values of R_E to the ratio R/X_C at 20 kc and 60 kc. Using this information as a guide, Table 9 was constructed to estimate the expected error in calculated R_E values as a function of R_E at 20 kc and 60 kc.

TABLE 9

ESTIMATES OF ERROR IN CALCULATED ELECTRICAL RESISTANCE, R_E, VALUES AS A FUNCTION OF ELECTRICAL RESISTANCE

20 kc			60 kc		
R_E (kΩ)	Approximate R/X_C Range	Estimated Error	R_E (kΩ)	Approximate R/X_C Range	Estimated Error
0-150	100-15	± 2%	0-200	5-1.3	± 2.5%
151-350	15-3	± 3.5%	201-600	1.3-0.3	± 3.0%
351-900	3-0.3	± 4%	601-1000	0.3-0.1	± 6.0%
> 900	< 0.3	± 5%	> 1000	< 0.1	± 20%

Uncertainty in locating the minimum of the R_E versus frequency curve. As mentioned previously, the resonant frequency of the crystal viscometer in a fluid is the frequency at which R_E versus frequency passes through a minimum. The resonant resistance, used in calculating η_R, is the value of R_E at this frequency. To determine the resonant frequency, R_E values were calculated as a function of frequency until a minimum was obtained. This procedure is satisfactory for liquids at high pressure, where ρ and η are relatively large, because R_E versus frequency is relatively flat, even near resonance. The minimum R_E may appear constant for ± 5 cps. in the extreme case. However, if the slope of the R_E versus

frequency curve is steep, corresponding to low ρ and η, this procedure is less satisfactory because it is impossible to make fine enough frequency adjustments to locate the minimum. Thus, if R_E values are obtained at 19,634 cps. and 19,635 cps., neither will give the correct minimum R_E if this minimum occurs at 19,634.3 cps. Errors in R_E and frequency measurements were large enough to make interpolation to a minimum R_E senseless. Therefore, the measured R_E values may be too large, especially when R_E is small, which corresponds to low ρ and η values and a steep R_E versus frequency curve. Estimates of this error are tabulated in Table 10.

TABLE 10

ESTIMATES OF UNCERTAINTY IN LOCATING THE MINIMUM OF THE ELECTRICAL RESISTANCE, R_E, VERSUS FREQUENCY CURVE

20 kc		60 kc	
R_E (kΩ)	Error (kΩ)	R_E (kΩ)	Error (kΩ)
0-150	+ 5	0-200	+ 5
151-350	+ 3	201-300	+ 3
351-600	+ 1	301-600	+ 1
> 600	0	> 600	0

The effect of oscillator instability on R_E. Although the oscillator had been warmed up for days prior to making measurements, the oscillator frequency varied while the bridge was being balanced. Thus, at low ρ and η, where R_E is a strong function of frequency, an absolute balance of the bridge was impossible because, while a bridge balance was being attempted, the frequency and thus the balance would change. The result was that a balance represented an average R_E over the frequency range caused by oscillator instability. This error was only appreciable at low R_E. As ρ and η became larger the frequency could vary slightly and only have a minor effect on the balance. Estimates of this error are tabulated in Table 11.

TABLE 11

ESTIMATES OF ERROR CAUSED BY OSCILLATOR INSTABILITY

20 kc		60 kc	
R_E (kΩ)	Error	R_E (kΩ)	Error
0-150	± 5%	0-200	± 5%
151-350	± 2%	201-300	± 2½%
351-600	± ½%	301-600	± ½%
600	0	600	0

Summation of the errors tabulated in Tables 9-11 provides an estimate of the maximum and minimum possible R_E

values for a given measurement. Inserting the maximum and minimum R_E into Equation (20) allows calculation of maximum and minimum expected values of η_R for a given measurement. These values are indicated in Figures 20-30.

Graphs of η_R versus pressure show agreement with previous investigations. If allowance for small experimental error in the previous investigations is made, the data from this investigation, with estimated error limits, will overlap the expected range of values for previous investigations.

Data obtained with the 60-kc crystal are less consistent than data obtained during runs with the 20-kc crystal. The discrepancy is probably caused by a poorer mounting of the 60-kc crystal. Evidence of the poorer mounting is the higher resonant resistance in air at atmospheric pressure (111kΩ for the 60-kc crystal opposed to 14kΩ and 2kΩ for different calibrations with the 20-kc crystals) which results in a smaller Q. The 60-kc crystal is much harder to mount because it is shorter than the 20-kc crystal. If the crystal is mounted somewhere other than at the nodal plane, or if solder is on the crystal other than at the nodal plane, the torsional motion of the crystal is distorted. Because the 60-kc crystal is three times shorter than the 20-kc crystal, mounting of the 60-kc crystal is much more critical than mounting a 20-kc crystal. Thus the greater inconsistency observed in the 60-kc data is assumed to be caused by a poorer mounting of this crystal.

Error in Frequency Measurements

Errors in the measured values of the resonant frequency arise from 3 sources: (A) Limits of the precision of the electronic counter, (B) Oscillator instability and (C) Inaccuracy in determining the resonant frequency, or minimum of the R_E versus frequency curve. These factors are discussed below.

Limits of the precision of the electronic counter. According to the manufacturer, the counter used to determine the frequency of the crystal oscillations had a precision of ± 1 cps., thereby limiting frequency determinations to a precision of ± 1 cps.

Oscillator instability. As soon as the impedance bridge was balanced, the oscillator frequency as determined by the counter was observed. Because the counter determined the frequency very often, the possibility of measuring the wrong frequency for a given balance was minimized. The error caused by oscillator instability is estimated to be less than ± 0.5 cps.

Inaccuracy in determining the resonant frequency. As the product $\rho\eta$ increases, the R_E versus frequency curve becomes flatter, making it progressively more difficult to determine the frequency at which R_E is a minimum; which is the resonant frequency. In the extreme case R_E may appear to be constant over a range of ± 5 cps. Thus, in this case it would be impossible to determine the resonant frequency to a greater precision than ± 5 cps. As $\rho\eta$, which is

related to R_E, increases, this error increases as estimated in Table 12.

TABLE 12

ESTIMATED ERROR CAUSED BY INACCURACIES IN DETERMINING THE RESONANT FREQUENCY

R_E (kΩ)	Error (cps)
0-300	0
301-1000	± 2
> 1000	± 5

These errors were not dependent on which crystal was being used. Summation of the frequency errors mentioned above allows estimation of the uncertainty of the measured frequency. The uncertainty in measured frequency can then be used to determine the expected range of calculated values of X_M.

Effect of Temperature Change Caused by Compression

Calculations in Appendix D demonstrate that the effect of any temperature change in the liquids caused by compression to high pressure is negligible. For an adiabatic compression, which greatly overestimates the possible temperature change, from 1 atm. to 10 katm., the temperature change in normal-

pentane is 58.5°C. However, because of heat loss through the wall of the high pressure cell to a surrounding oil bath with high heat capacity, calculations show that the temperature of the liquid in the high pressure cell will return to the temperature before compression after 20 minutes. Actually, for compressions at the highest pressures more than 45 minutes were allowed for the liquid to come to equilibrium and the pressure increases were usually only about 2.0 katm. (from 8.0 katm. to 10.0 katm. for instance). Therefore it is reasonable to assume that any temperature increase caused by compression had disappeared before viscosity data were obtained.

For the more representative compression from 3.0 katm. to 5.0 katm. the temperature increase caused by compression is only 1.2°C. and disappears in 10 minutes.

Viscoelastic Effects

If a liquid is not viscoelastic $\eta_2 = 0$ and $R_M = X_M$. If the R_M limits, calculated as described in the section, Effects of Errors in Measurement, (see pages 78-82 and Equation (20) overlap the X_M limits, calculated as described in the same section; (see pages 83-84 and Equation (21)), it is possible that $R_M = X_M$ within the experimental precision of the measurements. Therefore, the test of the criterion $R_M = X_M$ used in this investigation was if the limits of R_M overlapped the limits of X_M, $R_M = X_M$ and $\eta_2 = 0$. Information for evaluating this criterion is contained in Table 13. Maximum and minimum

TABLE 13

SUMMARY OF MAXIMUM AND MINIMUM LIMITS OF THE MECHANICAL RESISTANCE, R_M, AND THE MECHANICAL REACTANCE

Liquid	Pressure (katm.)	Maximum R_M	Minimum R_M	Maximum X_M	Minimum X_M	$R_M = X_M$ Satisfied
			Data Run 20kc-II			
Propane	0.37	10.04	7.86	12.31	4.73	x
	0.93	11.94	9.56	15.2	7.58	x
	2.40	15.39	12.56	22.73	15.15	x
	3.85	18.42	15.20	22.73	15.15	x
	4.39	19.51	16.94	26.52	18.94	x
	4.52	19.00	15.65	26.52	18.94	x
	5.50	20.73	18.03	25.57	17.99	x
	6.34	21.83	19.00	24.62	17.04	x
	7.17	23.18	20.22	22.73	15.15	x
	8.00	27.24	23.89	22.73	15.15	
normal-pentane	0	8.76	6.57	8.52	0.95	x
	0+	10.11	7.79	9.47	1.89	x
	0.4	11.53	8.95	13.26	5.68	x
	0.4	12.04	9.47	13.26	5.68	x
	2.16	19.45	16.74	22.73	15.15	x
	3.13	24.21	20.99	26.50	18.94	x
	3.83	27.62	24.02	29.36	21.78	x
	4.59	30.20	26.34	34.09	26.52	x
	5.57	35.61	31.23	34.09	26.52	x
	6.21	39.70	34.87	38.82	23.67	x
	7.00	45.59	39.02	50.19	35.04	x
	7.64	48.55	43.91	48.30	33.14	x

TABLE 13 (CONTINUED)

Liquid	Pressure (katm.)	Maximum R_M	Minimum R_M	Maximum X_M	Minimum X_M	$R_M = X_M$ Satisfied
iso-	0.75	13.84	11.01	17.04	9.47	x
pentane	2.05	21.06	18.22	23.67	16.10	x
	3.22	26.21	22.86	33.14	25.57	x
	3.93	31.42	27.43	28.41	20.83	x
	4.74	34.84	30.46	39.77	32.20	x
	5.50	39.70	34.87	45.45	30.30	x
	6.17	44.90	39.18	44.51	29.36	x
	6.85	49.64	44.88	53.03	37.88	x
	7.50	54.92	49.65	60.61	45.45	x
methyl-	0	18.80	16.10	23.67	16.10	x
cyclo-	0.49	24.21	21.00	27.46	19.89	x
hexane	1.00	30.33	26.46	35.98	28.41	x
	2.42	51.11	46.23	56.82	41.67	x
	2.46	53.57	48.42	60.61	45.45	x
	3.18	71.09	64.39	72.92	57.76	x
	3.97	88.79	81.71	92.80	77.65	x
	4.75	117.58	108.30	118.4	103.2	x
	6.12	178.2	161.0	199.8	161.9	x
	6.81	232.3	209.9	241.5	203.6	x
	7.96	301.3	272.3	343.8	305.9	
toluene	0	15.65	12.56	18.94	11.36	x
	0.3	19.45	16.74	18.94	11.36	x
	0.4	21.89	18.93	24.62	17.04	x
	0.4	21.51	18.54	24.62	17.04	x
	0.5	24.21	20.99	29.36	21.78	x
	2.02	37.80	33.16	35.98	28.41	x
	3.01	47.07	42.56	48.30	33.14	x
	3.92	59.37	53.57	61.55	46.40	x
	4.62	68.51	62.07	73.86	58.71	x
	5.47	88.09	81.13	92.80	77.65	x
	6.35	110.1	102.1	107.0	91.86	x
	7.37	148.6	134.2	161.0	123.1	x

TABLE 13 (CONTINUED)

Liquid	Pressure (katm.)	Maximum R_M	Minimum R_M	Maximum X_M	Minimum X_M	$R_M = X_M$ Satisfied
			Data Run 20kc-III			
normal-pentane	0.4	10.91	7.79	14.20	6.68	x
	2.00	21.74	18.28	25.76	18.13	x
	4.10	35.32	30.47	39.12	31.49	x
	5.00	37.53	32.41	55.34	40.08	
	6.20	44.04	39.47	49.62	34.35	x
	6.80	48.82	43.84	61.07	45.80	x
	8.01	59.62	53.67	66.79	51.53	x
	8.50	65.03	58.66	70.61	55.34	x
methyl-cyclo-hexane	1.04	30.37	26.00	34.35	26.72	x
	1.93	46.67	41.83	54.39	39.12	x
	3.93	104.71	96.12	105.9	90.65	x
	5.66	200.4	180.5	189.9	151.7	x
	5.66	201.8	181.8	204.2	166.0	x
	6.60	271.6	245.0	261.4	223.3	x
	7.74	365.9	330.7	376.0	337.8	x
	8.64	491.1	443.8	512.4	474.2	x
			Data Run 60kc-II			
iso-pentane	0.1	14.27	4.27	15.36	8.53	x
	2.21	44.64	36.18	30.72	10.24	
	4.80	66.36	56.55	61.43	40.96	x
	5.45	84.73	70.18	73.38	52.90	x
	6.89	94.73	82.73	88.74	68.26	x
	7.95	109.7	96.82	49.49	29.01	
normal-octane	0.3	27.64	16.36	30.72	23.89	x
	1.22	56.36	46.91	44.37	23.89	
	2.43	72.36	62.18	76.79	56.31	x
	2.44	72.82	62.46	73.38	52.90	x
	3.20	84.18	72.91	97.27	76.79	x
	4.09	121.5	107.6	98.98	78.50	

TABLE 13 (CONTINUED)

Liquid	Pressure (katm.)	Maximum R_M	Minimum R_M	Maximum X_M	Minimum X_M	$R_M = X_M$ Satisfied
normal-octane (cont'd)	4.10	123.6	110.1	95.56	75.09	
	5.31	186.7	155.3	155.3	134.8	x
methyl-cyclo-hexane	0.2	36.00	24.73	40.96	34.13	x
	0.73	61.09	48.73	56.31	49.49	x
	2.34	103.5	93.64	97.27	76.79	x
	3.56	133.3	121.3	143.4	122.9	x
	4.77	202.7	176.2	174.1	153.6	
	6.49	314.2	274.9	298.6	278.2	x
	7.94	478.2	345.1	426.6	392.5	x
toluene	0.1	32.91	23.46	37.54	30.72	x
	0.98	49.27	37.64	42.66	35.84	x
	2.22	71.82	60.91	66.55	59.73	x
	3.32	92.09	82.82	88.74	81.91	x
	4.67	124.6	114.0	110.9	90.44	
	5.82	164.8	151.6	121.2	100.7	
	7.29	244.2	214.0	182.6	162.1	
	7.93	290.0	254.7	198.0	177.5	

R_M and X_M values are given for all liquids at the pressures at which measurements were made. An "x" in the last column of this table indicates that $R_M = X_M$ is satisfied.

For all measurements at 20 kc $R_M = X_M$ within the limits of experimental precision, with an occasional sporadic exception. Thus, no viscoelasticity is observed at 20 kc. This frequency is equivalent to a shear rate of 1.25×10^5 sec.$^{-1}$. The assumption that all liquids were non-viscoelastic, and R_E versus frequency for these liquids would lie on a single straight line at a given pressure as used in Figures 16 and 17 is justified.

For the measurements at 60 kc, equivalent to a shear rate of 3.77×10^5 sec.$^{-1}$, the criterion $R_M = X_M$ is also generally obeyed, and the construction of Figure 18 is justified. Departures from this criterion, while being more frequent, are again sporadic, with the exception of measurements on toluene at the highest pressures where the departure is systematic. Thus, it appears that the behavior of toluene at the highest pressures exhibits viscoelasticity at 60 kc. This observation is supported by the fact that the high pressure data for toluene are not on the straight lines representing the behavior of Newtonian liquids in Figure 18. Therefore η_1 and η_2 were calculated, for toluene at the four highest pressures investigated, according to Equations (18) and (19). Maximum and minimum limits for η_1 and η_2 were also calculated.

Use of the reduced frequency, Equations (26) and Equations (6) and (7), which relate η_1/η_o and η_2/η_o to $\lambda\omega$ for a Maxwellian viscoelastic liquid, can be used to estimate the shear relaxation time for toluene.

Differentiating Equation (7) with respect to ω and using the fact that $\lambda\omega < 1$ for frequencies below the relaxation frequency gives:

$$\frac{d}{d\omega}(\eta_2/\eta_o)_{\lambda\omega < 1} = \lambda \qquad (7a)$$

Rearringing Equation (6) and taking square roots gives:

$$\sqrt{\eta_o/\eta_1 - 1} = \omega\lambda \qquad (6a)$$

Therefore, a plot of η_2/η_o versis $\omega = 2\pi f$ will have a slope of λ. Likewise a plot of $\sqrt{\eta_o/\eta_1 - 1}$ versis ω will have a slope of λ. A reduced frequency, see Equations (26), was used to reduce the 60 kc measurements at various pressures to a series of frequencies at atmospheric pressure.

η_2/η_o versus reduced frequency is plotted in Figure 31 and $\sqrt{\eta_o/\eta_1 - 1}$ versus reduced frequency is in Figure 32. The solid lines in Figures 31 and 32 represent a least squares fit of the data points. The dashed lines represent a least squares fit of the data points plus the additional points: $\eta_2/\eta_o = 0$ at $f_r = 0$ in figure 31; and $\sqrt{\eta_o/\eta_1 - 1} = 0$ at $f_r = 0$ in Figure 32. These points are the theoretical intercepts on the graphs of Figures 31 and 32 and may be

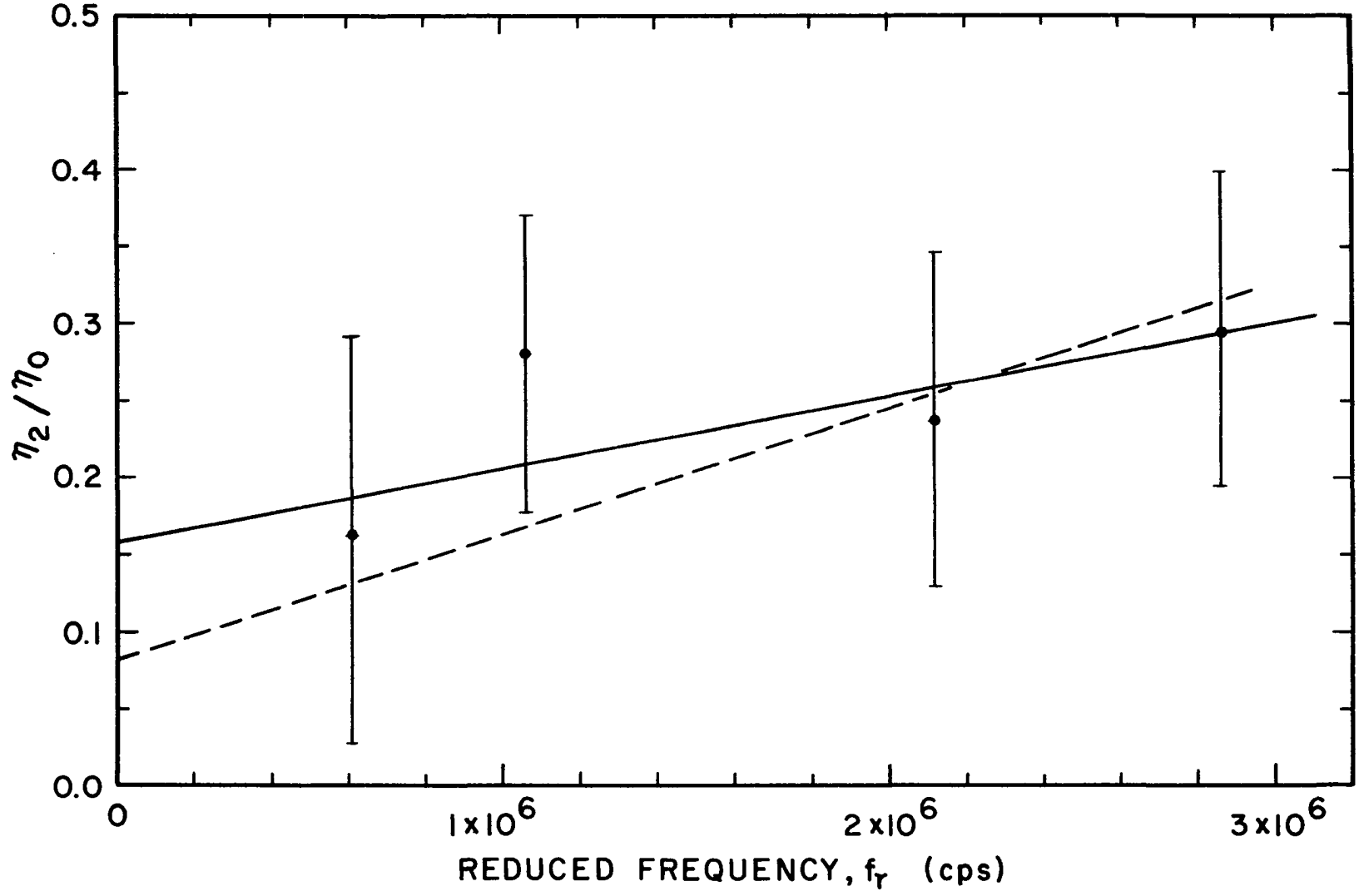

Figure 31. Correlation to Determine the Relaxation Time for Toluene (60kc-II) from the Imaginary Part of the Complex Viscosity

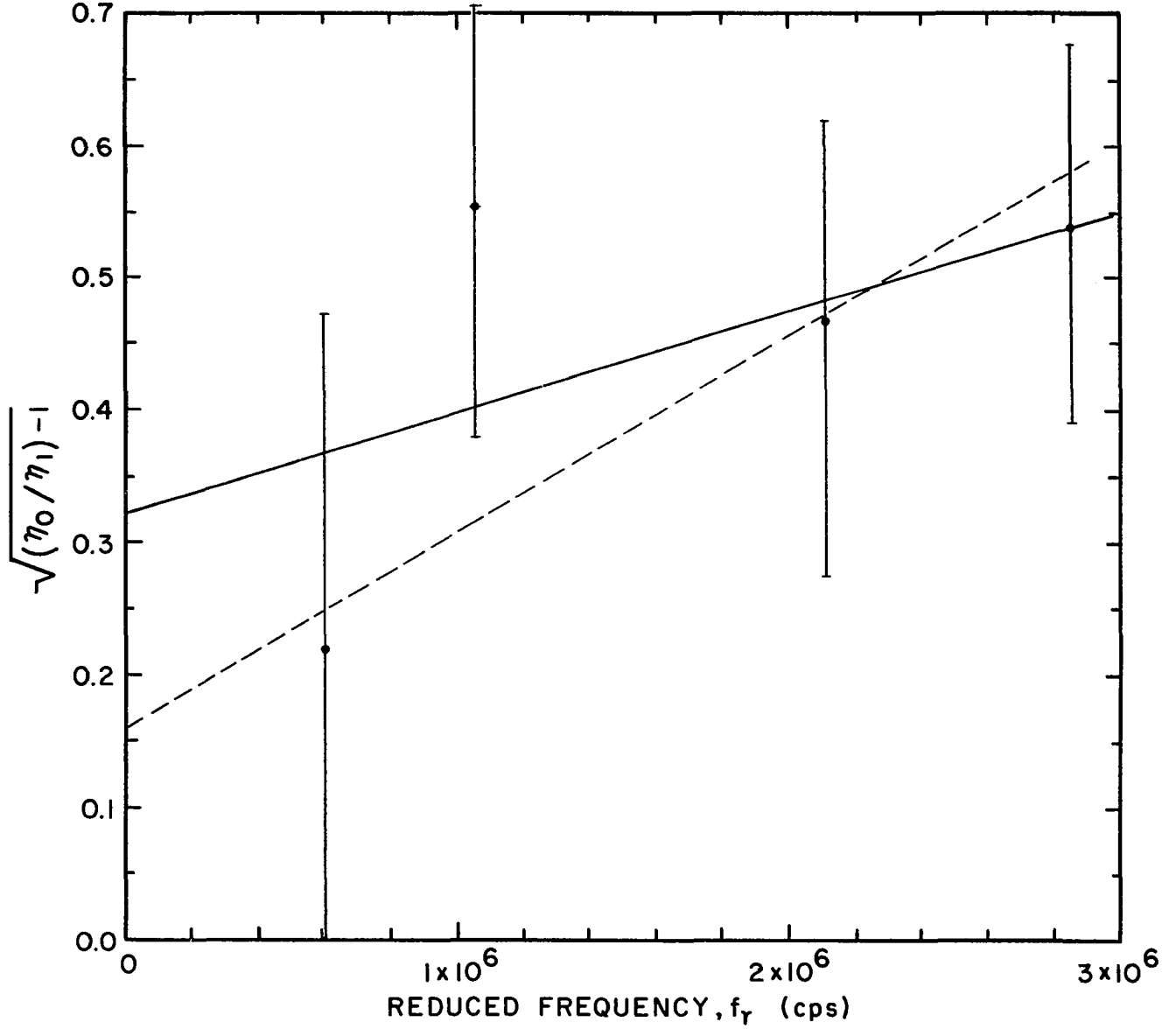

Figure 32. Correlation to Determine the Relaxation Time for Toluene (60kc-II) from the Real Part of the Complex Viscosity

assumed to be valid for this investigation because $\eta_2 = 0$ for toluene at low pressures, which correspond to low f_r, and because in toluene at low pressures, $\eta_1 = \eta_o$.

λ, obtained from the least squares slopes representing the data in Figures 31 and 32, together with ω_{relax} ($\omega\lambda = 1$ at the relaxation frequency) and f_{relax} are listed in Table 14. For both plots, the result of including the theoreti-

TABLE 14

SUMMARY OF CALCULATED VALUES FOR THE RELAXATION TIME, λ, AND THE RELAXATION FREQUENCIES, ω_{relax} AND f_{relax} FOR TOLUENE

	λ (sec.)	ω relax (radians/ sec.)	f_{relax} (cps.)
Calculations based on data obtained by least squares fit of data from Figure 31.			
Excluding the origin	7.48×10^{-9}	1.34×10^{8}	2.13×10^{7}
Including the origin	1.32×10^{-8}	7.58×10^{7}	1.21×10^{7}
Calculations based on data obtained by least squares fit of data from Figure 32.			
Excluding the origin	1.19×10^{-8}	8.40×10^{7}	1.34×10^{7}
Including the origin	2.35×10^{-8}	4.26×10^{7}	6.78×10^{6}

cal point ($y = 0$, $x = 0$) is that the slope, and thus λ, is

increased by a factor of 2. Notice that relaxation times calculated from η_2/η_o versus ω agree, within a factor of 2, with those calculated from the independent data; $\sqrt{\eta_o/\eta_i - 1}$ versus ω. Thus λ calculated from one set of data is confirmed by the other set. From these calculations it is apparent that toluene possesses a shear relaxation time of 7.5×10^{-9} to 2.4×10^{-8} sec., with the resultant relaxation frequency, f_{relax}, being between 6.8×10^6 cps. and 2.1×10^7 cps.

This range of values of the relaxation frequency for toluene is considerably less than 10^9 to 10^{10} cps. assumed by Barlow and Lamb (3) for monoaromatic liquids. Unfortunately, structures of the components in the lubricating oils investigated by Barlow and Lamb were not known in more detail. Therefore, it is impossible to discern if toluene is an exception to a general rule that monoaromatic liquids have a shear relaxation frequency of 10^9 to 10^{10} cps. or if the η_2 versus frequency peaks Barlow and Lamb observed were representative of a classification other than triaromatic, diaromatic, monoaromatic, saturate. From a structural consideration of shear it may be that perturbances from the main molecular structure, such as chain branches, and substitutions in aromatics are important in controlling shear relaxation in liquids. No shear relaxation was observed in the saturated hydrocarbons at reduced frequencies up to 3 megacycles which is in accord with Barlow's and Lamb's conclusions.

The probable relaxation times calculated for toluene are much lower than 5×10^{-7} sec. deduced from the data of Harrison, et al. (14). Evidently the shear relaxation of toluene in these solutions was restricted by interactions with the polymer molecules, thus giving higher relaxation times.

CHAPTER IV

CONCLUSIONS AND RECOMMENDATIONS

Conclusions

(1) The torsionally vibrating quartz rod may be used as a high pressure viscometer. Within the range of experimental error, this viscometer reproduces accepted viscosity as a function of pressure data for the following liquids, which were found to be Newtonian: propane, normal-pentane, iso-pentane, normal-octane, methyl-cyclohexane and toluene (low shear rate).

(2) When using the torsionally vibrating rod as a high pressure viscometer the effect of pressure on the resonant frequency of the rod must be considered. This pressure effect has been measured for 20-kc and 60-kc crystals. A graph indicating the change in resonant frequency with pressure is given. As predicted, the change in resonant frequency with pressure was 3 times as great for a 60-kc crystal as with a 20-kc crystal. The change in resonant frequency with pressure of any of the crystals can be represented within 1 cps. by $\Delta f_o/f_o = -2.601 \times 10^{-5} + 1.689 \times 10^{-4}P + 1.216 \times 10^{-5}P^2$, where P is in katm. and f_o is in cps. This relation is valid for 20-kc and 60-kc crystals in the pressure range 0.5 katm. to 8 katm.

(3) Of the liquids studied, only toluene exhibits viscoelasticity. Using a reduced frequency variable, 60-kc measurements at various pressures were reduced to a series of frequencies at atmospheric pressure, from which it was deduced that toluene has a shear relaxation time between 7.5×10^{-9} sec. and 2.4×10^{-8} sec. This value can be reconciled with a deduction from investigations of viscoelasticity of polystyrene solutions in toluene (14) by assuming that the shear relaxation of toluene in these polymer solutions is complicated by the polymer molecules. The measured relaxation time cannot be reconciled with the data of Barlow and Lamb (3) because sufficient data about the structures of the lubricating oils they used are not available.

(4) K_r depends on the electrical environment of the crystal while K_f is independent of the electrical environment. Assuming that the change in K_f with pressure is negligible so that the value of K_f obtained at atmospheric pressure is always applicable, Equation (30a) can be used to determine the effective K_r value for measurements in the electrical environment of the high pressure cell.

$$K_r = -(\Delta R_E/\Delta f)K_f \qquad (30a)$$

The random variation of $\Delta f/\Delta R_E$ with pressure is assumed to indicate that $\Delta f/\Delta R_E$ is independent of pressure and for each crystal an average of $\Delta f/\Delta R_E$ values for all pressures is used in Equation (30a).

Recommendations

(1) The greatest amount of experimental error is caused by inaccuracy of the impedance bridge, especially at 60 kc, and by a lack of precision of the electronic counter. In the calculation of viscosity this error is greatly magnified because the calculations involve functions of resistance squared and frequency squared. Therefore, for future investigations it is recommended that an impedance bridge be obtained which will have a maximum error at high parallel resistances, R_E, of not greater than ± 3% at all frequencies. The error will be less at low R_E. The bridge should be able to measure parallel resistance up to 50-60 megΩ. An impedance bridge fulfilling these requirements is not available commercially. Also, a counting device should be obtained which will be precise to at least ± 0.25 cps. A Hewlett-Packard Model #521-C Electronic Counter will fulfill the needs of a precise counter.

(2) Inconsistencies in the 60-kc measurements are attributed to a poor crystal mounting. The difficulty in mounting this crystal and smaller crystals might be overcome by using a different type of mounting. Although electrical connections to the crystal would be made on the electrodes, midway between the crystal ends, as in the present mounting, the crystal might be supported better in the center of the crystal ends.

(3) The combination of high pressure and high shear rates simulated by these experiments should be of value in

investigating the behavior of lubricating oils which may actually be subject to the conditions of high pressure and shear rate. Such an investigation is recommended. In addition, a detailed chemical analysis of the oils would be helpful in determining structural causes for viscoelasticity and corroborating the hypothesis of Barlow and Lamb (3) regarding gross structural causes of viscoelasticity.

(4) The atmospheric pressure frequency range of the torsionally oscillating crystal viscometer is increased by using reduced frequency in combination with high pressure and low temperature. High pressure is much more effective for increasing the reduced frequency than is low temperature. In the pressure range 1atm. - 10 katm. reduced frequency increases by approximately 2 decades for many simple liquids. Combined use of reduced frequency and high pressure might be used to investigate structural causes of viscoelasticity in simple liquids except that the method is subject to severe limitations. The limitations are: (a) the liquids must be non-conducting; (b) in order to benefit from the reduced frequency, the liquids must not freeze in the pressure range (freezing can be overcome by using higher temperatures, but using higher temperatures defeats the purpose of high pressure by decreasing the reduced frequency) and; (c) the practical upper limit of reduced frequency obtainable, even with pressures on the order of 10 katm. is 6-8 x 10^6 cps. Crystals that have a resonant frequency above 60-80 kc. in air at atmospheric pressure are so small that mounting

problems become very severe.

Although it would be interesting to investigate directly the effect of molecular structure of simple liquids on viscoelasticity with the torsion crystal, because of the limitations listed above, the author is unaware of a series of liquids which could be used for such an investigation.

BIBLIOGRAPHY

1. Appeldoorn, J. K., Okrent, E. H. and Philippoff, W., "Viscosity and Elasticity at High Pressures and High Shear Rates," Proceedings American Petroleum Institute, 42 [III] (1962), p. 163.

2. Babb, S. E., Jr., and Scott, G. J., "Rough Viscosities to 10,000 Bars," The Journal of Chemical Physics, 40 (1964), p. 3666.

3. Barlow, A. J. and Lamb, J., "The Viscoelastic Behavior of Lubricating Oils Under Cyclic Shearing Stress," Proceedings of the Royal Society, A253 (1952), p. 52.

4. Bridgman, P. W., "The Effect of Pressure on the Viscosity of Forty-Three Pure Liquids," Proceedings of the American Academy of Arts and Sciences, 61 (1926), p. 57.

5. Bridgman, P. W., "Viscosities to 30,000 kg/cm^2," Proceedings of the American Academy of Arts and Sciences, 77 (1949), p. 117.

6. Bridgman, P. W., "The Volume of Eighteen Liquids as a Function of Pressure and Temperature," Proceedings of the American Academy of Arts and Sciences, 66 (1931), p. 185.

7. Bridgman, P. W., The Physics of High Pressure, London: G. Bell and Sons, Ltd., 1952, p. 131.

8. Bridgman, P. W., "Further Rough Compressions to 40,000 kg/cm^2, Especially Certain Liquids," Proceedings of the American Academy of Arts and Sciences, 77 (1949), p. 129.

9. Cady, W. G., Piezoelectricity, New York: McGraw-Hill Book Company, Inc., 1946, p. 417.

10. DeWitt, T. W., Markovitz, H., Padden, F. J., and Zapas, L. J., Journal of Colloid Science, 10 (1955), p. 174.

11. Giebe, E. and Scheibe, A., "Piezoelektrische Erregung von Dehnungs-, Biegungsund und Drillungsschwingungen bei Quarzstäben," Zeitschrift für Physik, 46 (1927 and 1928), p. 607.

12. Greenidge, R. M. C., "The Mounting and Fabrication of Plated Quartz Crystal Units," The Bell System Technical Journal, 23 (1944), p. 234.

13. Hague, B., Alternating Current Bridge Methods, London: Sir Isaac Pitman and Sons, Ltd., 1943.

14. Harrison, G., Lamb, J. and Matheson, A. J., "The Viscoelastic Properties of Dilute Solutions of Polystyrene in Toluene," Journal of Physical Chemistry, 68 (1964), p. 1072.

15. Impedance Bridges Assembled from Laboratory Parts, Cambridge, Mass: General Radio Company. Reprinted from the General Radio Experimenter.

16. Mason, W. P., "Measurement of the Viscosity and Shear Elasticity of Liquids by Means of a Torsionally Vibrating Crystal," Transactions of the American Society of Mechanical Engineers, 69 (1949), p. 359.

17. Mason, W. P., Piezoelectric Crystals and Their Application to Ultrasonics, New York: D. Van Nostrand Company, Inc., 1950, p. 342.

18. Mason W. P., Ibid., p. 91.

19. Michels, A. and Pérez, J. P., "Déplacement de la Fréquence Piézoelectrique du Quartz Sous Haute Pression," Physica, 17 (1951), p. 563.

20. Philippoff, W., "Viscoelasticity of Polymer Solutions at High Pressures and Ultrasonic Frequencies," Journal of Applied Physics, 34 (1963), p. 1507.

21. Reiner, M., "Cross Stresses in Laminar Flow of Liquids," Physics of Fluids, 3 (1960), p. 427.

22. Rouse, P. E., Jr. and Sittel, K., "Viscoelastic Properties of Dilute Polymer Solutions," Journal of Applied Physics, 24 (1953), p. 690.

23. Rouse, P. E., Jr., Bailey, E. D. and Minkin, J. A., "Factors Affecting the Precision of Viscosity Measurements with the Torsion Crystal," Proceedings of American Petroleum Institute, 30M [III] (1950), p. 54.

24. Sage, B. H. and Lacey, W. N., Thermodynamic Properties of the Lighter Paraffin Hydrocarbons and Nitrogen, New York: American Petroleum Institute, 1950.

25. Spriggs, T. W. and Bird, R. B., "Some Nonlinear Viccoelastic Models with Inclusion of Results from Molecular Theory," I & EC Fundamentals, 4 (1965), p. 182.

APPENDIX A

NOMENCLATURE

A	A material constant = $\frac{1}{2}\sqrt{c_{66}/\rho}$, a constant
a_{TP}	Shift factor for reduced frequency
a_o, a_1, a_2	Constants for least squares fit of data
B	A material constant
C	Capacitance
C_{gap}	Capacitance in parallel with unknown in impedance bridge
C_{po}	Capacitance in parallel with C_1, P arm of impedance bridge
C_S	Capacitor in impedance bridge
C_{Seff}	Effective value of C_S, $(C_S + C_{sg})$
C_{sg}	Capacitance in parallel with C_S in impedance bridge
C_o	Capacitance in parallel with RLC representation of the crystal.
C_1	Variable capacitor in impedance bridge
C_{1eff}	Effective value of C_1, $(C_1 + C_{po})$
c_{66}	Elastic shear modulus for displacement in the Y direction with respect to X
D	Total extension of a spring and dashpot
f	Frequency; resonant frequency
f_r	Reduced frequency
f_o	Resonant frequency in air at atmospheric pressure

G	Shear modulus
G^*	Complex shear modulus
G_1	Imaginary part of complex shear modulus
G_2	Real part of complex shear modulus
i	Imaginary number, $\sqrt{-1}$
K_f	Calibration constant pertaining to frequency measurements
K_r	Calibration constant pertaining to resistance measurements
L	Inductance
ℓ	Length
P	Pressure; variable resistor in impedance bridge
Q	A resistor in the impedance bridge; quality factor
r	Radial direction in cylindrical coordinates
R	Resistance
T	Absolute temperature
T_o	Reference temperature for reduced calculations
t	Time
u, v, w	Displacements in x, y, and z directions respectively
V	Specific volume
V_{500}	Specific volume at 500 kg/cm^2
v	Velocity
X	Reactance
x, y, z	Principal directions
z	Axial direction in cylindrical coordinates
Z	Impedance

Greek Letters

$\alpha, \beta, \gamma, \delta$	Constants in Bridgman's average fluid equation
γ	Shear strain
γ_s	Shear strain of spring
γ_d	Shear strain of dashpot
$\dot{\gamma}$	Shear rate
ϵ	Linear strain
η	Viscosity coefficient
η_c	Cross viscosity coefficient
$\eta_{rel.}$	η solution/η solvent
η_R	Viscosity coefficient calculated from resistance measurements only
η_X	Viscosity coefficient calculated from measurements of mechanical impedance only
η_o	Viscosity coefficient at low shear rate; viscosity coefficient at reference conditions for reduced variable calculations
η_1	Real part of complex viscosity coefficient
η_2	Imaginary part of complex viscosity coefficient
η^*	Complex viscosity coefficient
θ	Tangential direction in cylindrical coordinates
λ	Relaxation time
ρ	Density
ρ_o	Density at reference conditions for reduced variable calculations
τ	Shear stress
ω	Angular velocity

Subscripts

C	Refers to a capacitive quantity
c	Refers to the crystal
E	Refers to an electrical quantity
Eo	Refers to an electrical quantity in air at atmospheric pressure
L	Refers to an inductive quantity
M	Refers to a mechanical quantity
max	Refers to the maximum value of a quantity
min	Refers to the minimum value of a quantity
n	Refers to the nth element
P	Refers to a quantity measured at a pressure P
relax	Refers to a value at shear relaxation
T	Refers to a quantity measured at a temperature T
x, y, z	Refers to the x, y, and z directions respectively
θ	Refers to the tangential direction

APPENDIX B

CALIBRATION DATA FOR NATIONAL BUREAU OF STANDARDS

LIQUIDS, SAMPLE #1 and SAMPLE #2

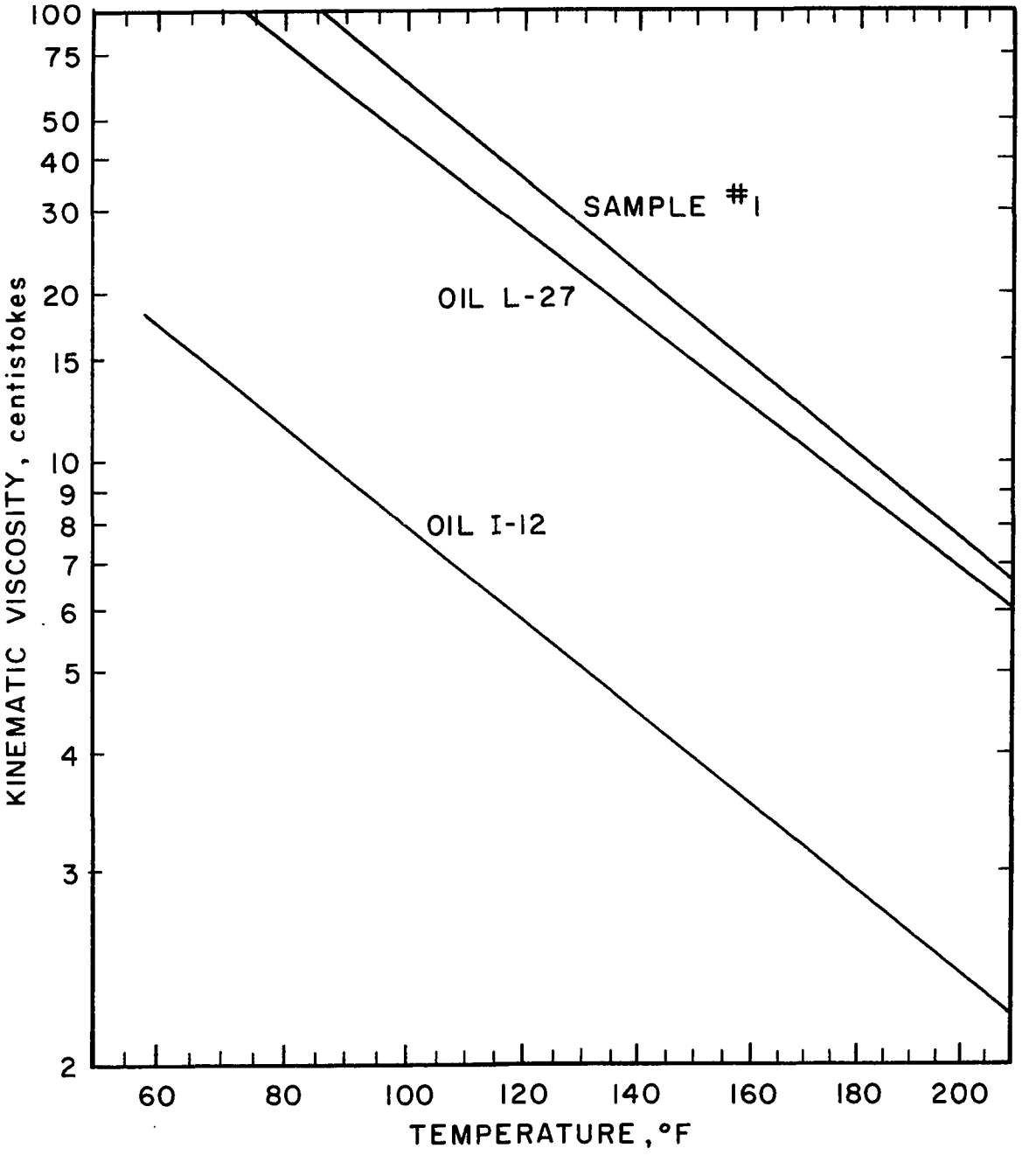

Figure B1. Changes in Viscosity with Temperature for National Bureau of Standards Liquids, Sample #1 and Sample #2 (Low Range).

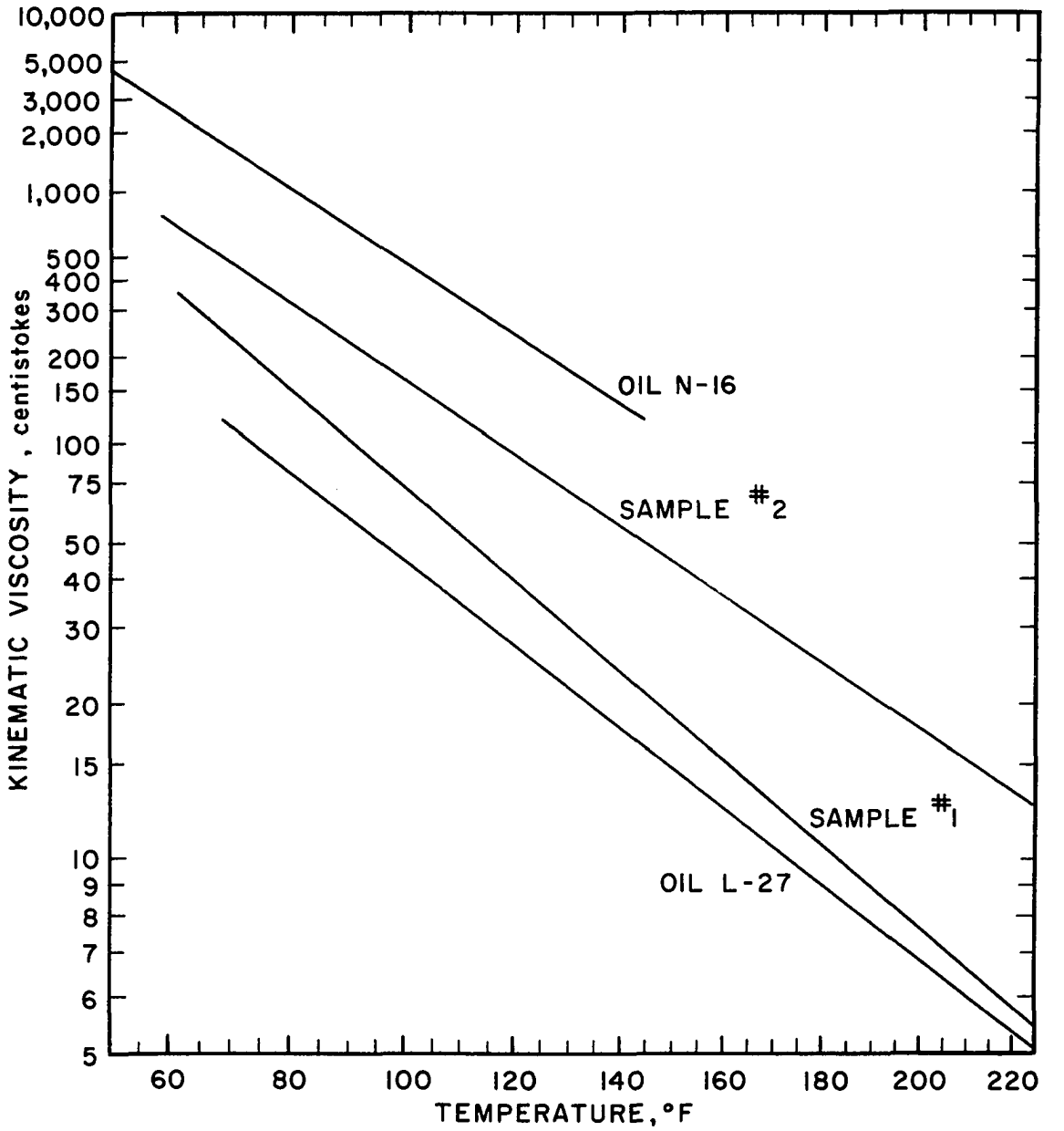

Figure B2. Changes in Viscosity with Temperature for National Bureau of Standards Liquids, Sample #1 and Sample #2 (High Range).

TABLE B1

DENSITY AS A FUNCTION OF TEMPERATURE FOR NATIONAL BUREAU OF STANDARDS LIQUIDS, SAMPLE #1 AND SAMPLE #2

Liquid	Temperature	Density (gm/cc)
Oil I-12	20°C	0.8439
	25°C	0.8406
	100°F	0.8322
	210°F	0.7915
Oil L-27	20°C	0.8745
	25°C	0.8713
	100°F	0.8633
	210°F	0.8249
Sample #1	75.5°F	0.879
	100°F	0.874
Sample #2	75.5°F	0.924
	100°F	0.918
Oil N-16	20°C	0.8873
	25°C	0.8843
	100°F	0.8766

APPENDIX C

DENSITY AS A FUNCTION OF PRESSURE

FOR LIQUIDS INVESTIGATED

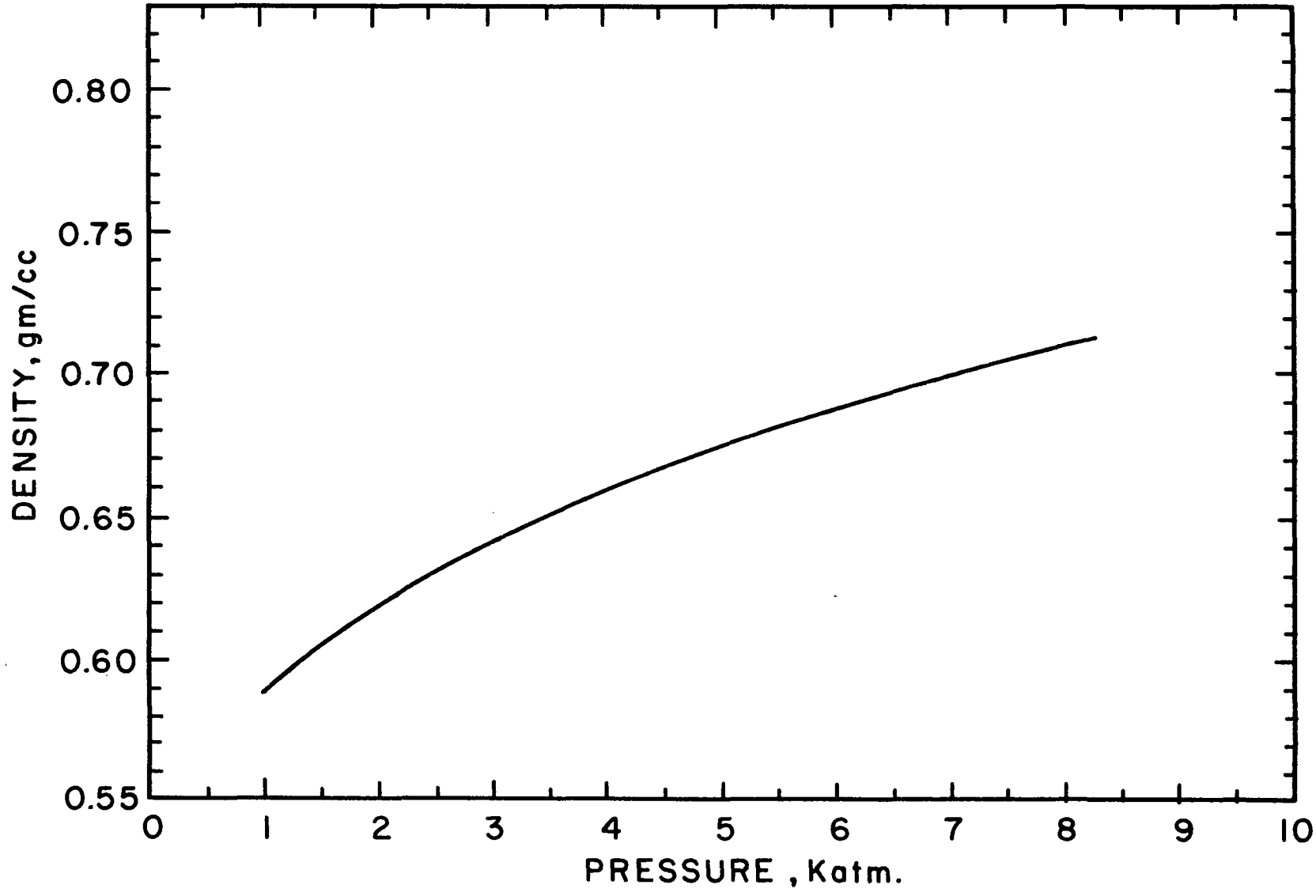

Figure C1. Dependence of the Density of Propane at 24°C on Pressure.

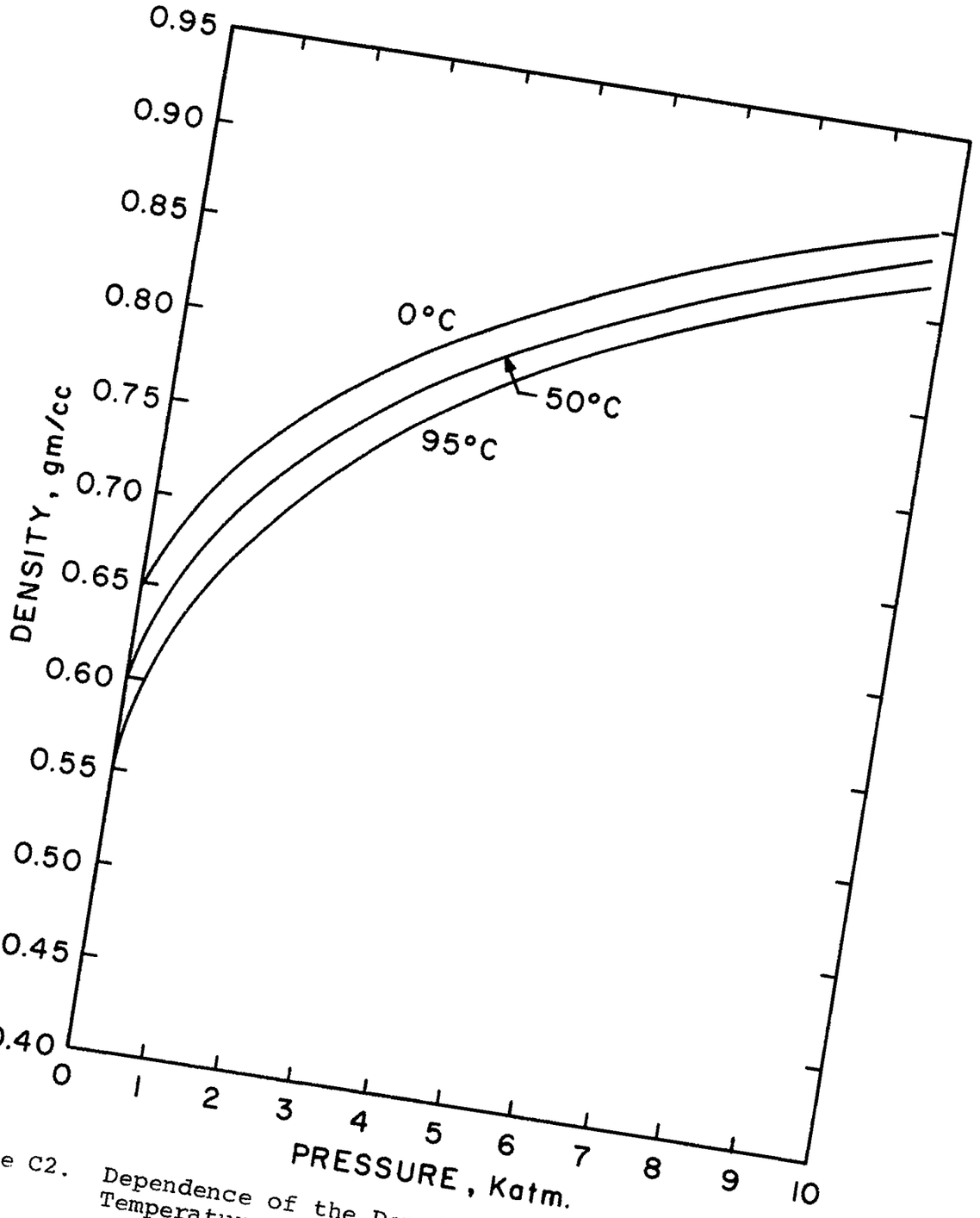

Figure C2. Dependence of the Density of n-Pentane on Temperature and Pressure.

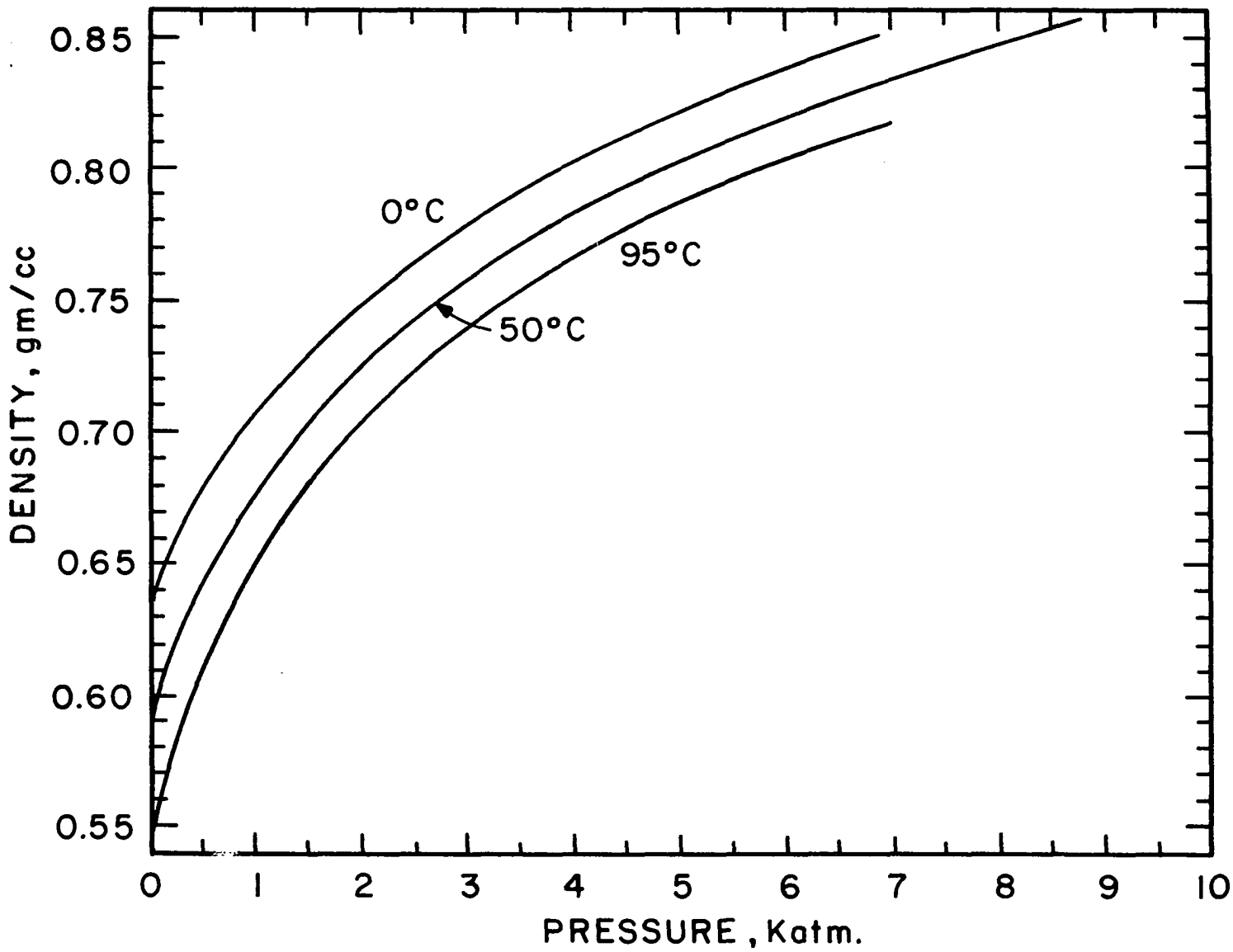

Figure C3. Dependence of the Density of i-Pentane on Temperature and Pressure.

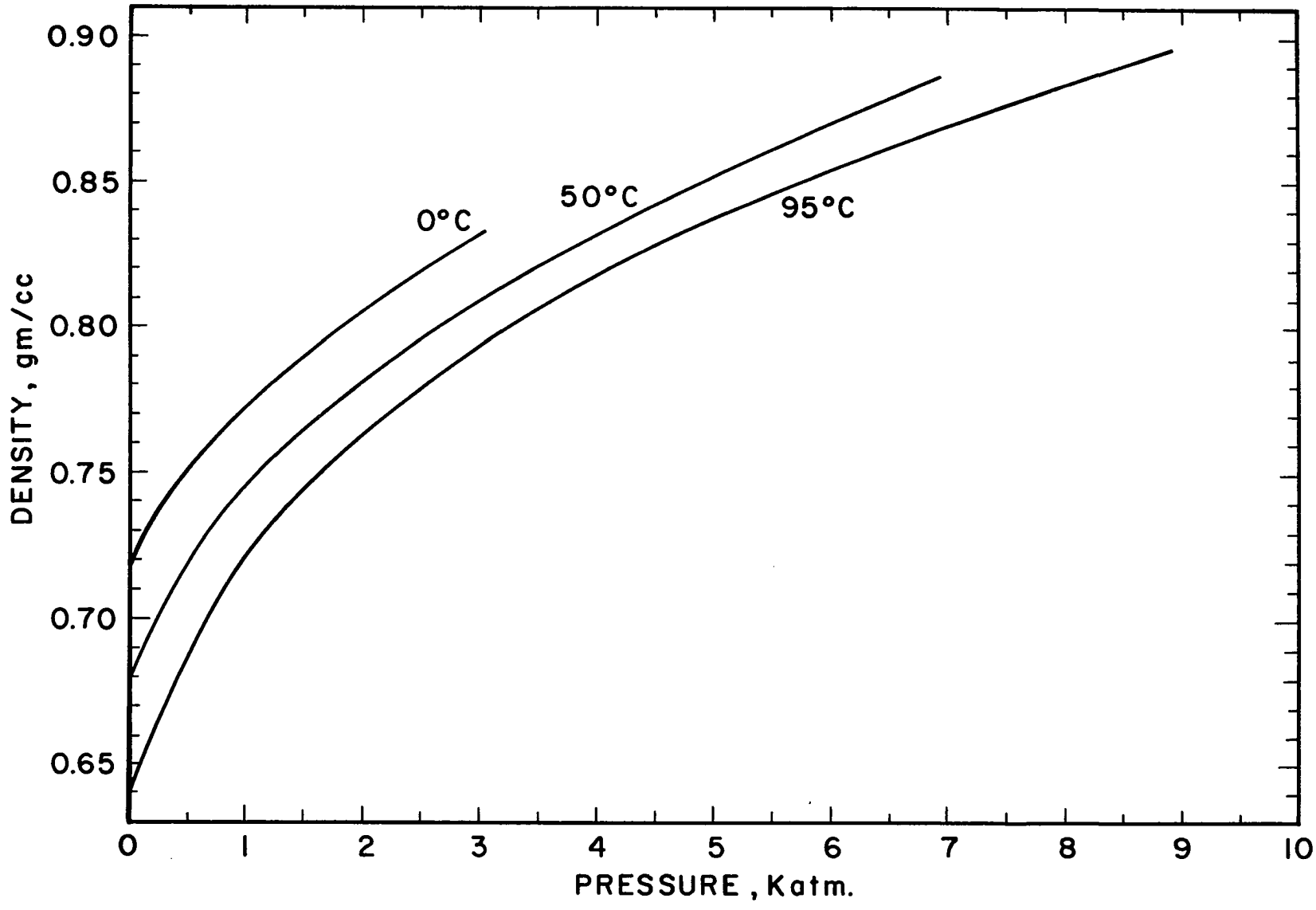

Figure C4. Dependence of the Density of n-Octane on Temperature and Pressure.

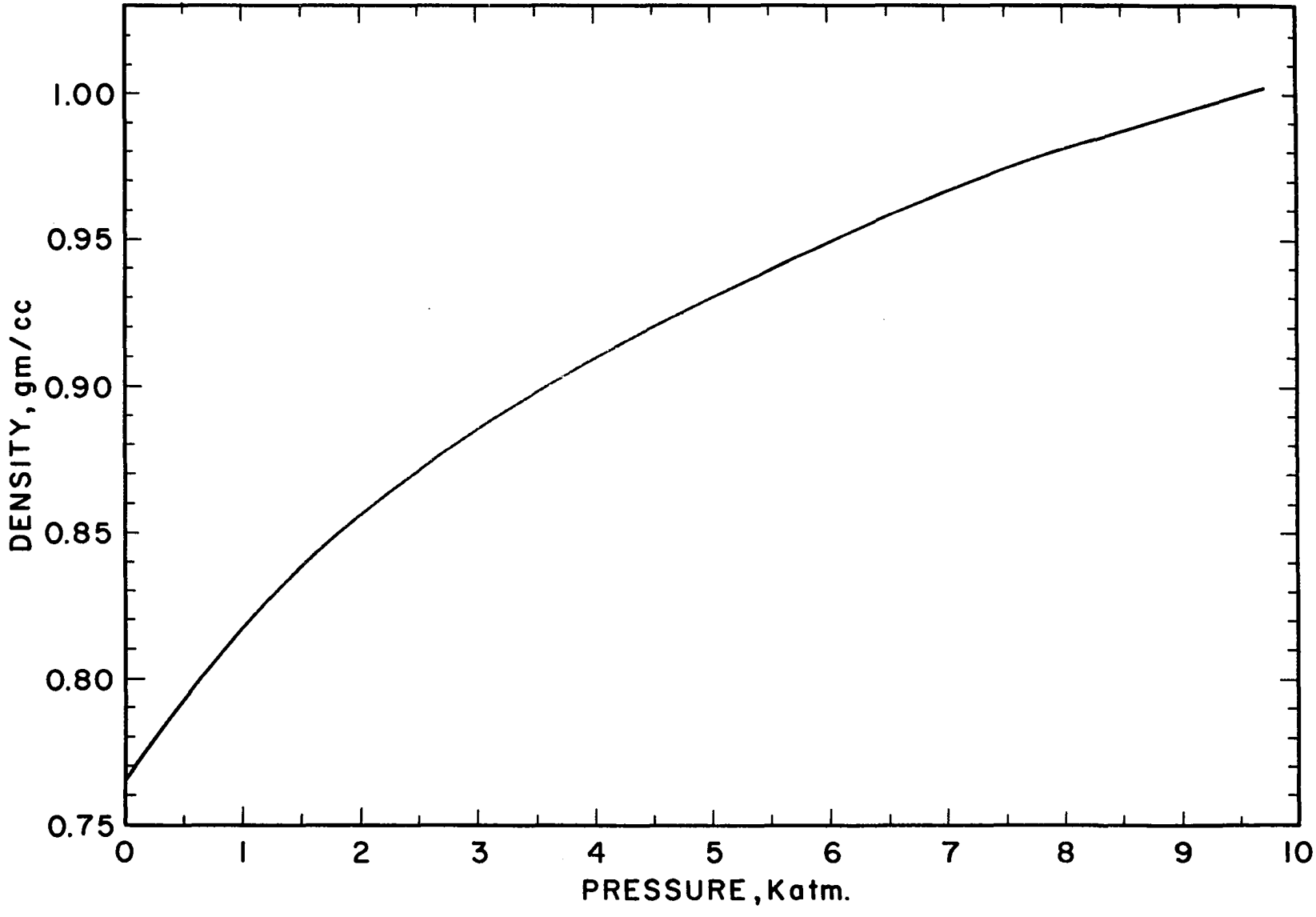

Figure C5. Dependence of the Density of Methylcyclohexane at 25°C on Pressure.

APPENDIX D

EFFECT OF PV WORK ON THE TEMPERATURE OF THE LIQUID IN THE HIGH PRESSURE CELL

The temperature change in the liquid subjected to a reversible, adiabatic, batch compression is considered. This assumption overestimates the actual temperature change because in reality as the liquid temperature is raised, the thermal capacity of the massive walls of the high pressure cell will soak-up most of the energy input. For a reversible, adiabatic compression

$$d\bar{H} = \bar{V}dP \tag{D1}$$

Also, considering temperature and pressure effects on enthalpy

$$d\bar{H} = \left(\frac{\partial \bar{H}}{\partial P}\right)_T dP + \left(\frac{\partial \bar{H}}{\partial T}\right)_P dT \tag{D2}$$

Noting that $\left(\frac{\partial \bar{H}}{\partial T}\right)_P$ is the heat capacity $\bar{C}_p$ and equating Equations (D1) and (D2) gives

$$\bar{V}dP = \bar{C}_p dT + \left(\frac{\partial \bar{H}}{\partial P}\right)_T dP \tag{D3}$$

or

$$dT = \frac{\bar{V}dP - \left(\frac{\partial \bar{H}}{\partial P}\right)_T dP}{\bar{C}_p} . \qquad \text{(D3a)}$$

Also

$$d\bar{H} = Td\bar{S} + \bar{V}dP \qquad \text{(D4)}$$

Since $\bar{S} = \bar{S}(P,T)$, then Equation D-4 becomes

$$\left(\frac{\partial \bar{H}}{\partial P}\right)_T = T\left(\frac{\partial \bar{S}}{\partial P}\right)_T + \bar{V} \qquad \text{(D4a)}$$

From the fact that

$$d\bar{F} = -\bar{S}dT + \bar{V}dP \qquad \text{(D5)}$$

is an exact differential the relation

$$\left(\frac{\partial \bar{S}}{\partial P}\right)_T = -\left(\frac{\partial \bar{V}}{\partial T}\right)_P \qquad \text{(D6)}$$

is obtained.

Substituting Equation (D6) into Equation (D4a) gives

$$\left(\frac{\partial \bar{H}}{\partial P}\right)_T = -T\left(\frac{\partial \bar{V}}{\partial T}\right)_P + \bar{V}. \qquad \text{(D7)}$$

Substitution of Equation (D7) into Equation (D3a) gives

$$dT = \frac{T\left(\frac{\partial \bar{V}}{\partial T}\right)_P dP}{\bar{C}_P} \qquad \text{(D8)}$$

Equation (D8) can be integrated if $\left(\frac{\partial \bar{V}}{\partial T}\right)_P$ and $\bar{C}_p$ are determined as functions of pressure.

$\bar{C}_p$ as a function of P may be obtained by noting that for a constant pressure process

$$d\bar{H} = Td\bar{S} = \bar{C}_p dT \tag{D9}$$

from which one attains

$$\frac{\bar{C}_p}{T} = \left(\frac{\partial \bar{S}}{\partial T}\right)_P \tag{D10}$$

Differentiating Equation (D10) with respect to P at constant T gives

$$\frac{1}{T}\left(\frac{\partial \bar{C}_p}{\partial P}\right)_T = \frac{\partial^2 \bar{S}}{\partial P \partial T}. \tag{D11}$$

Differentiation of Equation (D6) with respect to T at constant P gives

$$\frac{\partial^2 \bar{S}}{\partial P \partial T} = -\left(\frac{\partial^2 \bar{V}}{\partial T^2}\right)_P \tag{D12}$$

which upon substitution into Equation (D11) gives

$$\left(\frac{\partial \bar{C}_p}{\partial P}\right)_T = -T\left(\frac{\partial^2 \bar{V}}{\partial T^2}\right)_P. \tag{D13}$$

Bridgman (6) gives $\bar{V}(P)$ data for many liquids. His data for $\bar{V}(T,P)$ for n-pentane, a typical liquid used in this investigation, are shown in Figure 31. Notice that at all pressures except atmospheric, $\bar{V}$ is a linear function of T. $(\partial^2\bar{V}/\partial T^2)_P$ at atmospheric pressure is very small and can be neglected and $(\partial^2\bar{V}/\partial T^2)_P = 0$ at elevated pressures.

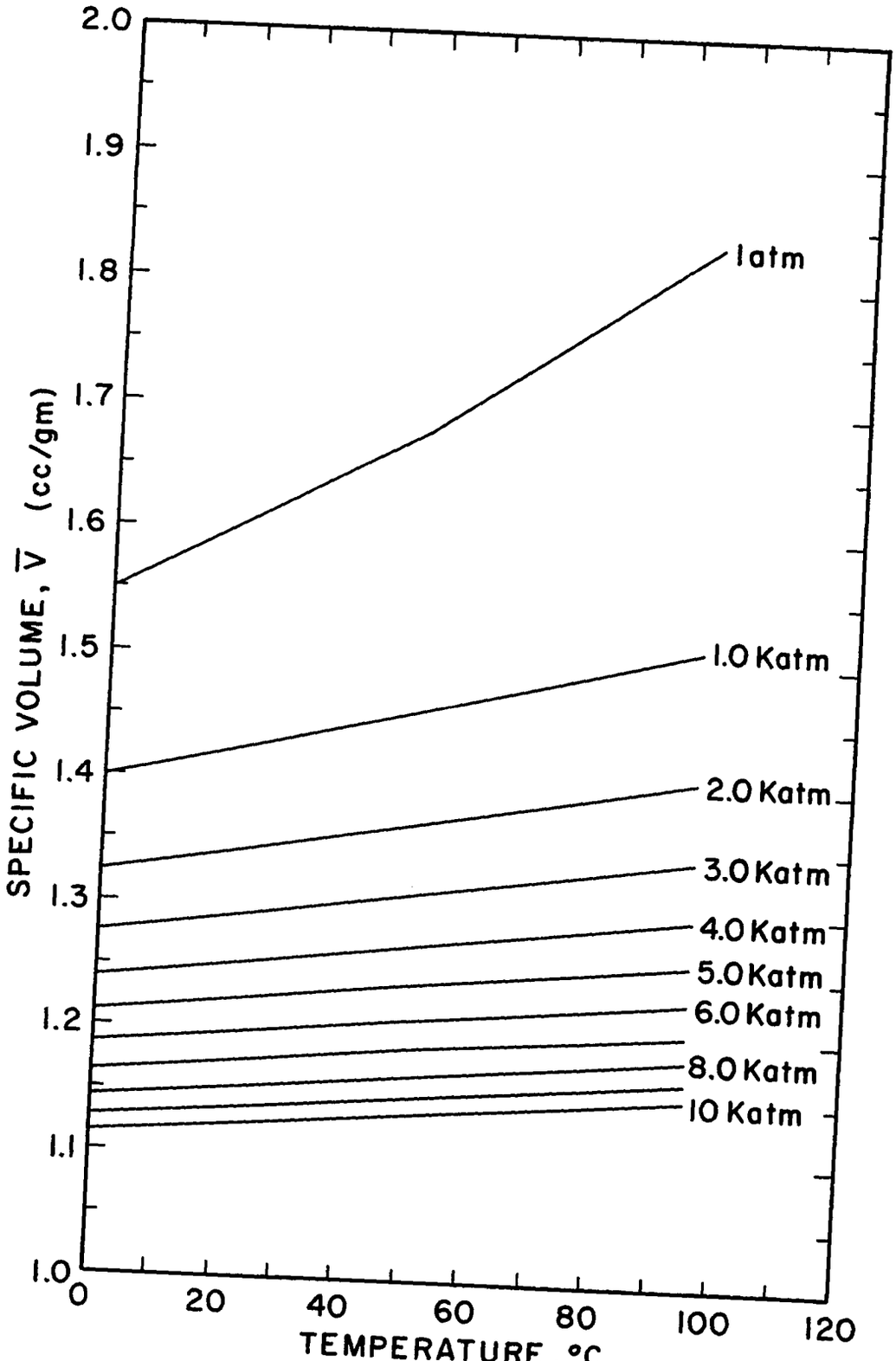

Figure D1. The Effects of Temperature and Pressure on the Specific Volume of n-Pentane.

It can thus be assumed that $\bar{C}_p$ is independent of pressure over the range 1 atm. to 10 katm. Then, assuming $\bar{C}_p$ is independent of temperature over the temperature range, Equation (D8) becomes upon integration

$$\bar{C}_p \ln \frac{T_2}{T_1} = \int_{1\text{ atm.}}^{10\text{ katm.}} \left(\frac{\partial \bar{V}}{\partial T}\right)_P dP \qquad \text{(D14)}$$

Using Bridgman's $\left(\frac{\partial \bar{V}}{\partial T}\right)_P$ data as a function of pressure and $\bar{C}_p = 0.527$ cal./gm.-^{o}C., integration of Equation (D3c) gives $\ln \frac{T_2}{T_1} = 0.341$. If $T_1 = 295^{o}$K, $T_2 = 415^{o}$K and $\Delta T = 120^{o}$C. However this temperature rise assumes that no heat is transferred to the vessel walls and oil bath.

Next consider the temperature rise that occurs in the liquid when the work of compression is absorbed by the cell walls as heat. The work $\int_{V_1}^{V_2} PdV$ can be calculated from the PVT data, given in Figure D1 for n-pentane. For a first approximation, calculate $\int PdV$ at 25^{o}C in order to obtain an order of magnitude of the energy input into the liquid. The work of the compression is equal to the sum of the heat lost to the high pressure cell and the increase in internal energy of the liquid. Thus at equilibrium

$$\int_{V_1}^{V_2} PdV = \left[(m\bar{C}_V)_{cell} + (m\bar{C}_V)_{liq.}\right] \Delta T \qquad \text{(D15)}$$

Since $\bar{C}_p$ is approximately equal to $\bar{C}_V$ for liquids and solids then D-15 becomes

$$\Delta T = \frac{\int_{V_1}^{V_2} PdV}{(mC_p)_{cell} + (mC_p)_{liq.}} \qquad \text{(D15a)}$$

$\int_{V_1}^{V_2} PdV$ for the reversible compression of the n-pentane at 25°C. in the cell to 10 katm. is 2,820 cal. For the steel cell $m\bar{C}_p$ is 20.65 cal./°C. $m\bar{C}_p$ of the liquid is 0.10 cal./°C. Therefore the temperature rise in the liquid after equilibrium is attained is 0.3°C. This temperature rise is still much greater than would be observed during the experiment because the 10 katm. compression used in the calculations is much greater than usual compressions. Normally pressure changes of 1-3 katm. were used. Also this calculation still neglects heat adsorbed by the oil bath surrounding the cell.

Temperature rises have been calculated for two extreme cases: (a) A reversible adiabatic compression in which no heat is adsorbed by the cell and (b) a reversible compression at 25°C in which the walls and liquid reach an equilibrium temperature.

It is desirable to determine the time required for the liquid to return to room temperature for the compression in (a) above, and for the liquid to attain the equilibrium temperature of (b) above if it had been subjected to an adiabatic compression.

For case (a) the heat associated with the temperature rise is transferred through the wall of the high pressure cell

to the surrounding oil bath. The thermal conductivity (k) of the cell is on the order of 0.041 (cal./sec.-cm.^{2}) (cm./$^\circ$C.). Bridgman (7), page 314, gives the thermal conductivity of n-pentane as a function of pressure up to about 12 katm. At 10 katm. the thermal conductivity of n-pentane is 0.00085 (cal./sec.-cm.^{2})(cm./$^\circ$C.). Because of the high thermal conductivity of the cell well, it is reasonable to assume that its temperature quickly reaches the temperature of the surrounding oil bath, which is at room temperature. It is then necessary to determine how long it takes the temperature of the liquid (n-pentane for these calculations) to come to room temperature. The differential equation for radial heat flow is:

$$\partial T/\partial t = \frac{k}{\rho C_p}\left[\frac{\partial^2 T}{\partial r^2} + \frac{1}{r}\frac{\partial T}{\partial r}\right] \qquad \text{(D16)}$$

McAdams* presents graphical solutions to Equation (D16) in terms of $Y = (T_a-T)/(T_a-T_b)$, $X = kt/C_p r_m^2$, $n = r/r_m$ and $m = k/r_m h$. The symbols used are:

T_a = Temperature of the surroundings (taken to be room temperature for these calculations)

T_b = Original temperature of the liquid in the cell

T = Temperature of the liquid in the cell at any time t

k = Thermal conductivity

*McAdams, William H. Heat Transmission, New York: McGraw-Hill Book Company, Inc., 1954, p. 41.

ρ = Density

C_p = Heat capacity of the liquid

r_m = Inside radius of the high pressure cell

r = Radial distance

h = Heat transfer coefficient between the liquid and the cell well

Using McAdam's solutions, and assuming negligible resistance to heat transfer between the liquid film on the cell wall and the cell wall (m = 0), the temperature of the liquid in the center of the cell, r = 0, is less than 0.1°C. above room temperature 20 minutes after the adiabatic compression of case (a).

Likewise, it would take less than 14 minutes for the average temperature of a liquid subjected to an adiabatic compression to attain the equilibrium ΔT of 0.3°C. calculated for case (b) in which heat adsorbed by the cell wall is included.

Because viscosity data were not taken until over 30 minutes after compression, it is apparent that temperature differences did not affect viscosity data.

APPENDIX E

DATA AND VISCOSITY CALCULATIONS

TABLE E1

DATA AND VISCOSITY CALCULATIONS FOR i-PENTANE AT 25°C (20kc-II)

Pressure (katm)	R_E (kΩ)	R_M (Ω)	R_M^2 (Ω^2)	f (cps)	f_o (cps)	ρ (gm/cc)	η_R (p)
.75	122	12.749	162.54	19900+	19903.75	.694	.00374
2.05	177	19.832	393.31	19903	19908.25	.736	.00855
3.22	215	24.726	611.38	19906	19913.75	.771	.0127
3.93	253	29.720	877.34	19911	19917.50	.786	.0179
4.74	278	32.839	1078.4	19913	19922.25	.804	.0215
5.50	314	37.475	1404.4	19917	19926.75	.817	.0275
6.17	350	42.112	1773.4	19921.50	19931.25	.828	.0343
6.85	391	47.392	2246.0	19924	19936	.830	.0429
7.50	430	52.414	2747.2	19928	19942	.846	.0560

$K_r = 7765$ $\quad K_f = -.264$

$R_o = 23k\Omega$ $\quad f_o = 19902$

TABLE E2

DATA AND VISCOSITY CALCULATIONS FOR n-PENTANE AT 25.6°C (20kc-II)

Pressure (katm)	R_E (kΩ)	R_M (Ω)	R_M^2 (Ω^2)	f (cps)	f_o (cps)	ρ (gm/cc)	η_R (p)
0	85	7.98	63.74	19900	19901.25	.621	.00164
0.05	95	9.27	85.97	19900	19901.50	.630	.00218
0.4	105	10.56	111.51	19900	19902.50	.668	.00267
0.4	109	11.08	122.66	19900	19902.50	.668	.00294
2.16	165	18.29	334.41	19904	19909	.748	.00715
3.13	200	22.79	519.57	19907+	19913	.777	.0107
3.83	225	26.01	676.73	19910	19916.75	.795	.0136
4.59	244	28.46	810.03	19913+	19921.25	.812	.0160
5.57	284	33.61	1129.8	19919	19927	.830	.0218
6.21	314	37.48	1404.4	19923	19931.25	.842	.0267
7.00	348	41.85	1751.8	19926	19937.25	.853	.0329
7.64	383	46.36	2149.3	19931	19941.75	.863	.0398

TABLE E3

DATA AND VISCOSITY CALCULATIONS FOR TOLUENE AT 23°C (20kc-II)

Pressure (katm)	R_E (kΩ)	R_M (Ω)	$R_{M_2}^2$ (Ω^2)	f_o (cps)	f (cps)	ρ (gm/cc)	η_R (p)
0	135	14.552	211.76	19901.25	19897+	.861	.00394
.3	165	18.287	334.41	19902	19898	.874	.00612
.4	183	20.605	424.57	19902.50	19897	.883	.00769
.4	180	20.218	408.77	19902.50	19897	.883	.00741
.5	200	22.794	519.57	19902.75	19896	.889	.00935
2.02	300	35.672	1272.5	19908.50	19900	.951	.0214
3.01	372	44.945	2020.0	19912.75	19902	.980	.0330
3.92	463	56.664	3210.8	19917.25	19903	1.003	.0512
4.62	531	65.421	4279.9	19921.50	19904	1.018	.0673
5.47	680	84.610	7158.8	19926.50	19904	1.035	.111
6.35	844	105.73	11179	19932.50	19906+	1.051	.170
7.37	1127	141.40	19995	19940.50	19903	1.067	.300

TABLE E4

DATA AND VISCOSITY CALCULATIONS FOR METHYLCYCLOHEXANE AT 25°C (20kc-II)

Pressure (katm)	R_E (kΩ)	R_M (Ω)	R_M^2 (Ω^2)	f (cps)	f_o (cps)	ρ (gm/cc)	η_R (p)
0	160	17.64	311.3	19896	19901.25	.765	.00651
.5	200	22.79	519.57	19896+	19902.50	.792	.0105
1.00	245	28.59	817.33	19896	19904.50	.817	.0160
2.42	402	48.81	2382.2	19897	19910	.868	.0439
2.46	420	51.13	2613.9	19896+	19910.25	.869	.0481
3.18	550	67.87	4606.1	19896+	19913.50	.889	.0829
3.97	685	85.25	7268.2	19895	19917.50	.908	.128
4.75	900	112.94	12756	19893	19922.25	.924	.221
6.12	1340	169.61	28767	19883	19930.75	.951	.484
6.81	1740	221.12	48894	19877	19935.75	.962	.813
7.96	2250	286.80	82254	19858	19943.75	.980	1.34

TABLE E5

DATA AND VISCOSITY CALCULATIONS FOR PROPANE AT 26°C (20kc-II)

Pressure (katm)	R_E (kΩ)	R_M (Ω)	R_M^2 (Ω^2)	f (cps)	f_o (cps)	ρ (gm/cc)	η_R (p)
.37	84	9.272	85.97	19900+	19902.50	.564	.00244
.93	98	11.075	122.66	19901	19904	.585	.00335
2.40	123	14.294	204.32	19905	19910	.627	.00521
3.85	145	17.128	293.37	19912	19917	.655	.00716
4.39	155	18.415	339.11	19914	19920	.664	.00817
4.52	149	17.643	311.28	19915	19921	.665	.00749
5.50	164	19.575	383.18	19921	19926.75	.681	.00900
6.34	172	20.605	424.57	19927	19932.50	.691	.00983
7.17	182	21.893	479.30	19933	19938	.700	.0110
8.00	212	25.756	663.37	19939+	19944.25	.710	.0149

R_o = 12 kΩ

TABLE E6

DATA AND VISCOSITY CALCULATIONS FOR n-PENTANE AT 22°C (20kc-III)

Pressure (katm)	R_E (kΩ)	R_M (Ω)	R_M^2 (Ω^2)	f (cps)	f_o (cps)	ρ (gm/cc)	η_R (p)
.4	125	9.695	93.99	19894+	19897	.665	.00226
2.00	201	20.221	408.89	19897+	19903	.742	.00882
4.10	294	33.102	1095.7	19903	19912.25	.802	.0213
5.00	309	35.180	1237.6	19905	19917.50	.822	.0241
6.20	357	41.828	1749.6	19914	19925	.841	.0333
6.80	390	46.398	2152.8	19916+	19930.25	.852	.0404
8.01	464	56.648	3209.0	19923	19938.50	.869	.0591
8.50	502	61.911	3833.0	19926	19942.50	.870	.0705

$K_r = 7220$ $K_f = -262$

$R_o = 55k\Omega$ $f_o = 19895$

TABLE E7

DATA AND VISCOSITY CALCULATIONS FOR METHYLCYCLOHEXANE AT 18°C (20kc-III)

Pressure (katm)	R_E (MΩ)	R_M (Ω)	R_M^2 (Ω^2)	f (cps)	f_o (cps)	ρ (gm/cc)	η_R (p)
1.04	.260	28.393	806.2	19890.50	19898.50	.819	.0157
1.93	.375	44.321	1964.4	19889.50	19901.75	.857	.0367
3.93	.780	100.42	10084	19885.50	19911.25	.912	.177
5.66	1.43	190.44	36267	19877.50	19922.25	.948	.612
5.66	1.44	191.83	36798	19874.75	19922.25	.948	.621
6.60	1.92	258.31	667 24	19865.50	19929	.964	1.11
7.74	2.57	343.34	121341	19843.50	19937	.982	1.98
8.64	3.43	467.52	218575	19814	19943.25	.994	3.52

TABLE E8

DATA AND VISCOSITY CALCULATIONS FOR i-PENTANE AT 25°C (60kc-II)

Pressure (katm)	R_E (kΩ)	R_M (Ω)	R_M^2 (Ω^2)	f (cps)	f_o (cps)	ρ (gm/cc)	η_R (p)
.10	222	0.818	096.40	59434.50	59438	.625	.000825
2.21	307	40.73	1659	59454.50	59460.50	.741	.0120
4.80	365	61.82	3822	59484.50	59499.50	.805	.0254
5.45	404	76.00	5776	59492.50	59514	.816	.0379
6.89	440	89.09	7937	59515.50	59538.50	.838	.0507
7.95	480	103.6	10740	59548.50	59560	.854	.0673

$R_o = 195k\Omega$ $f_o = 59437$

$K_r = 2750$ $K_f = -.293$

TABLE E9

DATA AND VISCOSITY CALCULATIONS FOR n-OCTANE AT 25°C (60kc-II)

Pressure (katm)	R_E (kΩ)	R_M (Ω)	R_M^2 (Ω^2)	f (cps)	f_o (cps)	ρ (gm/cc)	η_R (p)
.3	262	22.55	508.3	59431	59439	.720	.00378
1.22	343	52.00	2704	59438	59448	.766	.0189
2.43	386	67.64	4575	59444	59463.50	.805	.0304
2.44	387	68.00	4624	59445	59463.50	.805	.0307
3.20	417	78.91	6227	59449	59474.50	.825	.0404
4.09	516	114.9	13200	59462	59488	.845	.0836
4.10	521	116.7	13630	59463	59488	.845	.0836
5.31	673	172.0	29580	59466	59508.50	.868	.182
5.52	froze						

$R_o = 200k\Omega$

TABLE E10

DATA AND VISCOSITY CALCULATIONS FOR METHYLCYCLOHEXANE AT 26°C (60kc-II)

Pressure (katm)	R_E (kΩ)	R_M (Ω)	R_M^2 (Ω^2)	f (cps)	f_o (cps)	ρ (gm/cc)	η_R (p)
.16	174	31.273	978.00	59427	59438	.778	.00672
.73	238	54.546	2975.3	59428	59443.50	.805	.0198
2.34	360	98.910	9873.2	59437	59462.50	.865	.0605
3.56	439	127.64	16292	59440	59479	.898	.0971
4.77	609	189.46	35895	59451	59499	.924	.208
6.49	898	294.55	86760	59446	59530.50	.957	.485
7.94	1220	411.64	169447	59441	59560	.980	.925

R_o = 88kΩ

TABLE E11

DATA AND VISCOSITY CALCULATIONS FOR TOLUENE AT 25°C (60kc-II)

Pressure (katm)	R_E (kΩ)	R_M (Ω)	R_M^2 (Ω^2)	f (cps)	f_o (cps)	ρ (gm/cc)	η_R (p)
.13	139	29.091	846.29	59428	59438	.868	.00522
.98	181	44.000	1936.0	59434	59445.50	.913	.0113
2.22	243	66.910	4476.9	59442	59460.50	.957	.0250
3.32	296	86.183	7427.5	59451	59476	.988	.0402
4.67	388	119.38	14252	59468	59497.50	1.018	.0749
5.82	495	158.55	25138	59485	59517.50	1.040	.129
7.29	689	229.09	52482	59496	59546.50	1.066	.263
7.93	808	272.37	74185	59505	59560	1.076	.369

$R_o = 59k\Omega$